Synthesis of fumed titanium dioxide with a high content of rutile

structure by novel natural dropping thermal treatment

自然落下式新熱処理法による高ルチル化結晶を有したフュームド酸

化チタンの合成に関する研究

by

Yukiya Yamashita

January 2020

DOCTOR OF ENGINEERING

in

LIFE SCIENCE AND APPLIED CHEMISTRY

NAGOYA INSTITUTE OF TECHNOLOGY

NAGOYA

JAPAN

Synthesis of fumed titanium dioxide with a high content of rutile structure by novel natural dropping thermal treatment

自然落下式新熱処理法による高ルチル化結晶を有したフュームド酸化チタンの合成に関する研究

January 2020

Yukiya Yamashita

ABSTRACT

The synthesis of a new fumed TiO_2 having high content of rutile structure maintaining the high dispersibility was studied. The focuses were on the morphology of the precursors prepared by the modification of the fumed TiO_2 and thermal treatment conditions. The fumed TiO_2 was thermally treated in a vertical-type of a tubular furnace by a natural dropping method. The resulted thermally-treated TiO_2 showed drastically high content of the rutile structure and high dispersibility due to a sponge-like porous agglomerate. The new fumed TiO_2 modified with SiO_2 performed 100 % of the rutile structure content and excellent dispersibility due to both the sponge-like porous agglomerate and static electricity repellence by SiO_2 on the fumed TiO_2 surface. The relationships between the conversion ratio of the rutile structure and the morphology of the precursors are investigated.

Chapter 1 is dedicated to a brief and general background of titanium dioxide (TiO_2) especially fumed TiO_2 including the production process and applications. Accordingly, some studies to modify the morphology and crystal structure of the fumed TiO_2 are also introduced. The objective of this thesis is demonstrated.

Chapter 2 describes a new attempt to increase the content of rutile structure for the fumed TiO_2 by the novel thermal treatment, natural dropping method with preventing the sintering. Drastic increase in a polymorphism from the anatase to the rutile structure was observed by reducing the agglomerate size. The resulted thermally-treated fumed TiO_2 showed high dispersibility in the sedimentation test due to the porous sponge-like agglomerate. The relationships between the rutile structure conversion ratio and residence time of the agglomerate in the electrical furnace were investigated based on the thermal treatment temperature.

Chapter 3 describes the effect of a dry-type surface modification of the fumed TiO_2 to synthesis the new fumed TiO_2 having 100 % of the rutile structure content maintaining the high dispersibility. The fumed TiO_2 was modified with various metallic alkoxides to prepare preferable precursors for the next natural dropping thermal treatment. It is conformed that the dry-type surface modification without heating is very effective method for the preparation of the preferable precursors. The thermally-treated fumed TiO_2 modified with 2 wt.% of Tetraethoxysilane (TEOS) exhibited both 100% rutile structure and excellent dispersibility. This high dispersibility caused from both the sponge-like structural characteristic of the agglomerate and a static electricity repellence by coated SiO_2 layer.

Chapter 4 describes another new method for the synthesis of the new fumed TiO_2 having 100 % of the rutile structure content maintaining the high dispersibility by mixing with external additives. The new fumed TiO_2 with 100 % of the rutile structure having the excellent dispersibility was synthesized by the mixing of the surface modified fumed SiO_2 by both the sponge-like structural characteristic of the agglomerate and the static electricity repellence of SiO_2 on the fumed TiO_2 surface. The decrease of the crystal transformation temperature was observed for the thermally-treated fumed TiO_2 mixing with the fumed Al_2O_3 with the high thermal conductivity. Additionally, the remarkable acceleration of the transformation from the anatase to the rutile structure and sintering / grain growth of the thermally-treated fumed TiO_2 modified with calcium stearate was confirmed by the burning of the alkyl-group in calcium stearate. Small and low densified agglomerated precursors resulted in 100 % of the rutile structure conversion ratio.

Chapter 5 describes the new attempt to apply the natural dropping thermal treatment to other fumed oxides; fumed SiO_2 and fumed Al_2O_3. The crystal structures of both fumed oxides were not changed by the thermal treatment at 1450 °C while the fumed TiO_2 transformed at the same temperature. It was confirmed that the fumed SiO_2 and the fumed Al_2O_3 can be modified the morphology maintaining the original crystal structure by this natural dropping thermal treatment.

Finally, Chapter 6 furnished the overall concluding remarks of the present work and the future directions for research. The technique presented in this study provides a good foundation for the various future application of modification of the morphology and transformation of inorganic materials.

TABLE OF CONTENTS

CHAPTER 5 THE EXTENDED APPLICATION OF THE NOVEL NATURAL DROPPING THERMAL TREATMENT

CHAPTER 6 CONCLUDING REMARKS AND POTENTIAL DIRECTION FOR FUTURE RESEARCH

CHAPTER 1
INTRODUCTION

1.1 Titanium Dioxide (TiO₂)

1.1.1 General Introduction of Titanium Dioxide (TiO₂)

Titanium Dioxide (TiO_2) is widely used in our life. This paper is reported a new trial to synthesis a new fumed TiO_2 with high rutile structure content maintaining the high dispersibility. In this chapter, a general introduction of the TiO_2 and especially the fumed TiO_2 are described to clarify the purpose of this investigation.

TiO_2 has been applying as a white pigment in various industrial fields such as coatings, inks, papers, food, cosmetics and others. TiO_2 is chemically very stable material. It is not solved with weak acid, base and organic solvent. It is only reacted with hydrofluoric acid and hot concentrated sulfuric acid. There are no risk of explosion or fire. These chemically high stability is one of the superior points of TiO_2 as a white pigment compared with other typical ones, i.e., ZnO and Lithopone (Mixture of $BaSO_4$ and ZnS).

TiO_2 has three typical crystalline polymorphs, anatase, brookite and rutile. Generally, the anatase and the rutile structure are applied to the current industrial use. The brookite structure is not familiar due to lesser stability than the rutile structure due to a metastable phase and relatively complicated preparation method. Both the anatase and the rutile structure have tetragonal crystalline form. The anatase structure has 3.90 g/ml of density versus 4.27 g/ml of the rutile structure. This density difference results apparently difference of the Mohs' hardness, approximately 5.5 ~ 6.0 of the anatase structure and approximately 7.0 ~ 7.5 of the rutile structures.

For the white pigment, the refractive index is one of the most important properties. The refractive index of the anatase structure is 2.52 and the rutile structure is 2.72. These values are higher than the value of diamond; 2.42. The high refractive index results the high hiding power when it is dispersed to media such as a resin and a solvent. Further, TiO_2 powder also has relatively low density compared with other inorganic pigments. Low densified materials are preferred to the pigment because the coloring performance is related to the volume percentage in the media. Additionally, the low densified materials show less sedimentation and less separation coloring when it is applied to the

paint by a small difference of the density against the media. TiO_2 shows white color due to scattering a visible light with less adsorption. These properties are another reason which TiO_2 is applied as an excellent white pigment [1].

It is known that the most favored particle size for the pigment is 1/2 diameter against the wavelength of a visible light based on Mie-scattering effect. If the particle size reduces smaller than Mie-scattering region; Reyleigh scattering region, the particle decreases with the scattering performance and becomes to transmit the visible light. By this phenomenon, the particle size for the current TiO_2 is normally controlled between around 0.2 μm and 0.4 μm [2]. The standard physicochemical properties of TiO_2 base on the polymorphism are summarized in Table 1-1.

Table 1-1 Physicochemical properties of TiO_2

Crystal Structure	Rutile	Anatase	Brookite
Crystal Structure	Tetragonal	Tetragonal	Rhomic
Density (g/cm3)	4.27	3.90	4.13

Refractive index nD
  Normal light incidence for C-axis
  Parallel light for C-axis
	2.722
	2.613
	2.909
		2.52
		2.554
		2.493
			2.63

Mohs hardness	7.0 - 7.5	5.5 - 6.0	5.5 - 6.0
Specific heat (cal/℃・ g at 25℃)	0.169	0.169	
Thermal conductivity (cal/cm/sec/℃)	0.148	0.430	

Thermal expansion coefficient ($\times10^{-6}$/ ℃)
  a-axis
  c-axis
	7.19
	9.94
		2.88
		6.64	

Electrical conductivity (mho/cm)	10^{-13}-10^{-14}	10^{-13}-10^{-14} 5.5×10-8^{*1}	
Bandgap (eV)	3.0	3.2	3.0
Dielectric constant	114	48	78^{*2}
Melting point (℃)	1825	Transform to rutile	Transform to rutile
^{*1} at500℃　　　^{*2} direction to a-axis			

Besides the white pigment, there are many reports for the investigation of TiO_2 to other applications. For examples, an electrical conductive TiO_2 coated with Sb doped SnO_2 coating layer was synthesized for an antistatic white pigment [3], non-stoichiometric TiO_2-x powder produced by a reduction reaction with NH_3 gas as a black color pigment having electro-conductivity [4], a catalyst carrier of selective catalyst reduction of an

exhaust gas from an automobile [5] and from a coal boiler [6].

TiO_2 has around 3.0 ~ 3.2 eV of the bandgap. It shows an electro conductivity by the irradiation of the same energy to the bandgap. The wavelengths of the light corresponded with the bandgap is 388 nm for the anatase structure and 412 nm for both the rutile structure and the brookite structure. These wavelengths of the light exist a borderline between ultraviolet and visible light. Therefore, TiO_2 has a function of a photo-semiconductor by an irradiation of ultraviolet. Recently, many reports are demonstrated for the photocatalytic activities of the TiO_2. The detailed investigation examples are illustrated in Chapter 1.1.4 because later described a fumed TiO_2 has been mainly investigated as a photocatalytic material with its excellent performances. A heat ray shielding and infrared reflecting TiO_2 are also reported [7-8]. As another study, a high purified TiO_2 is studied as a raw material of a condenser; PZT ($Pb[Zr,Ti]O_3$) [9].

1.1.2 Production Process of TiO_2

(1) General Introduction

There are several production processes for the TiO_2. For the white pigment, a sulfate process and a chloride process are mainly applied [10]. A sol-gel process and a fumed process are generally applied to produce fine TiO_2 powders.

(2) Sulfate Process

An ilumenite ore is normally applied as a raw material of the TiO_2 in the sulfate process. A hydrogen sulfide reacts with the ilumenite ore and a titanyl sulfate is produced. The titanyl sulfate is next hydrolyzed and then dehydrated by the following equations (1-1).

$$FeTiO_3 + 2\,H_2SO_4 \rightarrow TiOSO_4 + F_2SO_4 + 2\,H_2O$$
$$TiOSO_4 + 2\,H_2O \rightarrow TiO(OH)_2 + H_2SO_4$$
$$TiO(OH)_2 \rightarrow TiO_2 + H_2O \qquad (1\text{-}1)$$
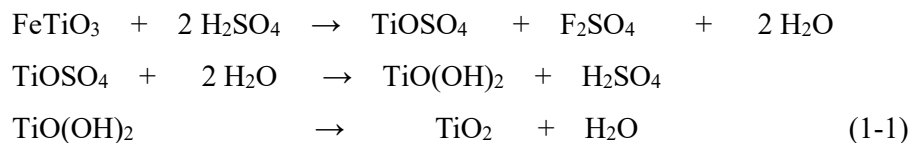
(3) Chloride Process

For the chloride process, a rutile ore is normally used as the raw material. The ilumenite ore is also available. The rutile ore is reacted with chlorine under reduction atmosphere and titanium tetrachloride ($TiCl_4$) is synthesized. The $TiCl_4$ is purified by the distillation

and next oxidized [11].

$$TiO_2 \; + \; C \; + \; 2\,Cl_2 \; \rightarrow \; TiCl_4 \; + \; CO_2$$
$$TiCl_4 \; + \; O_2 \qquad\qquad \rightarrow \quad TiO_2 \; + \; Cl_2 \qquad\qquad (1\text{-}2)$$
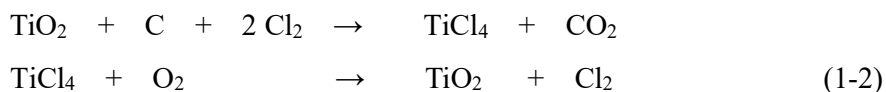
(4) Sol-gel Process

A sol-gel process can produce very fine and purified TiO_2 powders. It is normally investigated for the high functionalized materials. An organic titanate is applied as the raw material. The organic titanate is hydrolyzed and next heated [12]. An example of the reaction is shown equation (1-3) by using the titanium alkoxide.
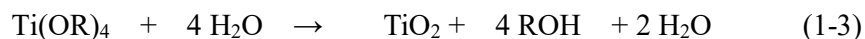
$$Ti(OR)_4 \; + \; 4\,H_2O \; \rightarrow \quad TiO_2 + \; 4\,ROH \; + 2\,H_2O \qquad (1\text{-}3)$$
$$\text{R: alkyl-group including functional groups}$$

(5) Fumed Process

$TiCl_4$ is applied as the raw material of the fumed process. The $TiCl_4$ is evaporated and inserted to an oxyhydrogen flame and next hydrolyzed by the equation (1-4).

$$TiCl_4 \; + \; 2H_2 \; + \; O_2 \; \rightarrow \quad TiO_2 \; + \; 4HCl \qquad\qquad (1\text{-}4)$$

The details of the fumed process are described in Chapter 1.2.

1.1.3 Phase Transformation and Morphology Investigations of The TiO_2

It is well known that the rutile structure is a stable phase in the TiO_2. Both the anatase and the brookite structure transform to the rutile structure at high temperature. This is generally irreversible transformation and the rutile structure does not return to the anatase and the brookite structure at normal conditions except for under special conditions. As a special case, an investigation reports that a stability of the anatase and the rutile structure may reverse and the anatase structure may be the stable phase with very small crystallite sizes [13]. As another study, an opposite transformation from the rutile to the anatase structure is reported at a negatively charged colloid surface [14]. There are several investigations regarding to the phase transformation and morphology

of the TiO_2 related to the production process.

As for the sulfate process, Cr- and Nb- ion accelerates the transformation from the anatase to the rutile structure [15]. A self-generated thermal hydrolysis method produces the anatase structure in various hydrolysis conditions [16].

For the chloride process, the final reaction is sometimes called to the oxidation reaction process. In this process, the production conditions are optimized to produce highly purified TiO_2 [17]. Suyama et al. obtained a highly densified TiO_2 by the sintering at 1200 °C for 2 hours [18]. They also reported the transformation from the anatase to the rutile structure in TiO_2-SiO_2 mixed system produced by the vapor phase reaction [19].

Regarding the sol-gel process, several investigations for the phase transformation were reported. A very fine TiO_2 with the anatase structure transforms to rutile structure at 600 °C for 3 hours [20]. Baorang et.al., obtained 100% of rutile structure by the thermal treatment at 800 °C for 2 hours for the very fine TiO_2 powders [21]. TiO_2 produced by the irradiation with ultrasound showed lower transformation temperature than without the ultrasound [22].

Some other investigations are reported the phase transformation based on the other synthesis methods, i.e., a vapor phase hydrolysis of $TiCl_4$ [23], fine TiO_2 particle synthesized from Ti-edta complex [24], Nb- and Ta-doped TiO_2 powders synthesized from precipitated method [25] and Cr doped TiO_2 film synthesized by RF magnetic sputtering method [26].

As other studies, the transformation related to the brookite structure is also reported [27-28]. There are also several investigations for the phase transformation and morphology of TiO_2 by the additional thermal treatment. Several additives like a SiO_2 exhibit remarkable inhibitory effect for the transformation from the anatase to the rutile structure by the solid stated reaction [29]. The phase transition of the anatase structure is investigated under high pressure by using Raman spectroscopy [30]. The crystalline of the TiO_2 powder calcined at 1000 °C for 3-24 hours was examined by using TEM electron diffraction patterns [31].

It is observed about several simulation reports for the transformation investigation of TiO_2, i.e., a gas-phase $TiCl_4$ reaction with O_2 [32], phase transition and stability of TiO_2 under high pressures [33], and the activation energy simulation for the transformation [34]. The above described contents are just examples. The research papers of TiO_2 are

enumerated. It means that TiO_2 is so important and attractive material for current our life.

1.2 Fumed Process

1.2.1 General Introduction

There is a special production process to synthesis very fine oxide powders as known the fumed process. For industrial purpose, silicon dioxide produced by this process is well known as AEROSIL® product (EVONIK GmbH, Nippon AEROSIL Co. Ltd.,). In this process, silicone tetrachloride ($SiCl_4$) is converted to the gas phase and then reacts spontaneously and quantitatively in an oxyhydrogen flame with the intermediately formed water to produce the desired silicon dioxide with the equation (1-5) [35].

$$2\,H_2 + \quad O_2 \quad \rightarrow \quad 2\,H_2O$$
$$SiCl_4 \quad + \quad 2\,H_2O \quad \rightarrow \quad SiO_2 \quad + \quad 4\,HCl$$
$$SiCl_4 \quad + \quad 2\,H_2 \quad + \quad O_2 \quad \rightarrow \quad SiO_2 \quad + \quad 4\,HCl \qquad (1-5)$$
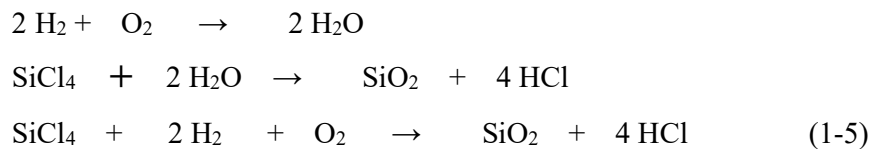
This fumed process is very environmentally friendly production process because a by-product is only gaseous hydrogen chloride and it is recycled to synthesis trichlorosilane ($HSiCl_3$) by the reaction with crude silicon metal for the semiconductor application. $SiCl_4$ is a byproduct of the production of $HSiCl_3$.

Other metallic oxides can be produced with changing the raw material to other metallic chloride in this fumed process. For industrial use, aluminum oxide (Al_2O_3) and titanium dioxide (TiO_2) are produced by using aluminum trichloride ($AlCl_3$) and titanium tetrachloride ($TiCl_4$) as the raw materials.

In the fumed process, the generated primary particles connect each other to make aggregate during the flame tube, and next the aggregate gathers to makes agglomerate with 3D networking structure. The scheme of the fumed process is demonstrated in Fig. 1-1.
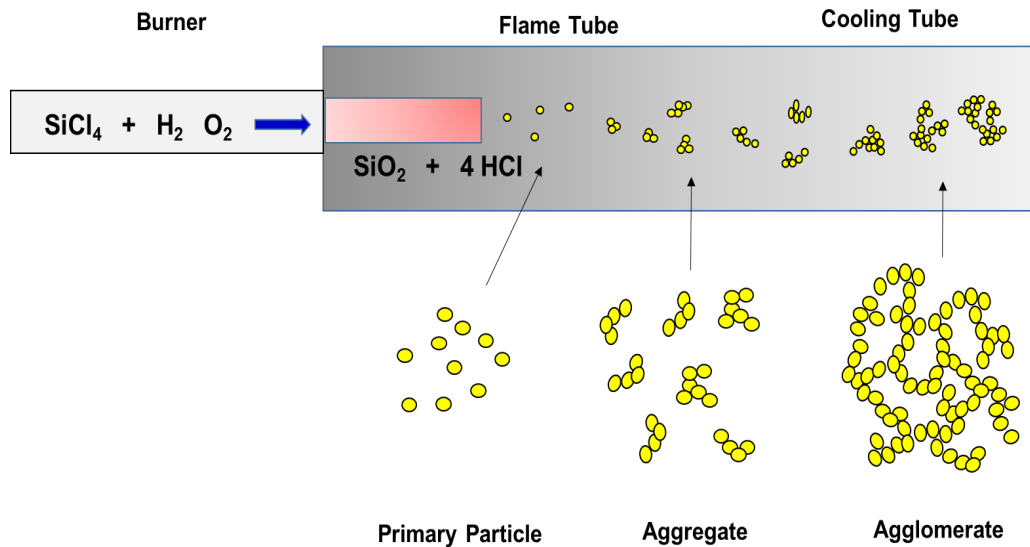
Fig. 1-1. Scheme of fumed process

This agglomerate is made by a week hydrogen bonding between the particles. The hydrogen bonding of the agglomerates is cleaved by the strong mechanical share when it dispersed in the media such as a solvent and a resin. When the mechanical share is released, the aggregates make the agglomerates again. By this phenomenon, the fumed oxides show excellent thixotropic performance. It is applied as a thickening agent [36]. This unique property is caused from the special production process of the fumed process. The process does not use a solvent during the production. There is no filtration, washing and drying process. Therefore, the particle produced by the fumed process has less coagulation agglomerate. The scheme of the thickening performance is shown in Fig. 1-2.
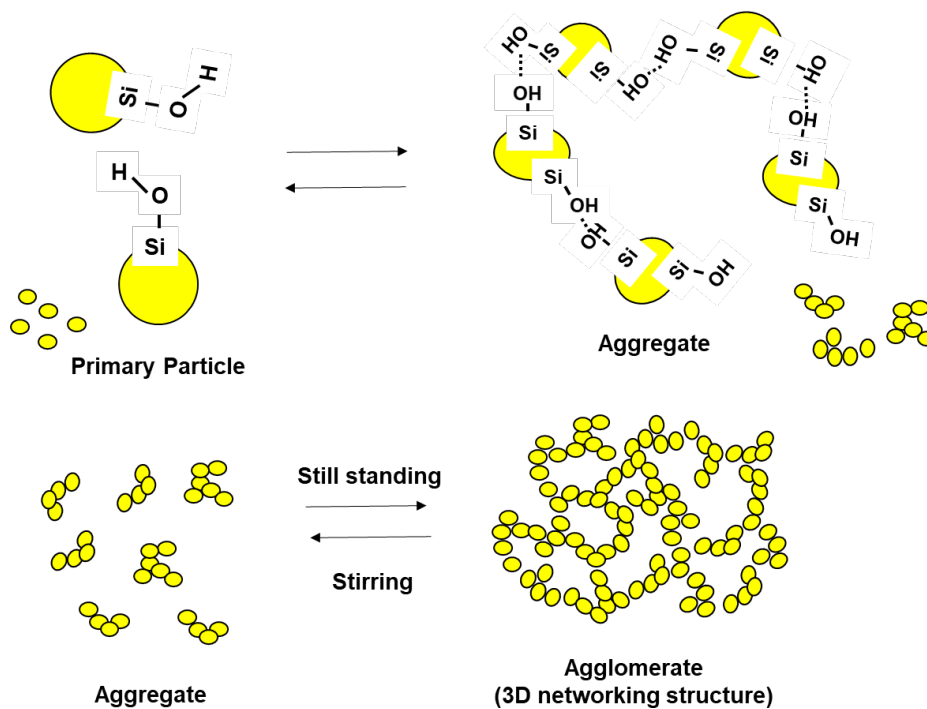
Fig. 1-2. Scheme of the thickening performance of the fumed oxides

1.2.2 Fumed TiO$_2$

Fumed TiO$_2$ is produced by the similar chemical reaction as the fumed SiO$_2$ by using TiCl$_4$ as the raw material. The TiCl$_4$ is colorless, extremely hydrolysis-sensitive liquid with a boiling point of 138 °C. The TiCl$_4$ is evaporated and hydrolyzed in an oxyhydrogen flame as shown in the equation (1-6).

$$2\,H_2 + O_2 \quad \rightarrow \quad 2\,H_2O$$
$$TiCl_4 + 2\,H_2O \quad \rightarrow \quad TiO_2 + 4\,HCl$$
$$TiCl_4 + 2\,H_2 + O_2 \quad \rightarrow \quad TiO_2 + 4\,HCl \qquad (1\text{-}6)$$
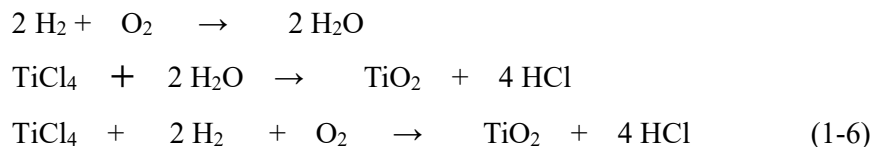
The fumed TiO$_2$ consists from a mixture of the anatase and the rutile structure. The main crystal phase is the anatase structure. The fumed TiO$_2$ has a mean primary particle size around 10 times smaller than the pigment grade of TiO$_2$. It has practically less pigment property due to low hiding power by a smaller primary particle size [37].

1.2.3 Application of The Fumed TiO$_2$

(1) General Introduction

As the fumed TiO$_2$, one of the famous fumed TiO$_2$, AEROXIDE® TiO$_2$ P 25 (EVONIK GmbH / Nippon AEROSIL Co. Ltd.,) (P25) has around 85 % of the anatase and 15 % of the rutile structure [38]. The primary particle size is around 21nm. A study confirmed that the anatase and the rutile particles are existing separately from their agglomerates and pure rutile particles are isolated by hydrogen fluoride (HF) treatment [39].

As shown in Chapter 1.1.1, the anatase structure has 3.2 eV of the bandgap. P25 can absorb ultraviolet light (UV) unless scattering the visible light. By these special properties, P25 has been mainly investigating and applying to a new material using its photo-semiconductor property and an ultraviolet shielding material with transparent for the visible light.

(2) Photocatalyst

It is known that the fumed TiO$_2$ (especially P25) has very excellent photocatalytic activities and has been investigating as a typical photocatalytic material [40].

TiO$_2$ absorbs UV and generates a charge carrier hole and an electron. The electron in a conduction-band reacts with oxygen (O$_2$) and forms a super oxide ion ($\cdot$O$_2$-), the hole in a valence-band reacts with water (H$_2$O) and forms hydroxyl radical ($\cdot$OH). The super oxide ion ($\cdot$O$_2$-), changes several radicals with its high reactivity. They decompose organic materials with hydroxyl radical ($\cdot$OH). This is very clean reaction because it uses only UV, H$_2$O and O$_2$ [41]. The scheme of photo-catalyst is shown in Fig. 1-3.
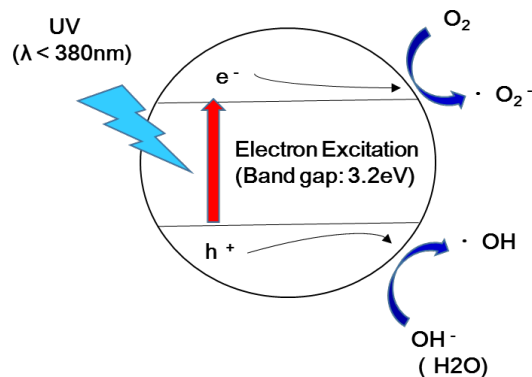
Fig. 1-3. Scheme of photocatalytic activity

The reason why P25 has been investigated as the photocatalytic materials is the very fine primary particle size, high anatase content (suitable bandgap), easy getting with a low price in a commercially and high photocatalytic activities [42]. The investigation of the P25 is mainly categorized to the following two types of researches.

One is the reference material of the evaluation of photocatalytic activities. Many investigations have been comparing the photocatalytic activities of their researching materials with P25. Some of them appeals the advantage of their developing materials compared with P25 for the decomposition performance of various materials under several conditions.

For example, TiO_2 nanocrystals prepared by precipitation method and next supercritical drying shows maintained the anatase structure at 800 ℃ and shows comparable photocatalytic activity to P25 [43]. Some studies are especially focusing on the improvement of the photocatalytic activities under visible light. S-doped TiO_2 prepared by the sol-gel method shows higher photocatalytic activities than P25 under visible light longer 500nm for the decomposition of methylene blue [44]. Mesoporous TiO_2 nanospheres with carboxylate ligands derived from oleic acid showed excellent photocatalytic decomposition ability for Rhodamine B (RhB) under visible light [45].

Another is a development of the new photocatalyst with P25. In this research, a combination or a modification of P25 with other materials are investigated to improve the photocatalytic performance. P25 is mixed with fumed SiO_2 and the photocatalytic activity is increased compared with pure P25 due to small increase in the bandgap [46]. P25 coated with peroxide titanate shows higher photodegradaiton ability of gaseous isopropyl alcohol under UV irradiation [47]. SiO_2 coated Cu doped P25 increases the photodegradation of methylene blue and self-cleaning ability under UV irradiation [48]. F_2O_3 coated P25 annealed at 600 ℃ performed better photocatalytic effect than the original P25 for the decomposition of phenol and nitrobenzene under UV irradiation [49]. Besides to make the composite, additional treatments are also applied to P25 for the enhancement of the photocatalytic activities. As some examples, the photocatalytic activities of P25 depended on the thermal treatment temperature for photodegradation of tartrazine dye [50] and the hydrothermal treatment of the P25 [51]. Not only materials but also decomposition conditions are also investigated. Horikoshi reported that the

photocatalytic activities of P25 can be improved under both irradiation of UV and microwave compared with only UV irradiation [52]. As a special case, addition of submicron sized Al_2O_3 to P25 improved to make a continuous film without clack and low quantity of P25 on the film [53]

For the industrial purpose, a transparent photocatalytic coating is developed by using P25. P25 has very small primary particle size and it can be made for the transparent coating under applying strong share to the dispersion [54-58].

There are many researches for the photocatalytic activities related to the fumed TiO_2 (P25). This is probably caused from the necessity of the development of a low energy resource and environmentally friendly materials.

(3) Dye-sensitized Solar Cell

Grätzel reported a low-cost, high-efficiency solar cell based on a dye-sensitized colloidal TiO_2 film; Grätzel cell [59]. When the dye molecule adsorbs a light, it gives rise to electron injection into the conduction band of the semiconductor, and next releases an electron to the TiO_2. The TiO_2 transfers the electron in turn to a conductive glass. The oxidized dye molecular is reduced by an iodide ion which is oxidized to elemental iodine. The iodine receives the electron from the cathode, and it is transformed back to iodide, closing the circuit. The schematic design is shown in Fig. 1-4.
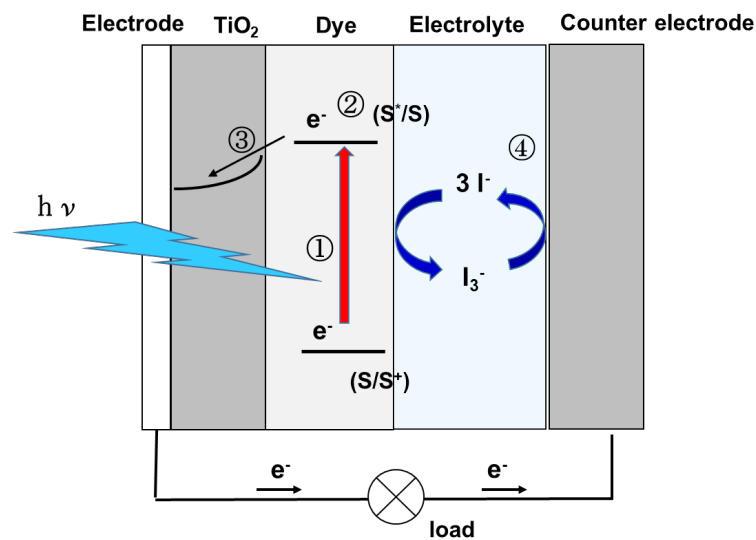
Fig. 1-4. Schematic design of the dye-sensitized solar cell

In the original paper of Grätzel cell, TiO_2 electrode was synthesized by the sol-gel method. After publication of this report, many investigations applied the fumed TiO_2 (P25) to the TiO_2 electrode [60-64] because of the suitable bandgap and the same reason as the photocatalyst investigation such as very fine primary particle size, high anatase contents and easy getting with a low price and additionally high purified TiO_2. Okai et. al. improves the adhesion of a coating with P25 by low temperature calcination over 350 ℃ maintaining around 4 % of the efficiency [65]. A composite of nano SiO_2 and P25 as the photo-anode achieves 8.4 % of energy conversion efficiency [66]. Another research confirms that composite of nanocrystalline titania containing nanotube structure (TiNT) with 2 wt.% of P25 shows 8.43 % of the energy conversion efficiency [67]. Natural dyes sensitized solar cell is made by using porous TiO_2 film anode by using P25 [68]. Double layer composite consisted of P25 gives 5.78 % of the energy-conversion efficiency [69]. A solid stated solar cell; P25/dye/CuSCN shows around 2 % of energy efficiencies [70]. A perovskite solar cell based on P25 was investigated as low costed solar cell [71]. TiO_2 nanaowire produced from P25 by the hydrothermal treatment for the application to the solar cell [72]. Some investigation compared the performance of their researching materials with P25 as the electrode of Grätzel cell [73-75] like a photocatalytic activity investigation. As a special case, a new pressing method using pre-coated powder appeals to be a low costed method for the dye sensitized-solar cell using Cd coated P25 [76].

This solar cell technology seems to be one of the attractive fields to cultivate the next generation energy source because it has some possibilities to make a flexible film type of the solar cell and apply various industrial fields.

(4) Sunscreen

TiO_2 has an excellent UV cutting performance. Further, the fumed TiO_2 is applied to the UV cutting material with maintaining the transparent due to the low scattering effect of the visible light made from the small sized primary particle. The UV absorption ability of the fumed TiO_2 was compared with other white pigments and it was utilized to the UV cutting material for sunscreens in Japanese cosmetic producers [77-78]. Fig. 1-5. demonstrates one of the experimental results.
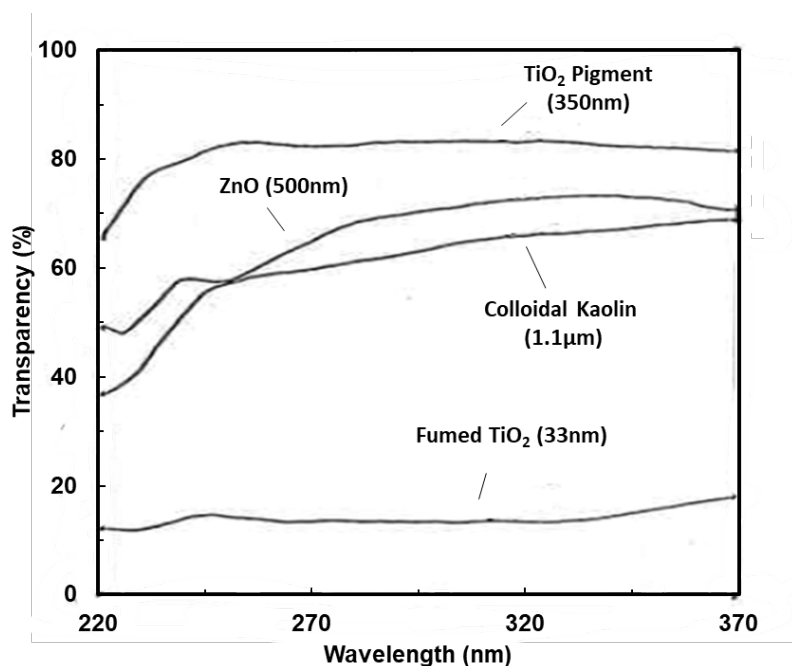
Fig. 1-5. UV absorption ability for metal oxides

A surface modified fumed TiO_2 with octyl silane; AROXIDE® TiO_2 T 805 (Evonik GmbH), is applied to the sunscreen [79]. An analytical trial is carried out to determine the titanium content directly in composite of the sunscreen by using laser-induced breakdown spectroscopy [80]. As a very similar to the investigation of the photocatalyst and the dye-sensitized solar cell, the performance Cinnamido group modified silica gels was compared with P25 for the UV shielding properties [81]. Other various TiO_2 materials are also compared [82].

The sunscreen agent with the fumed TiO_2 is already widely applied to the society and it is a mature industry.

(5) Other Applications

A silicone rubber with P25 shows excellent physical properties under UV-C radiation and increased the crosslinking density, high retention ratio in tensile properties, especially elongation at break [83]. P25 improves the flame resistance in polyimide foams [84] and smoke and fire resistance of silicone [85]. An examination of P25 to an ingredient of a tooth paste is reported to give bactericidal activity [86]. P25 is also applied to a catalytic support for silica-gel and the generation of H_2 from ethanol [87].

As other studies, naphthalene hydrogenation catalyst Pt-Pd supported P25 is reported [88], and the surface modified TiO_2 is applied to toner application as an external additive [89-90].

1.3 Object of Thesis

Among above mentioned various applications for the fumed TiO_2, the sunscreen seems to be one of the most important applications in the current society because the photocatalyst and the dye-sensitized solar cell with the fumed TiO_2 is still under developing stage.

For the sunscreen, the rutile structure is preferred as the UV cutting agent because of the different of the absorbing UV light wavelength between the rutile and the anatase structure which is caused from the energy bandgap. The rutile structure can absorb longer UV light than the anatase structure [91]. Comparatively, it is reported that the anatase structure is not preferred to be used for the cosmetics application because of the high photocatalytic activities [92]. Additionally, other studies are also appealed that TiO_2 nanoparticle with the anatase structure damages DNA under UV irradiation [93-94]. To improve these situations, it is considered to increase the rutile structure content of the fumed TiO_2 by the additional thermal treatment.

As a basic examination, Porter et al. reported a study for the additional thermal treatments to the P25. They obtained nearly 100 % rutile structure contents at 1000 ℃ for 3 hours [95]. As another study, 100 % of the rutile structure content was obtained by the thermal treatment of P25 at 900 ℃ for 4 hours [96]. However, in both investigations, the drastic increase of the primary particle size and rapidly decrease of the surface area are observed. In generally, it has been considered that the sintering of the fumed TiO_2 are not affordable by the additional thermal treatment and it resulted a big louse of the high dispersibility.

These issues are probably caused from the calcination method. Previous calcination process would mainly have three big problems to apply the fumed TiO_2 maintaining the high dispersibility. The first one is a long calcination time. The previous calcination time such as from 3 to 4 hours is too long to prevent the sintering of the fumed TiO_2. The second one is a closely contact of each agglomerate during the thermal treatment. The closely contacted agglomerate tends to induce the sintering. To avoid the sintering,

each agglomerate should be apart separately as good as possible.

The final one is low productivity. The fumed TiO_2 has very low bulk density around 0.1 Kg/L. When the additional thermal treatment is applied to the fumed TiO_2 with the current calcination method, i.e., put into a crucible and next the calcination with a muffle furnace, the obtained weight is very small against the volume of the muffle furnace and the crucible. This problem is related to the second problem above mentioned because if the agglomerate was packed closer to increase the bulk density, it would easily result the sintering due to closely contacted each particle.

In this study, a new approach was carried out to solve these problems for the development of the new fumed TiO_2 with high rutile content maintaining the high dispersibility. The newly thermal treatment method is tried to reduce the thermal treatment time as short as possible by applying a natural dropping method. This new calcination process did not use the crucible. It has a possibility to preserve the sintering of agglomerate of the fumed TiO_2 during the calcination by separating each agglomerate. The thermal treatment condition was investigated as a function of the size of agglomerate and residence time in the electrical furnace.

Next, the effect of the morphologies of the fumed TiO_2 before the thermal treatment (Precursor) was investigated by the surface modification of the fumed TiO_2 with the metallic alkoxides with liquid state. As the modification method, a dry-type of the surface modification process without heating was attempted to simplify the process. Additionally, the dry-type of the surface modification process was applied to another modification process controlling the morphology of the agglomerate by mixing of solid stated external additive.

Finally, the novel natural dropping thermal treatment is applied to the other fumed oxides, fumed SiO_2 and fumed Al_2O_3 to confirm the availability.

1.4 Thesis Organization

The thesis consists of following 6 chapters.

Chapter 1 is dedicated to a brief and general background of titanium dioxide (TiO_2) especially the fumed TiO_2 including the production process, applications and crystalline polymorphs investigations.

Chapter 2 describes the new attempt to increase the content of rutile structure for the

pure fumed TiO_2 by the novel natural dropping thermal treatment with changing the agglomerate size passing through the sieves. The crystal structure and dispersibility of the resulted thermally-treated pure fumed TiO_2 were examined. The thermal treatment conditions are also investigated by the residence time in the electrical furnace based on the size of the agglomerate.

In Chapter 3, the new trial to make a precursor before the thermal treatment was tried to synthesize 100 % rutile fumed TiO_2 maintaining the high dispersibility after the thermal treatment. The effect of the dry-type surface modification of the fumed TiO_2 with metallic alkoxide to make the preferable precursor and dispersibility of thermally-treated fumed TiO_2 were studied.

Chapter 4 describes the results of the study to another new method to make the preferred precursor as a mixing of a solid stated external additive. The focus of this investigation was on the external additive species, agglomerates of the fumed TiO_2 of the precursors. The conversion ratio from the anatase to the rutile structure of the resulted thermally-treated fumed TiO_2 was investigated as a function of the agglomerate of the precursors.

In Chapter 5, the natural dropping thermal treatment is applied to other fumed oxides; the fumed SiO_2 and the fumed Al_2O_3 to confirm the possibility.

Finally, Chapter 6 furnishes the overall concluding remarks of the present works. The technique presented in this study provides a good foundation for the various future investigation.

References

[1] K. Asumu, Titanium Dioxide Pigment, Shikizai 31(1958) 349-351.

[2] A. Tsugita, Optical Properties of Pigments and Their Applications, J. Soc. Cosmet. Chem. Japan 27 (1993) 119-129.

[3] Mitsubishi Metals, JP S56-41603.

[4] Mitsubishi Metals, JP S60-200827.

[5] I. Hoshiyama and H. Yonejima, The Catalysts for the Exhaust Gases Produced by Ultrafine Metal Powders, The Chemical Society of Japan 6 (1984) 1035-1041.

[6] K. Adachi, K. Uchida, A. Yukimura, H. Kamata, A. Nakahima and T. Haruyama, Deactivation Characteristics of DeNOx Catalyst for Coal and Biomass Co-fired Boilers,

Journal of the Japan Institute of Energy 94 (2015) 1371-1377.

[7] K. Isobe, Particle Shape of Titanium Dioxide and Application for Functional Materials, J. Jpn. Soc. Color Mater. 88 (2015) 67-72.

[8] T. Yamakawa, T. Ezaki, M. Ishii and S. Takahashi, The Influence of $MnCO_3$ Addition on the Sintering Behavior of PZT Ceramics, J. Jpn. Soc. Powder Powder Metallurgy 42 (1995) 582-586.

[9] J. Fukuda, Development of functional titanium dioxide, Manufacturing & Technology 66 (2014) 54-59.

[10] U. Reiziro, Some Aspects of TiO_2 Pigment Industry, Sikizai 41 (1968) 36-43.

[11] Y. Yasuda and K. Kobashi, Titanium Dioxide, Journal of Aerosol Research 5 (1990) 24-31.

[12] X. Chen and S. S. Mao, Titanium Dioxide Nanomaterials: Synthesis, Properties, Modifications, and Applications, Chem. Rev. 107 (2007) 2891-2959.

[13] A. A. Gribb and J. F. Banfield, Particle size effects on transformation kinetics and phase stability in nanocrystalline TiO_2, American Mineralogist 82 (1997) 717-728.

[14] S. Kittaka, K. Matsuno and S. Takahara, Transformation of Ultrafine Titanium Dioxide Particles from Rutile to Anatase at Negatively Charged Colloid Surfaces, Journal of Solid State Chemistry 132 (1997) 447-450.

[15] S. Karvinen, The effects of trace elements on the crystal properties of TiO_2, Solid State Sciences 5 (2003) 811-819.

[16] T. Cong-xue, D. Jian-qiao, C. Xin-hong, M. Wei-ping, L. Zhi-qiang, C. Xia-zhe, H. Hong-fei and L. Dai-jun, Influence of hydrolysis in sulfate process on titania pigment producing, Trans. Nonferrous Met. Soc. China 19 (2009) s829-s833.

[17] T. Go, T. Hara, M. Honda and K. Kato, Property Control of High Purity Titanium Dioxide by Vapor Phase Oxidation Process, The Society of Chemical Engineers, Japan 22 (5) (1996) 1167-1173.

[18] Y. Suyama and A. Kato, Sintering of Fine TiO_2 Powders Prepared by Vapor-phase Reaction, Yogyo-Kyokai-Shi 89 (1981) 140-147.

[19] Y. Suyama, E. Ura and A. Kato, TiO_2-SiO_2 Powders Produced by the Vapor Phase Reaction of the $TiCl_4$-$SiCl_4$-O_2 System, The Chemical Society of Japan 3 (1978) 356-360.

[20] N. Wetchakun, B. Incessungvorn, K. Wetchakun and S. Phanichphant, Influence of calcination temperature on anatase to rutile phase transformation in TiO_2 nanoparticles synthesized by the modified sol-gel method, Materials Letters 82 (2012) 195-198.

[21] B. Li, X. Wang, M. Yan and L. Li, Preparation and characterization of nano-TiO_2 powder, Materials Chemistry and Physics 78 (2002) 184-188.

[22] K. Prasad, D. V. Pinjari, A. B. Pandit and S. T. Mhaske, Phase transformation of nanostructured titanium dioxide from anatase-to-rutile via combined ultrasound assisted sol-gel technique. Ultrasonics Sonochemistry 17 (2010) 409-415.
Journal of Solid State Chemistry 132 (1997) 447-450.

[23] B. Xia, H. Huang and Y. Xie, Heat treatment on TiO_2 nanoparticles prepared by vapor-phase hydrolysis, Materials Science and Engineering B57 (1999) 150-154.

[24] T. Nishide, Crystal structure and optical property of TiO_2 gels and films prepared from Ti-edta complexes as titania precursors, Journal of Materials Science 35 (2000)

465-469.

[25] S.V. Zaitsev, J. Moon, H. Takagi and M. Awano, Preparation and characterization of nanocrystalline doped TiO_2. Advanced Powder Technol. 11 (2000) 211-220.

[26] A. Hajjaji, A. Atyaoui, K. Trabelsi, M. Amlouk, L. Bousselmi, B. Bessais, M. A. E. Khakani and M. Gaidi, Cr-Doped TiO_2 Thin Films Prepared by Means of a Magnetron Co-Sputtering Process: Photocatalytic Application, American Journal of Analytical Chemistry 5 (2014) 1-10.

[27] J-G. Li and T. Ishigaki, Brookite $\rightarrow$ rutile phase transformation of TiO_2 studied with monodispersed particles, Acta Materialia 52 (2004) 5143-5150.

[28] T. Wakamatsu, T. Fujiwara, K. N. Ishihara and P. H. Shingu, Formation of Brookite-type TiO_2 Titania by Mechanical Alloying, Journal of the Japan Society of Powder and Powder Metallurgy 48 (2001) 950-954.

[29] Y. Suyama and A. Kato, Mechanism of Action of Additives on Anatase-Rutile Transition, Zairyo 27 (1978) 632-637.

[30] T. Sekiya, S. Ohta, S. Kamei, M. Hanakawa and S. Kurita, Raman spectroscopy and phase transition of anatase TiO_2 under high pressure, Journal of Physics and Chemistry of Solids, 62 (2001) 717-721.

[31] P. I. Gouma and M. J. Mills, Anatase-to-Rutile Transformation in Titania Powders, J. Am. Chem. Soc. 84 (2001) 619-622.

[32] A. Kobata, K. Kusakabe and S. Morooka, Growth and Transformation of TiO_2 Crystallites in Aerosol Reactor, AIChE Journal 37 (1991) 347-359.

[33] Q-J. Liu, Z. Ran, F-S, Liu and Z-T. Liu, Phase transitions and mechanical stability of TiO_2 polymorphs under high pressure, Journal of Alloys and Compounds 631 (2015) 192-201.

[34] H. Zhang and J. F. Banfield, Understanding Polymorphic Phase Transformation Behavior during Growth of Nanocrystalline Aggregates: Insights from TiO_2, J. Phys. Chem. B 104 (2000) 3481-3487.

[35] Degussa, Basic Characteristics of AEROSIL® Fumed silica, Technical Bulletin Fine Particles 11 (2003) 1-70.

[36] T. Sukawa and H. Shirono, Fumed Silica, Resources Processing 38 (1991) 131-137.

[37] Degussa. Titanium Dioxides P25 Manufacture-Properties-Applications, Technical Bulletin Fine Particles 80 (2003) 1-26.

[38] B. Ohtani, O. O. Prieto-Mahaney, and D. Li and R. Abe, What is Degussa (Evonik) P25? Crystalline composition analysis, reconstruction from isolated pure particles and photocatalytic activity test, Journal of Photochemistry and Photobiology A: Chemistry, 216 (2010) 179-182.

[39] T. Ohno, K. Sarukawa, K. Tokieda and M. Matsumura, Morphology of a TiO_2 Photocatalyst (Degussa, P-25) Consisting of Anatase and Rutile Crsytalline Phases, Journal of Catalysts 203 (2001) 82-86.

[40] B. Ohtani, O. O. P. Mahaney, F. Amano, N. Murakami and R. Abe, What are Titania Photocatalysts? –An Exploratory Correlation of Photocatalytic Activity with Structural and Physical Properties, J. Adv. Oxide. Technol. 13 (2010) 247-261.

[41] M. R. Hoffmann, S. T. Martin, W. Choi and D. W. Bahnemann, Environmental Applications of Semiconductor Photocatalysis, Chem. Rev. 95 (1995) 69-96.

[42] EVONIK, AEROXIDE®, AERODISP® and AEROPERL® Titanium Dioxide as

Photocatalyst, Technical Information 1243 (2015) 1-12.

[43] D. He and F. Lin, Preparation and photocatalytic activity of anatase TiO_2 nanocrystallites with high thermal stability, Materials Letters 61 (2007) 3385-3387.

[44] T. Ohno, M. Akiyoshi, T. Umebayashi, K. Asai, T. Mitsui and M. Matsumura, Preparation of S-doped TiO_2 photocatalysts and their photocatalytic activities under visible light, Applied Catalysis A: General 265 (2004) 115-121.

[45] J. Cao, X-Z. Song, X. Kang, Z. Dao and Z. Tan, One-pot synthesis of oleic acid modified monodispersed mesoporous TiO_2 nanospheres with enhanced visible light photocatalytic performance, Advanced Powder Technology 29 (2018) 1925-1932.

[46] H. R. Jafry, M. V. Liga, Q. Li and A. R. Barron, Simple Route to Enhanced Photocatalytic Activity of P25 Titanium Dioxide Nanoparticles by Silica Addition, Environmental Science & Technology 45 (2011) 1563-1568.

[47] H. Ichinose and H. Katsuki, Photocatalytic Activities of Film Prepared from Peroxo-Modified Anatase Sol with Added TiO_2 Powder, Journal of the Ceramic Society of Japan 107 (1999) 73-77.

[48] I. Harya, F. Izinilah, I. R. Hakiki and S. Slamet, Study of Self Cleaning Fabric Modified by Cu Doped TiO_2 with the addition of Tetraethyl OrthoSilicate (TEOS), AIP Conference Proceeding 2024 (2018) 020071-1 – 020071-7.

[49] T. K. Kim, M. N. Lee, S. H. Lee, Y. C. Park, C. K. Jung and J.-H. Boo, Development of surface coating technology of TiO_2 powder and improvement of photocatalytic activity by surface modification, Thin Solid Films 475 (2005) 171-177.

[50] I.P.A.F. Souza, O. Pezoti, K. C. Bedin, A. L. Cazetta, S. A. R. Melo, L. S. Souza, M. C. Silva and V. C. Almeida, Chemometric study of thermal treatment effect on the P25 photoactivity for degradation of tartrazine yellow dye, Ceramics, International 44 (2018) 12292-12300.

[51] J. Yu, H. Yu, B. Cheng, M. Zhou and X. Zhao, Enhanced photocatalytic activity of TiO_2 powder (P25) by hydrothermal treatment, Journal of Molecular Catalysis A: Chemical 253 (2006) 112-118.

[52] S. Horikoshi, Microwave Effect in Titanium Dioxide Photocatalyst, Journal of the Society of Inorganic Materials, Japan 16 (2009) 251-259.

[53] S. Hayashi, F. Oguri and F. Kagaya, Preparation of Composite Film by Simultaneous Electrophoretic Deposition Using Titanium Oxide Nanoparticles and Submicron-sized Aluminum Oxide Particles, J. Soc. Powder Technol, Japan 51 (2014) 686-693.

[54] Mitsubishi Materials, JP3291559.

[55] Mitsubishi Materials, JP3291560.

[56] Mitsubishi Materials, JP3291563.

[57] Mitsubishi Materials, JP4110799.

[58] Mitsubishi Materials, JP4525041.

[59] B. O'Regan and M. Grätzel, A low-cost, high-efficiency solar cell based on dye-sensitized colloidal TiO_2 films, Nature 353 (1991) 737-740.

[60] L. Han, R. Yamanaka and T. Obata, Effect of the Cell Structure Elements on Performance of Dye-Sensitized Solar Cell, Sharp Technical Journal 83 (2002) 49-53.

[61] X. Yin, Z. Xue, L. Wang, Y. Cheng and B. Liu, High-Performance Plastic Dye-sensitized Solar Cells Based on Low-Cost Commercial P25 and Organic Dye, ACS Appl. Mater. Interfaces 4 (2012) 1709-1715.

[62] P. Cheng, S. Du, Y. Cai, F. Liu, P. Sun, J. Zheng and G. Lu, Tripartite Layered

Photoanode from Hierarchical Anatase TiO_2 Urchin-Like Spheres and P25: A Candidate for Enhanced Efficiency Dye Sensitized Solar Cells, The Journal of Physical Chemistry C 117 (2013) 24150-24156.

[63] G. Boschloo, H. Lindström, E. Magnusson, A. Holmberg and A. Hagfeldt, Optimization of dye-sensitized solar cells prepared by compression method, Journal of Photochemistry and Photobiology A: Chemistry, 148 (2002) 11-15.

[64] M. Hamadanian, J. Safaei-Ghomi, M. Hosseinpour, R. Masoomi and V. Jabbari, Uses of new natural dye photosensitizers in fabrication of high potential dye-sensitized solar cells (DSSCs), Materials Science in Semiconductor Processing 27 (2014) 733-739.

[65] T. Okai and H. Tsubakihara, Highly efficient dye-sensitized solar cells sintered at low temperature, Research Reports of the School of Engineering Kinki University 41 (2007) 51-56.

[66] H. Niu, L. Liu, H. Wang, S. Zhang, Q. Ma, X. Mao, L. Wan, S. Miao and J. Xu, Significant influence of nano-SiO_2 on the performance of dye-sensitized solar cells based on P25, Electrochemical Acta 81 (2012) 246-253.

[67] S. Ngamsinlapasathian, S. Sakulkhaemaruethai, S. Pavasupree, A. Kitiyanan, T. Sreethawong, Y. Suzuki and S. Yoshikawa, Highly efficient dye-sensitized solar cell using nanocrystalline titania containing nanotube structure, Journal of Photochemistry and Photobiology A: Chemistry 164 (2004) 145-151.

[68] S. Hao, J. Wu, Y. Huang and J. Lin, Natural dyes as photosensitizers for dye-sensitized solar cell, Solar Energy 80 (2006) 209-214.

[69] G. Dai, L. Zhao, S. Wang, J. Hu, B. Dong, H. Lu and J. Li, Double-layer composite film based on sponge-like TiO_2 and P25 as photoelectrode for enhanced efficiency in dye-sensitized solar cells, Journal of Alloys and Compounds 539 (2012) 264-270.

[70] B. O'Regan, F. Lenzmann, R. Muis and J. Wienke, A Solid-State Dye-Sensitized Solar Cell Fabricated with Pressure-Treated P25-TiO_2 and CuSCN: Analysis of Pore Filling and IV Characteristics, Chem. Mater. 14 (2002) 5023-5029.

[71] P. Liu, Z. Yu, N. Cheng, C. Wang, Y. Gong, S. Bai and X.-Z. Zhao, Low-cost and Efficient Hole-Transport-Material-free perovskite solar cells employing controllable electron-transport layer based on P25 nanoparticles, Electrochimica Acta 213 (2016) 83-88.

[72] S. Uchida and Y. Sanehira, Hydrothermal Synthesis of Titania Nanowire and Their Application for the Photo-Electro Functional Electrodes, Bulletin of The Society of Scientific Photography of Japan 69 (2006) 112-115.

[73] Y. Li, J. Hagen, W. Schaffrath, P. Otschik and D. Haarer, Titanium dioxide films for photovoltaic cells derived from a sol-gel process, Solar Energy Materials and Solar Cells 56 (1999) 167-174.

[74] A. Otavio, T. Patrocinio, E. B. Paniago, R. M. Paniago and N.Y. M. Iha, XPS characterization of sensitized n-TiO_2 thin films for dye-sensitized solar cell applications, Applied Surface Science 254 (2008) 1874-1879.

[75] S. Ngamisinlapasathian, T. Sreethawong, Y. Suzuki and S. Yoshikawa, Single- and double-layered mesoporous TiO_2/P25 TiO_2 electrode for dye-sensitized solar cell, Solar Energy Materials & Solar Cells 86 (2005) 269-282.

[76] K. G. U. Wijayahtha, L. M. Peter and L.C. Otley, Fabrication of CdS quantum dot sensitized solar cells via a pressing route, Solar Energy Materials & Solar Cells 83 (2004) 363-369.

[77] Shiseido, JP S47-42502.

[78] Pola Chemical, JP S49-450.

[79] J. Schulz, H. Hohenberg, F. Pflücker, E. Gärtner, T. Will, S. Pfeiffer, R. Wepf, V. Wendel, H. Gers-Barlag and K.-P. Wittern, Distribution of sunscreens on skin, Advanced Drug Delivery Reviews 54 Suppl. 1 (2002) S157-S163.

[80] J. Menneveux, F. Wang, S. Lu, X. Bai, V. Motto-Ros, N. Gilon, Y. Chen and J. Yu, Direct determination of Ti content in sunscreens with laser-induced breakdown spectroscopy: Line selection method for high TiO_2 nanoparticle concentration, Spectrochimica Acta Part B 109 (2015) 9-15.

[81] K. Suetsugu, Y. Yamada and H. Konishi, Preparation of Silica Gels Carrying Cinnamamido Group and Their Protectional Function from Ultraviolet Rays, The Chemical Society of Japan 1 (2000) 33-36.

[82]] K. M. Tyner, A. M. Wokvich, D. E. Godar, W. H. Doub and N. Sadrieh, The state of nano-sized titanium dioxide (TiO_2) may affect sunscreen performance, International Journal of Cosmetic Science 33 (2011) 234-244.

[83] H. Zhang, H. Yang, B. Shentu, S. Chen and M. Chen, Effect of titanium dioxide on the UV-C ageing behavior of silicone rubber, Journal of Applied Polymer Science 10 (2018) 46099-1-46099-7.

[84] Sorrento Engineering, US5,000,813.

[85] Dow Corning, US5,861,451.

[86] H. Miura, E. Isogai, H. Isogai, H. Wakizaka, I. Ueda and N. Ito, Clinical Application of Tooth Paste Containing Semi-conductor TiO_2 Powder – Its Relation to Cariogenic Bacteria -, Journal of Dental Health 39 (1989) 711-715.

[87] K. Iimura, H. Haruyama, H. Satone and M. Suzuki, Preparation of TiO_2 Porous Gel for the Application as Catalytic Support, J. Soc. Powder Technolo. Japan 54 (2017) 10-16.

[88] K. Ito, K. Satou, T. Tomino, M. Miyake, M.-aki. Ohshima, H. Kurokawa, K. Sugiyama and H. Miura, Sulfur-tolerance of Al_2O_3- and TiO_2- supported Bimetallic Pt-Pd Catalysts for Naphthalene Hydrogenation, Journal of the Japan Petroleum Institute 46 (2003) 315-321.

[89] EVONIK, AEROSIL® Fumed Silica and AEROXIDE® Fumed Metal Oxides for Toner, Technical Information TI1222 (2008) 1-20.

[90] Y. Amano, External Additive of Toner, The Imaging Society of Japan 47 (2008) 527-531.

[91] M. Saitoh, Properties and Applications of Ultrafine Ceramic Powders, Solids handling & processing industry Powder science & engineering 30 (1998) 35-40.

[92] H. Ishii, S. Matsumoto, Y. Matsui, Y. Terada, T. Tanabe, I. Uchiyama and J. Kawai, Individual particle analysis for the risk assessment induced by TiO_2 photocatalytic particles, Environmental Science 19 (2006) 209-216.

[93] M. Ema, N. Kobayashi, M. Naya, S. Hanai and J. Nakanishi, Genotoxicity Evaluation of Titanium Dioxide Nanoparticles, Jpn. J. Environ. Toxicol. 12 (2009) 71-84.

[94] T. Sato, Generation and Control of Active Oxygen Species by the UV irradiation on Semiconductor Particles, Annual Report of Cosmetology 14 (2006) 9-15.

[95] J. F. Porter, Y.-G. Li and C. K. Chan, The effect of calcination on the microstructural characteristics and Photoreactivity of Degussa P-25 TiO_2, J. Materials Sci. 34, (1999) 1523-1531.

[96] K J. A. Raj and B Viswanathan, Effect of surface area, pore volume and particle size of P25 titania on the phase transformation of anatase to rutile. Indian Journal of Chemistry 48A (2009) 1378-1382.

CHAPTER 2

THE SYNTHESIS OF A POROUS-TYPE OF FUMED TITANIUM DIOXIDE WITH RUTILE STRUCTURE

2.1 Introduction

There is a popularity to increase the rutile structure content for the fumed TiO_2 as described in Chapter 1. For the fumed TiO_2, some investigations about the additional thermal treatment are reported related to the morphologies as basic examinations. For examples, the particle size of the fumed TiO_2 (P25) is increased depended on the increase of the content of rutile structure by rising the thermal treatment temperature up to 1000 ℃ for 3 hours [1]. Around 100 % of the rutile structure contents are obtained by the additional thermal treatment at 900 ℃ for from 3 to 4 hours [2]. In both cases, drastic decreases of the surface area for the P25 were observed due to sintering of the P25. These investigations are applied by a normal calcination method with a muffle furnace for the thermal treatment. This traditional thermal treatment would be insufficient to synthesis the fumed TiO_2 maintaining the high dispersibility. It is necessary to preserve the sintering keeping the high dispersibility. The thermal treatment time is preferably as short as possible under conditions exceeding the temperature required for crystal transformation for the purpose.

As another thermal treatment with short calcination time, Ikuma et al., reported combination of the normal calcination and microwave heating for the anatase TiO_2 (not fumed TiO_2) and achieved the high rising rate of the temperature up 900 ℃ for around 1 minute. However, TiO_2 with 100 % of rutile structure did not get in this investigation probably due to the short calcination time [3].

As for sintering of TiO_2, Goto et al., investigated the relationship between sintering time and the primary particle size based on the calcination temperature and demonstrated the equation of the sintering time [4]. It is known that the crystal transformation is influenced by the primary particle size. Nano particle transforms lower temperature and faster time than the large ones. If the primary particle size downs enough to the nano-size, a possibility is considered that the crystal transformation proceeds faster than the sintering at the relative temperature by the optimization of the thermal treatment

conditions. It would be able to apply to P25 because it is very fine nanoparticle around 21 nm of the primary particle size.

Herein, in this chapter, we would like to report the new thermal treatment technology to synthesis the new fumed TiO_2 with high rutile structure content maintaining the high dispersibility due to preserving the sintering for the pure TiO_2.

The fumed TiO_2 is thermally treated by a natural dropping method from top to the bottom of the electrical furnace set up vertically to reduce the thermal treatment time and preserve the sintering by separating the agglomerated particle as far as possible. The crystalline morphology and dispersibility of the resulted thermally-treated TiO_2 are investigated.

The experimental results suggest that the newly thermally-treated fumed TiO_2 shows remarkable high rutile structure content maintaining the high dispersiblity due to containing many pores in the agglomerate, a sponge-like agglomerate. The thermal treatment conditions are investigated depended on the residence time during the heating unit in the electrical furnace as a function of agglomerate size.

2.2 Experimental Details

2.2.1 Materials and Preparation

As fumed TiO_2, commercially produced TiO_2 with different surface areas and primary particle sizes, (AEROXIDE® TiO_2 P 25: 50 m^2/g; 21 nm; (P25), AEROXIDE® TiO_2 P 90: 90 m^2/g; 14 nm; (P90) produced by Nippon AEROSIL Co., Ltd.) were used. An electric tubular furnace (OSK 55DB125B Ogawa Seiki Co., Ltd.) was vertically placed and equipped with 2 L glass conical beaker at the bottom with a wrapped opening by oven cloth to protect the upstream inserted air. The length of a core tube and a heating unit were 1,200 mm and 600 mm respectively. A sample of the fumed TiO_2 was directly dropped from top of the furnace to the bottom by a natural dropping method without a sieve or through several mesh sizes of sieves (0.5 mm, 1.0 mm, 1.4 mm and 2.8 mm) fixed on the top of the electric furnace. The sieve was vibrated by a vibration device (THRIVE Handy Vibe MD-01 Daito Electric Machine Industry Co., Ltd.). The electric furnace was heated at several temperatures from 800 ℃ to 1450 ℃ under air atmosphere. Without the oven cloth wrapped opening, doing the thermal treatment was impossible because the fumed TiO_2 bursts from the sieve following the inserted air

upstream by the very light bulk density. The thermal treatment time was observed by checking the dropping time of the fumed TiO_2 from the top to the bottom by visual inspection. A schematic outline of experimental apparatus for thermal treatment is illustrated in Fig. 2-1.
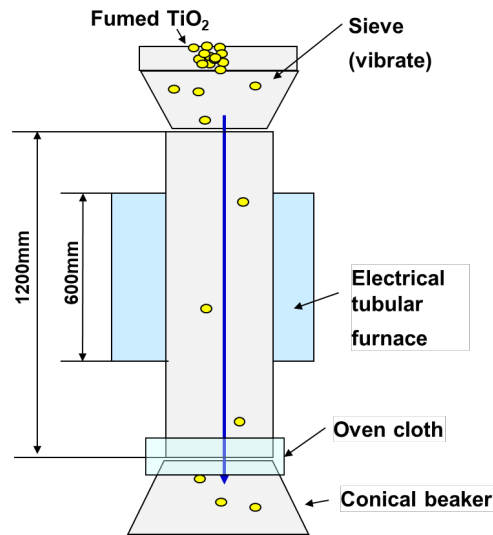
Fig. 2-1. Outline of the thermal treatment method

2.2.2 Characterization

The crystalline phases were analyzed by an X-ray diffractometer (XRD-6100 Shimazu Corp.) using Cu-Kα radiation to identify the content of the rutile and the anatase structure of the thermally-treated fumed TiO_2. The content of the rutile (f rutile) structure was calculated by using the following equation (2-1) [5].

$$f \text{ rutile} = 1 - f \text{ anatase} ;$$
$$f \text{ anatase} = 1/ (1 + 1.26 (I \text{ rutile} /I \text{ anatase})) \tag{2-1}$$

I rutile, I anatase: XRD peak intensity of rutile (110) and anatase (101) structure

The average crystal size of the fumed TiO_2 (D in nanometers) can be estimated by Scherrer's equation (2-2).

$$D = 0.89*\lambda / B (2\theta)*\cos\theta \tag{2-2}$$

λ: X-ray wavelength (nanometer),

B (2θ): width of the XRD peak at half-peak height in radians,

θ: angle of diffracted peak in degrees.

The particle size distribution was measured by a MT3300EX2 from the MicrotracBEL Corp. The surface area was measured by the BET technique (Macsorb HM-1200S Mountech Co., Ltd.) using the one-point measurement method with nitrogen as an absorbent [6]. For the sedimentation test, 0.5 wt.% of a TiO_2 water dispersion was prepared by an ultrasonic homogenizer (US-300CCVP Nihon Seiki Kaisha, Ltd.,) at 300 W for 5 minutes. The resulting dispersion was poured into a 15 ml sedimentation tube graduated on the outside of the wall. One ml of the dispersion was taken from the 8-ml point of the sedimentation tube and the absorbance of the water dispersion was measured by a spectrophotometer (V-670 JASCO Corp.) at a 700 nm light wavelength. The appearance of the water dispersion in the sedimentation tube was also visually observed. The water vapor adsorption-desorption isotherms were measured by a BELSOP-max (MicrotracBEL Corp.). The nanostructure and morphology were observed by a transmission electron microscope (TEM, JEM-1010 JEOL Ltd.).

2.3 Results and Discussion
2.3.1 Conversion Ratio from Anatase to Rutile Structure
Table 2-1 summarizes the results of the thermal treatment of P25 at 1450 ℃ without the sieve and through the 0.5 mm mesh sieve. The thermal treatment time was observed at less than 1 second in the case of without the sieve. The original P25 before the thermal treatment has 16% of the content of rutile structure. After the thermal treatment at 1450 ℃ without the sieve, P25 showed a very slight change of the content of the rutile structure; from 16 % to 18 %. However, just by passing the P25 through the 0.5 mm mesh sieve, a drastic increase in the content of the rutile structure was observed. The rutile content is reached 94 %. The surface area decreased with around 1/5 (9 m^2/g) against before the thermal treatment.

Table 2-1 Rutile ratio and S.BET of the thermally-treated P25

Temperature (℃)	Mesh size of sieve (μm)	Rutile ratio (%)	S_{BET} (m²/g)
Room temperature	-	16	51
1450	-	18	49
1450	500	94	9

Fig. 2-2 shows the X-ray diffraction (XRD) peaks of the anatase (101) and rutile (110) for the P25 treated at several temperatures through the 0.5 mm mesh sieve. The XRD data indicates that the content from anatase to rutile (%) was significantly affected by the temperature rise. The anatase gradually decreased depending on the increase in the thermal treatment temperature and the content of rutile (%) increased relative to the decrease of anatase.
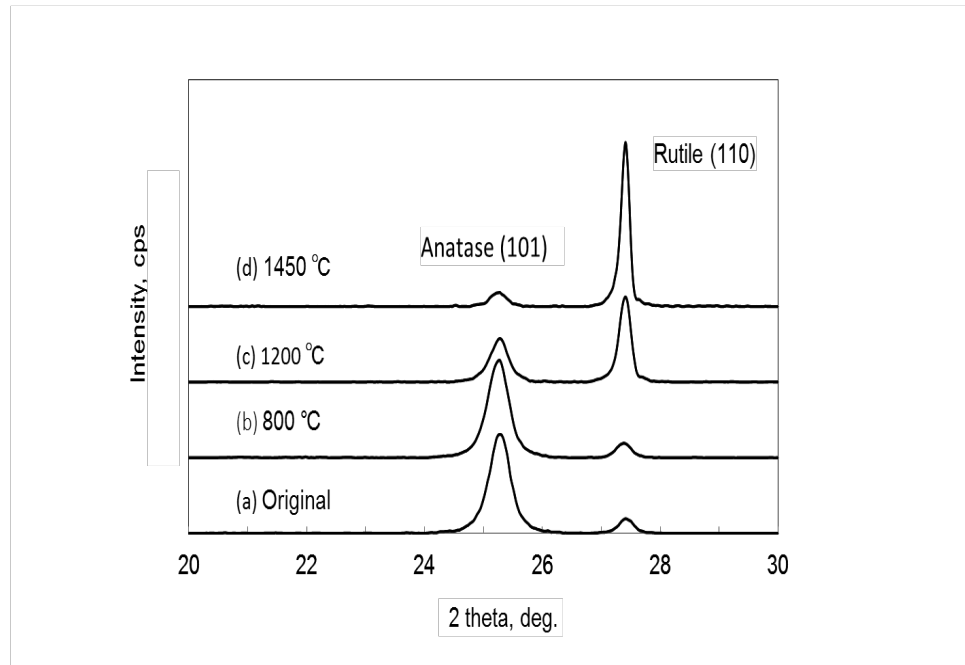
Fig. 2-2. XRD patterns of the thermally-treated P25

Fig. 2-3 confirms the content of the rutile structure for P25 at several temperatures from 800 ℃ to 1450 ℃ through the 0.5 mm mesh sieve. It was observed the content of the rutile structure was increased liminary related to the increase of the thermal treatment temperature.
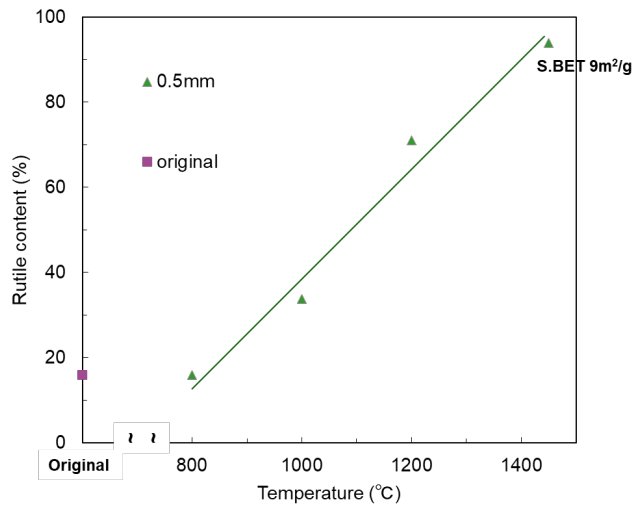
Fig. 2-3. Rutile conversion ratio of the thermally-treated P25

2.3.2 Dispersibility

The particle size distribution of the thermally-treated P25 at 1450 ℃ through the 0.5 mm mesh sieve was measured and compared to the other types (Chloride process) of TiO_2 (CR-EL (7 m^2/g) Ishihara Sangyo Co. Ltd.,) with the rutile structure and similar surface area as a reference. The results of the original P25 before the thermal treatment is also measured. Fig. 2-4 confirms the particle size distribution, (a) without ultrasonic irradiation and (b) ultrasonic irradiation at 40 W for 3 minutes. Without ultrasonic irradiation in Fig. 2-4 (a), the main peak of the thermally-treated P25 appears around 200 μm and it indicates very wide range from 1μm to 1000 μm. The main peak of CR-EL appears around 1.8 μm with a narrower particle size distribution than the thermally-treated P25. As the ultrasonic irradiation at 40 W for 3 minutes as shown in Fig. 2-4 (b), the main peak of the thermally-treated P25 shifts to a lower range. However, it still shows a larger particle size than CR-EL. The particle sized distribution of CR-EL was very similar to the original P25. These results indicate that the thermally-treated P25 demonstrates a quite larger particle size and broader particle size distribution than that of both CR-EL and original P25.

(a) Without ultrasonic irradiation   (b) Ultrasonic irradiation 40W 3 minutes
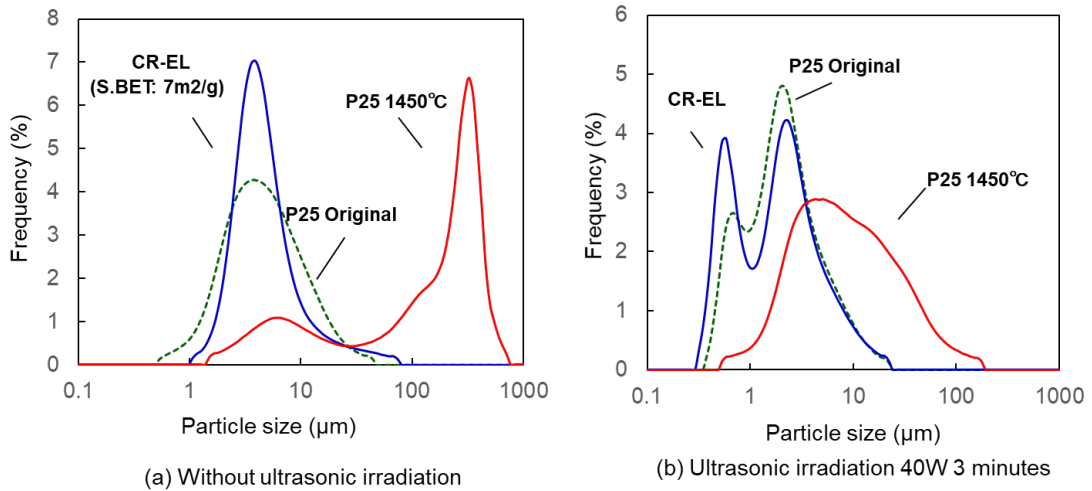
Fig. 2-4. Particle sized distribution of the thermally-treated P25

The absorbance measurement of the water dispersion is an effective method for the evaluation of the dispersibility of the powders in media [7]. Fig. 2-5 indicates the relationships between the absorbance of water dispersion and storage time for the thermally-treated P25 at 1450 ℃ comparing with original P25 and CR-EL. The original P25 shows highly stable absorbance values and the values are not downed at 50 hours storage time. Comparatively, the thermally-treated P25 has a higher absorbance than CR-EL from just after forming the dispersion up to 50 hours storage even though the values were lower than original P25. This absorbance value is directly related to the transparency of the water dispersion. These results suggest that the thermally-treated P25 has a slower sedimentation velocity and higher dispersibility in the water dispersion than CR-EL although it displays larger particle size distribution than CR-EL.
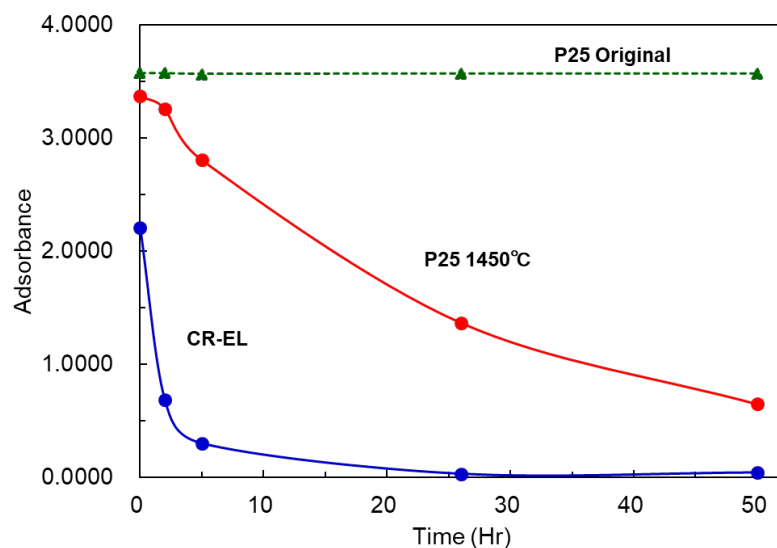
Fig. 2-5. Absorbance of the thermally-treated P25 at 1450 ℃

The photos of the dispersion for the original P25, the thermally-treated P25 and CR-EL in the sedimentation test at 7 hours and 50 hours storage are illustrated in Fig. 2-6. It is confirmed that the water dispersion of original P25 shows a turbid color with a low transparency during 50 hours of storage by visual inspection. On the other hand, the water dispersion of CR-EL became clear from the middle to top of the sedimentation tube for less than 7 hours storage. Obviously, the particles of CR-EL are easily precipitated. The thermally-treated P25 at 1450 ℃ demonstrated a slightly light turbid color compared with original P25.
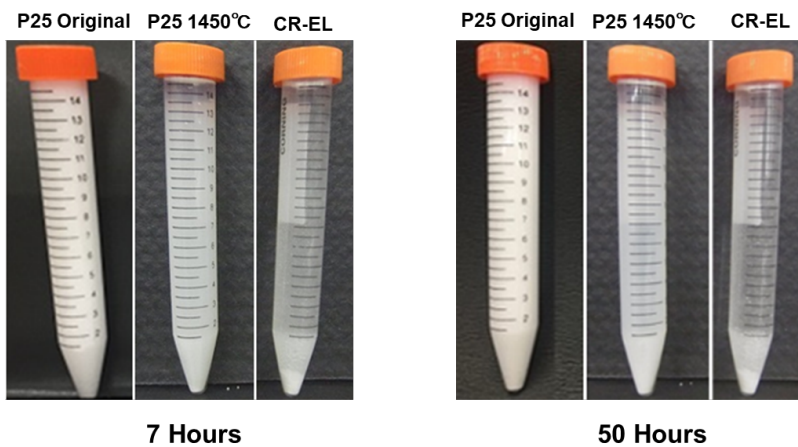
Fig. 2-6. Photos of TiO$_2$ dispersion in water for the sedimentation test

For estimation of the sedimentation velocity, the Stokes's equation was used. By applying the 1 μm diameter for CR-EL particles measured by the particle size distribution shown in Fig. 2-4 (b), to the Stokes's equation, a 0.56 cm/hour sedimentation velocity was obtained. This result shows a relatively good consistency with the result of the sedimentation test for CR-EL.

Comparatively, for the thermally-treated P25 at 1450 ℃, by applying a 2 μm diameter shown in Fig. 2-4 (b), a 2.2 cm/hour sedimentation velocity was obtained.

This calculation result is quite different from the current sedimentation result, and in fact, a totally opposite result. From the Stokes's equation, not only the particle size, but also the particle density influenced on the sedimentation velocity. This difference suggested that the thermally-treated P25 has a much lower powder density with larger average particle size than CR-EL. The thermally-treated P25 would contain many pores in the agglomerate.

2.3.3 The Nanostructure and Morphology

It is well known that vapor adsoption-desoprtion isotherm is an effective method for characterizing the nanostructure and morphology of porous particles. Water vapor is selected as the measurement vapor of it because it can detect micro pores based on smaller molecular size than nitrogen [8]. For the fine powders produced by the fumed process, water vapor was applied to characterize nanostructure of both the original core particles and surface modified ones [9-11].

Fig. 2-7 shows the water adsorption-desorption isotherms for the thermally-treated P25 at 1450 ℃. The original P25 without the thermal treatment exhibits a type-II isotherm according to the BDDT classification. This result is different from the result of the fumed silica, which shows a type-III isotherm [12], although both oxides are produced by the same fumed process. However, the thermally-treated P25 at 1450 ℃ exhibits a different type pf isotherm, i. e., a type-IV isotherm with hysteresis loops, under the higher pressure range from 0.5 to 0.9.

(a) P25 without thermal treatment   (b) Thermally-treated P25 at 1450℃
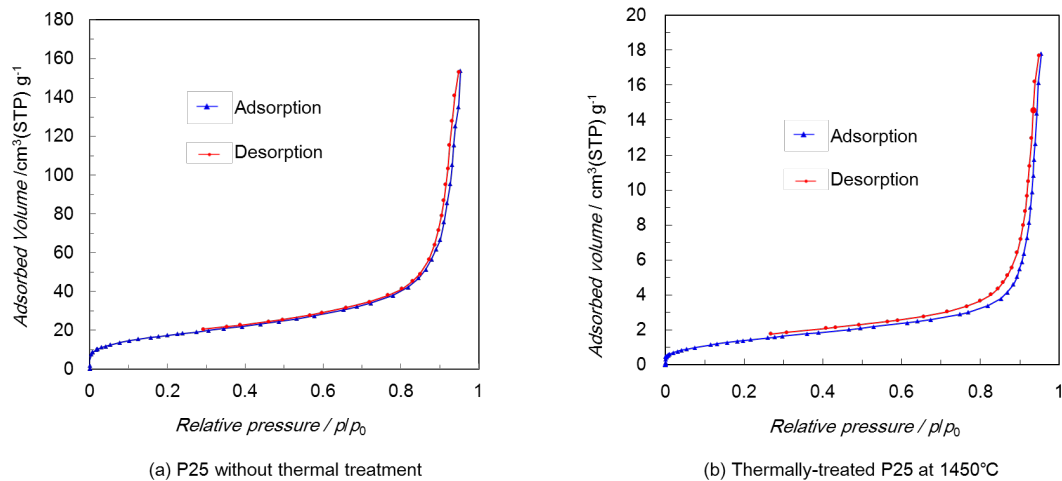
Fig. 2-7. Adsorption / desorption curves of the thermally-treated P25

It is known that the hysteresis loop in this range is due to mesopores. The thermally-treated P25 at 1450 ℃ confirms this hysteresis although the original P25 does not show it. This result indicates that the thermally-treated P25 contains many pores made by closing the open pores by partial sintering between the particles. Some pores made by small particles act like pseudo-mesopores. Based on this characterization, the thermally-treated P25 acts like a pseudo-large particle during the measurement of the particle size distribution. It is a low densified particle and shows a low sedimentation velocity in the water dispersion. Additionally, water would be able to enter some of the large pores by strong ultrasonic irradiation when it was dispersed in the water.

The crystal size of the original P25 was estimated to be around 20 nm from the anatase (101) and 26 nm from rutile (110) diffraction peaks. On the other hand, the crystal size of the thermally-treated P25 at 1450 ℃ was estimated to be around 20 nm from anatase (101) and 32 nm from the rutile (110) diffraction peaks.

Fig. 2-8 illustrates the image scheme of the porous-type of morphology for the thermally-treated fumed TiO_2. Thermally-treated P25 with 94 % of the rutile structure contents contains two type of pores in the agglomerate; a normal type of pore and a small type of pore. The normal type of pore is made by closing of the open spaces of pores in P25 agglomerate with the connection of normal and large sized of particles by the partial sintering. On the other hand, small type of pore is made by closing of the

open pores among small particles by the partial sintering. These small pores act like pseudo-mesoporous type of phenomena. Thermally-treated P25 also exhibits pseudo-large particles in the particle size distribution measurement. Each particle is connected partially and make large particles in appearance containing many porous.
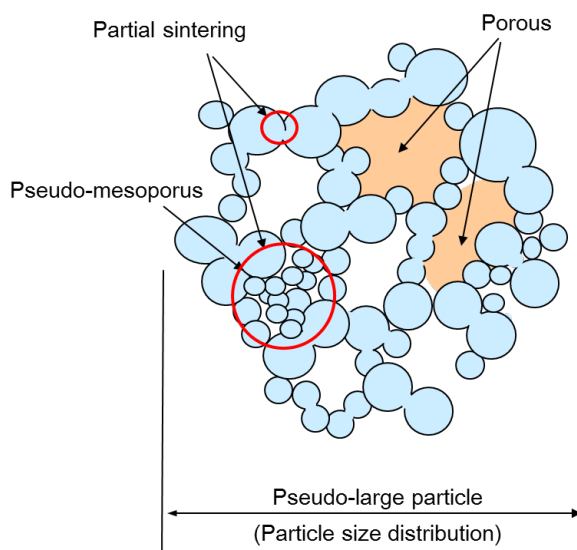
Fig. 2-8. Image of agglomerate for the thermally-treated fumed TiO_2 (P25)

The transmission electron microscope images of the thermally-treated P25 at 1450 °C are shown in Fig. 2-9. The connections of each particle by partial sintering and grain growth are observed in the agglomerate and they formed many pores in the agglomerate. These results support the formation of a porous-type of fumed TiO_2.

There are several studies related to the porous or mesoporous TiO_2. Some of them are related to the photocatalytic activity of the TiO_2 coating made by the sol-gel process [13-14]. The porous-type of morphology in this study is different from these previous studies.
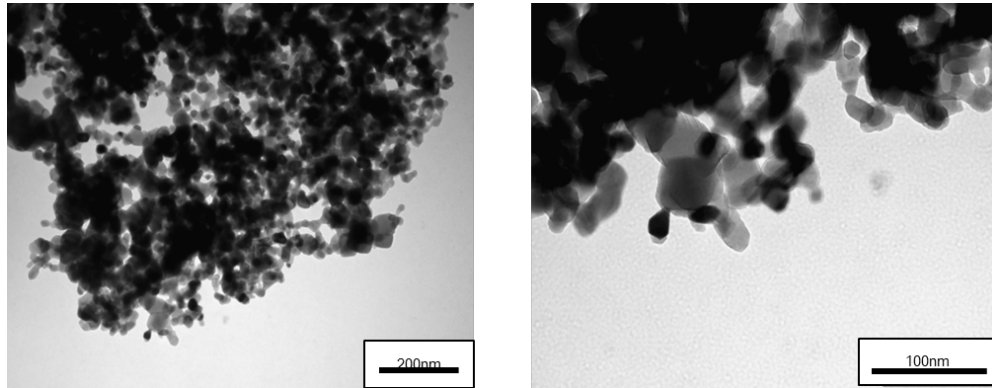
Fig. 2-9. TEM images of thermally-treated P25 at 1450 ℃

2.3.4 Thermal Treatment Conditions

Fig. 2-10 confirms the content of the rutile structure of P25 treated at several temperatures from 800 ℃ to 1450 ℃ using the 0.5 mm, 1.0 mm and 1.4 mm mesh sieve.

The same contents of the rutile structure; 94 %, were obtained by passing through 0.5 mm and 1.0 mm mesh sieves at 1450 ℃. Comparatively, the content of the rutile structure was stayed at 73 % with the 1.4 mm sieve.
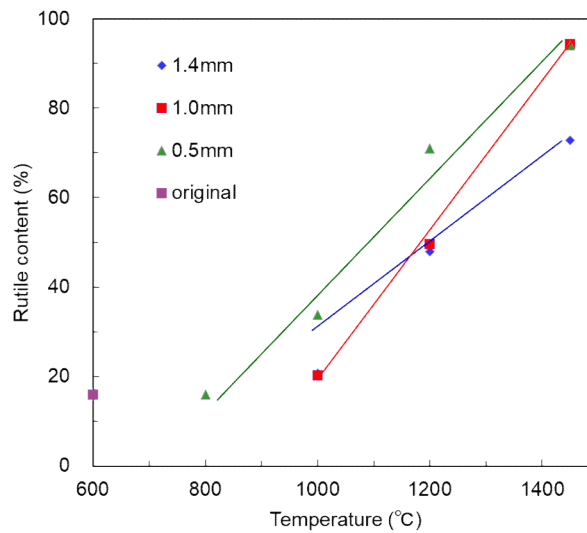
Fig. 2-10. Rutile conversion ratio of P25

For estimation of the residence time of the particle in the heating unit of the electrical furnace (600 mm), the terminal velocity of the Stokes's equation (2-3) was applied based on the bulk density of P25, particle size and the related media temperature (air). The particle diameter is assumed to the same size as the mesh size of the sieve. The residence time is calculated by the terminal velocity from the length of the heating unit.

$$v = \left[\frac{\rho_s \, g}{9} \sqrt{\frac{2r^3}{\rho\mu}} \right]^{2/3} \qquad (2\text{-}3)$$

v: terminal velocity, ρ: density of media (air) g: gravitational constant

r: diameter of particle   ρ: density of media   μ:viscosity coefficient of media (air)

The relationship between rutile structure content and particle residence time at 1450 ℃ is appeared in Fig. 2-11 with the result of 2.8 mm mesh sieve and the image of the agglomerate. From 0.00 to 0.48 seconds of residence time, the rutile structure content is increased related to the increase of the residence time. After 0.48 seconds, the rutile structure contents sustained at 94% up to around 1.00 seconds. This result suggests that the crystal transformation from the anatase to the rutile structure of P25 is mainly proceeded before 0.48 seconds and after 0.48 seconds the applying heat energy is not mainly used to the transformation but sintering or grain growth.
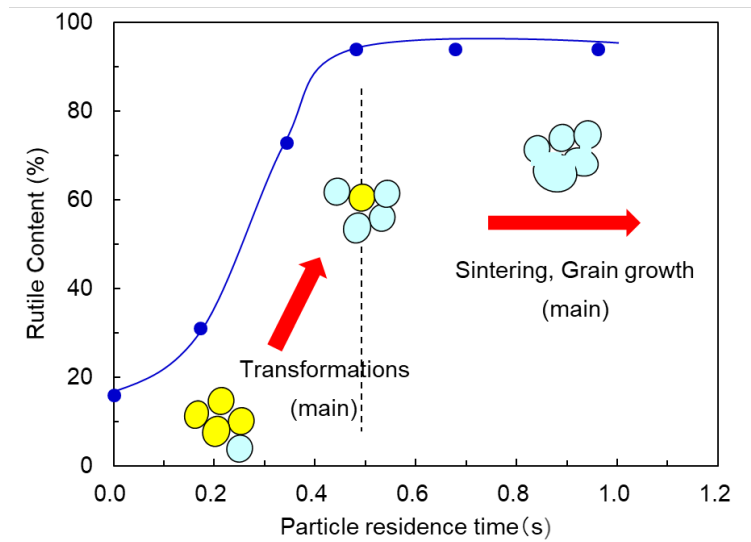
Fig. 2-11. Illustration of thermal treatment based on particle residence time

The temperature of the P25 agglomerate is estimated by using the unsteady heat transfer equation (2-4) by assuming that the agglomerate particle is a spherical shape based on the quantity of heat calculated by heat capacity of TiO_2 under the related temperature.

$$T_0^{P+1} = 6\Theta_r T_1^P + (1-6\Theta_r) T_0^P \qquad \Theta_r = \alpha\Delta t/(\Delta r)^2 \qquad (2\text{-}4)$$

P: time   T: temperature   r: radial coordinates   α: thermal diffusivity

The applied heat energy is also estimated by the rise of temperature. The results are shown in Fig. 2-12 with related to the residence time.
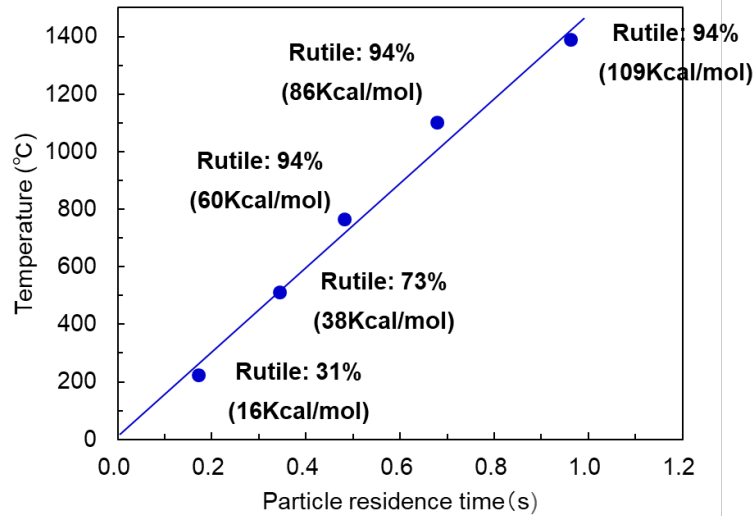
Fig. 2-12. Estimated applied energy for the thermal treatment

These results also demonstrate that the applied heat energy to P25 after 0.48 seconds of the residence time is not used effectively for the crystal transformation. Even though, the residence time arrived at around 1.00 seconds, the rutile structure content remained to the same level as 0.48 seconds. It is probably caused from the deviations of agglomerate density or re-agglomerate of P25. The residence time of P25 is calculated by using the bulk density of P25. When some small agglomerates have higher bulk densities than that of whole original P25 agglomerate, the terminal velocity of the small agglomerates become higher than the normal ones and the residence times also become shorter than the ones. Additionally, P25 has very easy re-agglomerated property. After through the sieve, when P25 re-agglomerates and makes large agglomerate, the terminal velocity becomes fast and the residence time also becomes short.

Before the thermal treatment, original P25 was classified by using the sieve with 0.3 mm mesh size to make more smaller agglomerate than the original P25. Next, the obtained P25 with small agglomerate was thermally treated at 1400 ℃ by passing through 0.5 mm mesh sieve equipped top on the electrical furnace. It was difficult to carried out the natural dropping thermal treatment by using 0.3 mm mesh sieve set top on the electrical furnace due to very less quantity of obtained thermally-treated P25 by the upstream. The yield of the classification of original P25 under 0.3 mm sieve was 30 wt.% and the thermal treatment through 0.5 mm sieve was 60 wt.%. The total yield was

18 wt.% for this method. The surface area of the thermally-treated P25 at 1400 ℃ was 3 m^2/g.

The rutile conversion rate is shown in Table 2-2. A 100 % of rutile structure conversion ratio was obtained. The residence time in the electrical furnace is estimated at 1.60 seconds by the assumption of the agglomerate diameter to 0.3 mm. This result suggests that the rutile structure conversion ratio is increased by making small agglomerate although the sintering is also proceeded by the prolonging the thermal treatment time.

Table 2-2 Classification of P25 before thermal treatment

Before thermal treatment (Classification)	After thermal treatment (Sieve: 0.5 mm)		
Mesh size of sieve (mm)	Temperature (℃)	Rutile ratio (%)	Estimated residence time (s)
Under 0.3	1400	100	1.60

It seems that one of main reasons of the remaining rutile structure contents at 94 % for the thermally-treated P25 is probably cased from the deviation of the density for small agglomerates in original P25. The residence time of P25 was estimated 0.96 seconds at 1450 ℃ under 0.5 mm sieve based on the bulk density of the P25 by 0.1 Kg/L.

It was confirmed that the bulk density of the P25 is increased by the addition of high mechanical share to P25 agglomerate destroying the 3D network structure. For an example, 5 times higher bulk density of the P25 (0.5 Kg/L) was easily obtained by 10 minutes of the ball milling process. This result suggests a possibility that the small agglomerate in P25 would have higher density than whole P25 agglomerate. By the estimation of slightly higher agglomerate density than the bulk density of P25; i. e., 0.3 Kg/L, the residence time is calculated to 0.46 seconds with 0.5 mm mesh sieve. This value seems to be short to complete the crystal transformation. Comparatively, By the estimation of the agglomerate size to 0.3 mm with the same bulk density; 0.3 Kg/L, the residence time is calculated to 0.77 seconds. This time is satisfied the transformation time.

The quantity of densified small agglomerates is assumed to around 6 % for the P25 because of the saturation of rutile structure content at 94 %. Fig. 2-13 illustrates the image of this assumption.
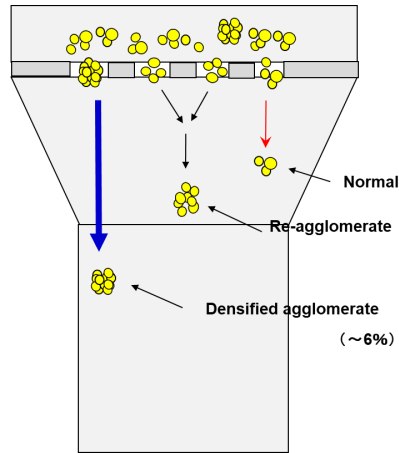
Fig. 2-13. Illustration of the thermal treatment through the sieve

As another fumed TiO_2; P90 with smaller primary particle size than P25 was thermally treated by the same temperatures and the same sizes of the mesh sieves as P25. The rutile conversion ratio is demonstrated in Fig. 2-14.
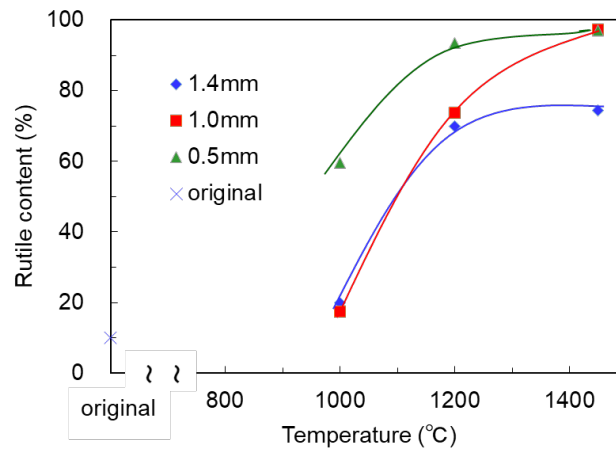
Fig. 2-14. Rutile conversion rate of P90

The contents of the rutile structure maintained 74 % at 1.4 mm sieve and 97 % at both 1.0 mm and 0.5 mm mesh of sieve. These results suggest that the P90 probably has around 3 % of densified small agglomerates. The surface area of the thermally-treated P90 at 1450 ℃ passing 0.5 mm sieve was 2 m^2/g. Obviously, sintering of P90 occurred. The small primary particle size of P90 results the easily sintering.

2.4 Conclusions

In summary, the fumed TiO_2 powder with a high content of rutile (P25: 94 %, P90: 97 %) were synthesized by the novel thermal treatment by passing sieve from 0.5 to 1.0 mm sieve at 1450 ℃. The thermally-treated TiO_2 (P25) keeps the high dispersibility in the water dispersion with many pores in the agglomerated. The high dispersibility is caused from closed open pores by partial sintering of the particles of the agglomerate. It makes the porous-type of morphology with a sponge-like agglomerate.

The conversion rate of the rutile structure is highly depended on the residence time passing the heating unit in the electrical furnace. The crystal transformation from anatase to rutile structure is mainly finished at around 0.48 seconds at 1450 ℃ and other residence time would be used mainly not the crystal transformation but the sintering. The remained rutile structure contents at 94 % for the thermally-treated P25 is probably cased from the deviation of densified small agglomerates in P25. The same tendency to P25 is observed to another fumed TiO_2, P90 with smaller primary particle size than P25. P90 performed easily sintering with the small primary particle size.

References

[1] J. F. Porter, Y.-G. Li and C. K. Chan, The effect of calcination on the microstructural characteristics and photoreactivity of Degussa P-25 TiO_2, J. Materials Sci. 34 (1999) 1523-1531.
[2] K J. A. Raj and B Viswanathan, Effect of surface area, pore volume and particle size of P25 titania on the phase transformation of anatase to rutile, Indian Journal of Chemistry 48A (2009) 1378-1382.
[3] Y. Ikuma and T. Shigemura, Rapid-Rate Sintering of Anatase-Type TiO_2 by Microwave Heating, Journal of the Ceramic Society of Japan 101 (1993) 900-904.
[4] M. Goto, S. Takahashi, K. Hamaguchi, T. Ihara and K. Wakai, Surface Modification by Oxide Particles Spray Burner, Journal of the Combustion Society of Japan 55 (2013) 73-80.

[5] R. A. Spurr, H. Myers, Quantitative Analysis of Anatase-Rutile Mixtures with an X-ray Diffractometer, Analytical Chemistry 29 (1957) 760-762.

[6] Determination of the specific surface area of powders (solids by gas adsorption-BET method, JIS Z8830 (2013) 1-24.

[7] Y. Mitani, T. Teshima, Y. Yoshida and N. Yamazoe, Dispersibility of Fumed Silica in Simple Media, J. Ceramic Society of Japan 101 (1993) 707-712.

[8] H. Naono, Characterization of Powder by Adsorption of Nitrogen Gas and Water Vapor, J. Powder Tech. Soc. Jpn. 28 (1991) 34-39.

[9] M. Fuji, H. Iwata, T. Takei, T. Watanabe and M. Chikazawa, The change in the water vapor affinity of fine silica particles loaded with trimethylsilyl groups, Advanced Powder Technol. 8 (1997) 325-334.

[10] M. Fuji, H. Iwata, T. Takei, T. Watanabe and M. Chikazawa, The Change in Wettability and Structure of Silica Powder Surfaces Modified with Hexamethyldisilazane, J. Soc. Powder Technol., Japan 33 (1996) 740-746.

[11] M. Fuji, H. Iwata, T. Takei, T. Watanabe and M. Chikazawa, The Change in the Water Vapor Affinity of Fine Particles Loaded with Trimethylsilyl Group, J. Soc. Powder Technol., Japan, 32 (1995) 649-654.

[12] M. Fuji, M. Araki, T. Takei, T. Watanabe and M. Chikazawa, Structure and Wettability of Various Silica Surfaces – Evaluation in Nano and Macro Levels -, J. Soc. Powder Technol., Japan, 36 (1999) 528-533.

[13] J. Yu, X. Zhao, J. Du and W. Chen. Preparation, Microstructure and Photocatalytic Activity of the Porous TiO_2 Anatase Coating by Sol-Gel Processing, J. Sol-gel Science and Technol. 17 (2000) 163-171.

[14] M. Zhou, J. Yu, B. Cheng and H. Yu, Preparation and photocatalytic activity of Fe-doped mesoporous titanium dioxide nanocrystalline photocatalysts, Materials Chemistry and Physics 93 (2005) 159-163.

CHAPTER 3

DEVELOPMENT OF FUMED TITANIUM DIOXIDE HAVING HIGH CONTENT OF RUTILE STRUCTURE AND DISPERSIBILITY USING A DRY-TYPE OF SURFACE MODIFICATION AND THERMAL TREATMENT

3.1 Introduction

The high rutile structure contents of the fumed TiO_2 (94 % for P25 and 97 % for P90) were obtained as shown in Chapter 2. However, these rutile structure contents insufficient for the practical use because 100 % of the rutile structure content is required by the cosmetic application. It is also confirmed that the conversion ratio of the rutile structure from anatase structure to rutile structure is highly depended on the size and density of agglomerate for the pure fume TiO_2. These results suggest that it has a possibility to increase in the content of the rutile structure or decrease with the transformation temperature by using a small agglomerate and preserving the densification of the small agglomerate. Low temperature is preferred to preserve the sintering. However, it is also difficult to complete the natural dropping thermal treatment by using under 0.5 mm size sieve treatment due to the upstream.

This means that the application of smaller agglomerate less than 0.5 mm size is difficult for the natural dropping thermal treatment. Additionally, the fumed TiO_2 has quite re-agglomerated property. It easily and quickly re-agglomerates during storage even though under room temperature.

Regarding the dispersibility, the thermally-treated P25 showed higher dispersibility than Chloride type of TiO_2; CR-EL although it is not achieved to the same level of dispersibility for the original P25. By these reasons, further investigations of the transformation to 100% of the rutile structure and to increase the dispersibility with the same level of original P25 are necessary by controlling the agglomerate of the fumed TiO_2.

There are several studies to control the morphologies of the fumed TiO_2 (P25) with the combination of other materials, i.e., mixing with SiO_2 particle [1-2], surface

modification with various materials and alkylalkoxysilanes [3-12], pheylphosphnic acid [13] and alumina coating [14]. Especially, it is reported that SiO_2 coated TiO_2 shows high dispersibility by the static electricity repellence of the SiO_2 coated layer [15-16]. These investigations always apply a wet-type process for the surface modification. It has an advantage to modify the fumed TiO_2 uniformly. On the other hand, the wet-type process needs multiple steps such as preparation of fumed TiO_2 dispersion, adjustment of pH of the dispersion, filtration or centrifugation, washing, drying and next heating. By these processes, normally the resulted fumed TiO_2 loses the high dispersibility due to a coagulation during the drying process. This is a weak point of the wet-process to apply to fumed TiO_2.

Regarding the surface modification, a dry-type surface modification is applied to the fumed oxide to give unique functions [17-18]. The dry-type surface modification is consisted from simply only two processes, mixing and heating. This dry-type surface modification process has mainly big two advantages. One is a maintaining the high dispersibility of the fumed oxides due to no use of the solvent. Another is a very simple production process. However, it also has a disadvantage, the necessity of a large volume heating reactor to complete the reaction due to low bulk density of the fumed oxides.

In this study, the fumed TiO_2 is modified with mainly silicone alkoxides to achieve high dispersiblity after thermal treatment to give the static electricity repellence of the SiO_2 coated layer. Titanium alkoxide is also applied as the surface modifier comparing to the effectiveness of the silicone alkoxides. For the surface modification process, the dry-type surface modification without the heating is tried to produce a precursor avoiding the large heating unit. The effectiveness of the species of the metallic alkoxides; silicone alkoxide and titanium alkoxide, as a surface modification agent is examined for the acceleration of the crystalline transformation and maintaining the high dispersibility.

Herein, in this chapter, we mainly demonstrate two investigations. One is a possibility of the dry-type surface modification of the fumed TiO_2 with the metallic alkoxides; silicone alkoxide and titanium alkoxide, without heating to synthesis the preferable precursor for the crystalline transformation. Another is the morphology examination of the resulted thermally-treated fumed TiO_2 with 100 % of the rutile structure content.

Especially, we focused on the dispersibility of the new fumed TiO_2 with 100 % of the rutile structure content.

3.2 Experimental Details

3.2.1 Materials

As fumed TiO_2, commercially produced TiO_2 (AEROXIDE® TiO_2 P 25: 50 m^2/g; 21 nm; (P25), produced by Nippon AEROSIL Co., Ltd.) was used. As silicone alkoxides, Silicon tetraethoxide $(Si(C_2H_5O)_4)$: (TEOS), 3--aminopropyltriethoxysilane $(H_2N(CH_2)_3Si(OC_2H_5)_3)$: (APTES): Shin-Etsu. Co. Ltd., and Octyltrimethoxysilane $(C_8H_{17}Si(OCH_3)_3)$: (OCTMO): EVONIK GmbH) were used. As a titanium alkoxide, Titanium tetra-isopropoxide $(Ti(i-C_3H_7O)_4)$: (TTIP), Sigma-Aldrich: CP grade: Merck Co. Ltd) was used, Ammonium hydroxide and ethanol were provided by reagent grades (Kanto Chemical Co., Inc.) for the wet-type of the surface modification.

3.2.2 Preparation of The Surface Modified Fumed TiO_2 with Metallic Alkoxides (Precursors)

For the preparation of surface modification of P25 with metallic alkoxides (precursor), the dry-type surface modification was performed without heating at room temperature (A). Another dry-type surface modification with heating (B) and a wet-type surface modification (C) were also carried out as a comparison of the dry-types surface modification.

(A): Dry-type surface modification without heating at room temperature: Specified quantities of TEOS, TTIP and APTES were added from the top of a mixer (VA-W27 Hitachi, Ltd.) in small portions of the droplet stirring with P25 (20.0 g) over 60 seconds individually. After finishing the addition, the mixed powder was stirred two times at 30 seconds intervals. The mixed powder was stored at room temperature under air atmosphere until the next thermal treatment.

(B): Dry-type surface modification with heating: OCTOMO (1.6 g) and P25 (20.0 g) were mixed with the same procedure described in (A). After the mixing, the mixed powder was transferred to 2 L glass flask and heated at 180 ℃ for 2 hours under nitrogen stream with mechanical stirring.

(C): Wet-type surface modification with heating: P25 (20.0 g) and ammonium hydroxide (25 wt.% aq. 7.0 g) were dispersed in a mixture of deionized distilled water (150 ml) and ethanol (400 ml) via Homomixer (PRIMIX Corp.) at 1400 rpm for 3 minutes. Next, the mixture was dispersed via an ultrasonic homogenizer (US-300CCVP Nihon Seiki Kaisha, Ltd.,) at 300 W for 5 minutes. A solution of TEOS (1.5 g) dissolved in ethanol (10 ml) was added to the dispersion during magnetically stirring. The dispersion was then continued by stirring in a dark environment at room temperature for 18 hours. Then the dispersion was filtrated and resultant silica-coated P25 was washed several times with deionized distilled water and several times ethanol individually. The silica coated P25 was next dried at 105 °C for 50 hours and finally pulverized using an agate mortar.

Sample coding for all used and prepared conditions are listed in Table 3-1. The weight percentage of the metal oxide in Table 3-1 is calculated from the added quantity of the metallic alkoxides converting to corresponding metal oxides.

Table 3-1 Sample cording of the surface modified P25 with metallic alkoxides (precursors)

No.	Sample coding	Description of sample preparation [*1]
1	P25 Original	P25 without the surface modification
2	TE(2)	P25 modified with TEOS (SiO_2: 2wt%) Dry-type without heating at room temperature
3	TE(5)	P25 modified with TEOS (SiO_2: 5wt%) Dry-type without heating at room temperature
4	TT(2)	P25 modified with TTIP (TiO_2: 2wt%) Dry-type without heating at room temperature
5	TT(5)	P25 modified with TTIP (TiO_2: 5wt%) Dry-type without heating at room temperature
6	AP(5)	P25 modified with APTES (SiO_2: 5wt%) Dry-type without heating at room temperature
7	OC(2)	P25 modified with OCTMO (SiO_2: 2wt%) Dry-type with heating at 180°C for 2 hours
8	W-TE(2)	P25 modified with TEOS (SiO_2: 2wt%) Wet-type with heating at 105°C for 50 hours

*1) The weight percentage of metal oxide is calculated from the addition quantity of the metallic alkoxide converted   corresponding metal oxide.

3.2.3 Thermal Treatment of The Surface Modified Fumed TiO₂ with Metallic Alkoxides (Precursors)

The same thermal treatment was carried out with the same conditions of the electric tubular furnace described in Chapter 2.2.1. The electric furnace was heated at several

different temperatures from 1000 ℃ to 1400 ℃. The electric tubular furnace maker, Ogawa Seiki Co., Ltd. recommend us to use 1400 ℃ as the maximum temperature due to exhaustion of a heating element of the furnace. The precursors produced by the same procedure in Chapter 3.2.2 were then directly dropped from top of the furnace to the bottom through a 0.71 mm sieve fixed to the top of the electric furnace under vibration. In the previous examination described in Chapter 2, it was confirmed that the less different of rutile conversion ratio between 0.5 mm and 1.0 mm sieve. When using 0.5 mm sieve, powder blowing from the sieve flowing air upstream was severe and dust problem of the operation environment occurred. Additionally, the yields were low. By this reason, 0.71 mm sieve was selected taking a balance among rutile conversion ratio, operation / environment conditions and yields.

3.2.4 Characterization

The carbon content of the precursor was measured by Carbon Meter (SUMIGRAPH NC-22F, Sumika Chemical Analysis Service, Ltd.) The thermogravimetric analysis (TGA) was done in air at a heating rate of 10 ℃/min from room temperature to 500 ℃ by DTA / Thermogravimetric analyzer (Thermo Plus EVO2; Rigaku Corp.).   The adsorption of the precursor was evaluated by FT-IR (Nicolet 670, Thermo Fischer Scientific Inc.) collecting 32 scans in the $400 - 4000$ cm^{-1} range with 4 cm^{-1} resolution. The crystalline phases were analyzed by an X-ray diffractometer (XRD-6100 Shimazu Corp.) using Cu-Kα radiation with XRD peak intensity of the rutile (110) and the anatase (101) structure [19]. The average crystal size of the thermally-treated fumed TiO_2 (D in nanometers) was estimated by Scherrer's equation.

The particle size distribution was measured by a MT3300EX2 (MicrotracBEL Corp.). The Carr Cohesion value was applied as the index of the agglomerate by a weight measurement passing through the 355 μm, 250 μm and 155 μm of the sieves with 60 seconds vibration [20-21]. The sedimentation test was carried out with the same method described in Chapter 2.2.2 using a spectrophotometer (V-670 JASCO Corp.) at a 700 nm [22]. The surface area was measured by the BET technique (Macsorb HM-1200S Mountech Co., Ltd.) using the one-point measurement method with nitrogen as an absorbent [23]. The morphology and nanostructure were observed by a scanning electron microscopy (SEM, JSM-IT300LA, JEOL Ltd.) and a transmission electron

microscope (TEM, JEM-1010 JEOL Ltd.). The average crystal size (D in nanometers) of the thermally-treated P25 was estimated by Scherrer's equation. The zeta potential of the thermally-treated P25 dispersion in water was measured by nano Partica SZ-100 (HORIBA Corp.). Colorimetric tests were performed using a color meter (Color Cute i Suga Test Instruments Co. Ltd.,)

3.3 Results and Discussion

3.3.1 Surface Modification

Table 3-2 summarizes the carbon content of the precursors with storage time at room temperature. For the dry-type surface modification without heating at room temperature, TE(2), TE(5), TT(2) and TT(5) showed low carbon content less than 0.5 wt.% just after 1 day of storage.

Table 3-2 Carbon content of P25 modified with the metallic alkoxides (precursors)

Sample coding	Surface modification conditions	Carbon content (wt%)			
		Additive carbon content[*1]	Theoretical carbon content[*2]	1 day of storage	6 days of storage
P25 Original	-	-		-	-
TE(2)	Dry-type without heating at room temperature	2.0	0	0.3	0.2
TE(5)	Dry-type without heating at room temperature	7.0	0	0.5	0.3
TT(2)	Dry-type without heating at room temperature	2.9	0	0.4	0.2
TT(5)	Dry-type without heating at room temperature	6.7	0	0.5	0.3
AP(5)	Dry-type without heating at room temperature	7.5	2.7	-	7.1
OC(2)	Dry-type with heating at 180°C for 2 hours	4.1	3.7	-	3.0
W-TE(2)	Wet-type with heating at 105°C for 50 hours	2.0	0	0.0	-

*1) Additive carbon content is calculated by the addition quantity of the metallic alkoxide.
*2) Theoretical carbon content is calculated by the assumption that all of metallic-alkoxy groups react with P25 and generated alcohols are removed from P25.

After 6 days of storage, the carbon content of these precursors slightly decreased to less than 0.3 wt.%. Regarding AP(5), it showed similar carbon content; 7.1 wt.% to the additive one; 7.5 wt.% even after 6 days of storage. For the dry-type surface modification with heating, OC(2) showed less carbon content; 3.0 wt.% than the theoretical one; 3.7 wt.%.   The wet-type surface modification, W-TE(2) displayed no carbon content.

Fig. 3-1 presents the FT-IR spectra of the precursors after 6 days of storage. The spectra of the metallic alkoxides and original P25 are shown as references. The metallic alkoxides, TEOS, TTIP, APTES and OCTMO show absorption peaks at around 2840-2900 cm^{-1} attributed to symmetric and asymmetric stretching of C-H bonds [24]. Regarding to the original P25 and precursors, broad absorption bands at regions 400-800 cm^{-1} are attributed to Ti-O and Ti-O-Ti bonds [25]. The adsorption bands around 1600 cm^{-1} correspond to the bending vibrations of O-H, and 3400 cm^{-1} are stretching modes of the O-H bond related to the surface adsorbed water and hydroxyl groups [26].
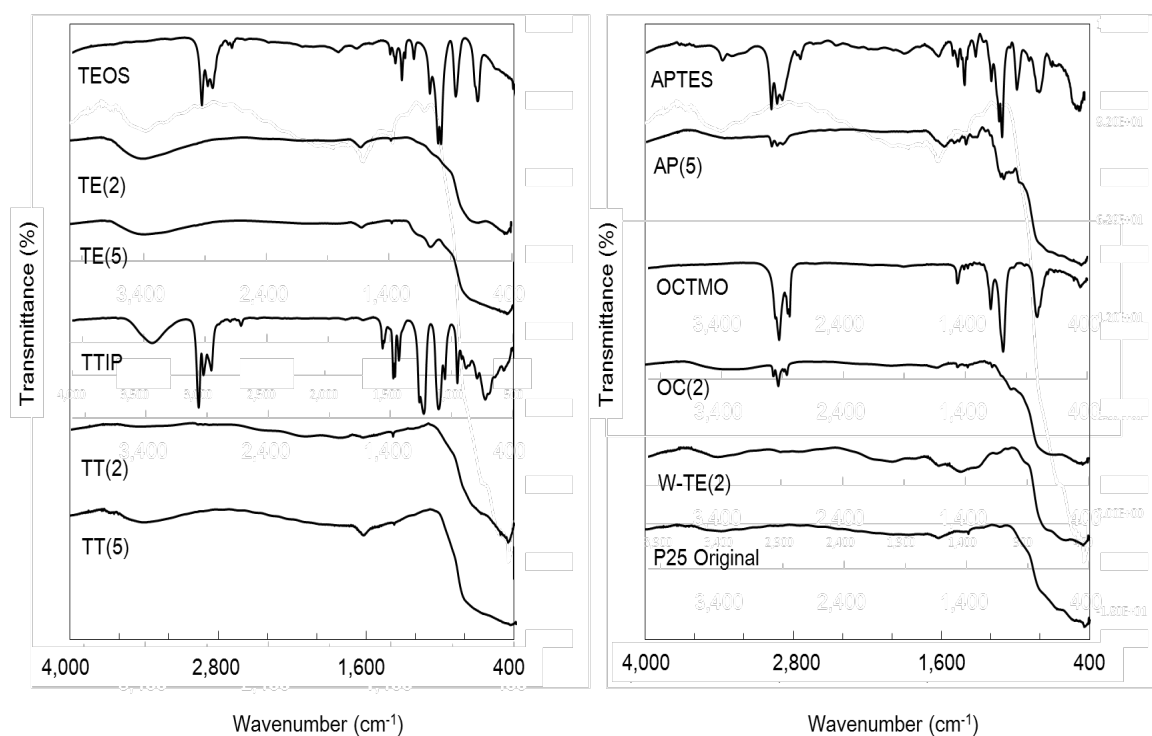
Fig. 3-1. FT-IR spectra of the surface modified P25 with metallic alkoxides (Precursors)

In the precursors modified with APTES and OCTMO, the symmetrical and asymmetrical stretching vibration of the C-H bonds were observed as presented in spectra AP(5) and OC(2). Comparatively, other precursors modified with TEOS and TTIP showed no C-H adsorption bands presented in spectra TE(2), TE(5), TT(2), TT(5) and W-TE(5). APTES and OCTMO have an alkylene-group bonded to Si atom. On the

contrary, TEOS and TTIP do not have an alkylene-group connected to Si or Ti atom and only have an alkoxy-group. These results suggest that the alkoxy-groups of TEOS and TTIP react with the hydroxyl-groups on the P25 surface and the generated alcohols are removed from the P25.

Fig. 3-2 presents TG curves of the precursors after 6 days of storage. The result of the original P25 is also displayed as a reference. The small weight losses observed in the original P25 for 1.16 wt.% and W-TE(2) for 1.11wt% attributed to the removal of physically absorbed water. The weight losses of TE(2), TE(5), TT(2) and TT(5) were probably due to both physically absorbed water and the remaining small quantities of organic molecules. The weight loss of OC (2) for 3.81 wt.% can be attributed to the oxidative thermal decomposition of the alkyl-group of OCTMO at over 200 ℃. The considerable weight losses for AP(5) for 6.62 wt.% can be attributed to the removal of unreacted APTES with P25 and oxidative thermal decomposition. These weight losses for all materials confirmed the results of the carbon contents data shown in Table 3-2.
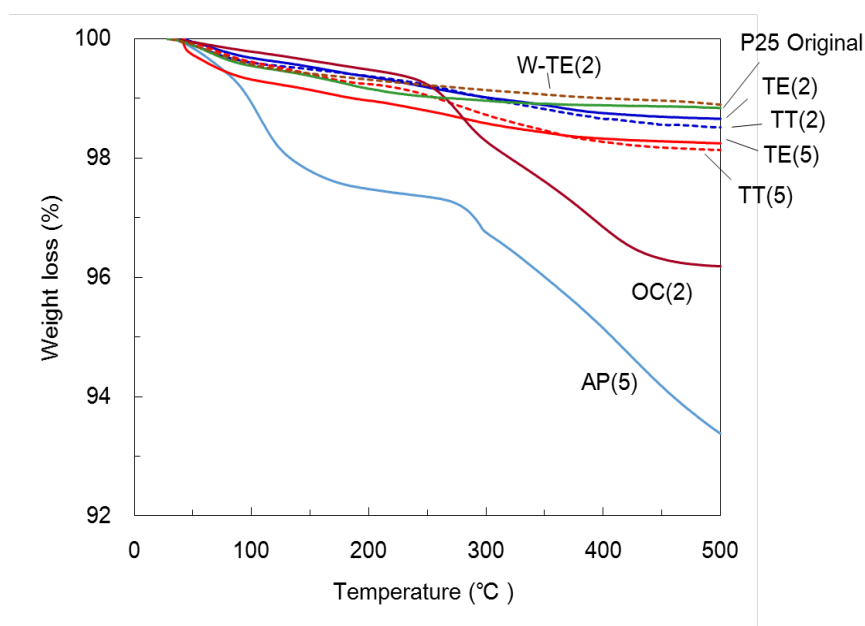
Fig. 3-2. TG thermographs of P25 modified with metallic alkoxides (Precursors)

These results suggest that the reactivity of the metallic alkoxides with P25 is highly dependent on the species of metallic alkoxides in the dry-type surface modification. The

proposed reaction schemes are shown in Fig. 3-3. TEOS and TTIP can react with P25 at room temperature as shown in Fig. 3-3 (a). The decrease of small carbon content after 6 days of storage as shown in Table 3-2 probably caused from the reaction of remaining alkoxy-group and leaving the alcohol generated by the reaction during storage at room temperature.

APTES has less reactivity with the P25 at the same temperature (Fig. 3-3 (b)). Regarding the dry-type surface modification with heating, unreacted OCTMO probably removed from P25 surface during the heating process as illustrated in Fig. 3-3 (c). The heating process can be skipped for the dry-type surface modification with TEOS and TTIP from these results.
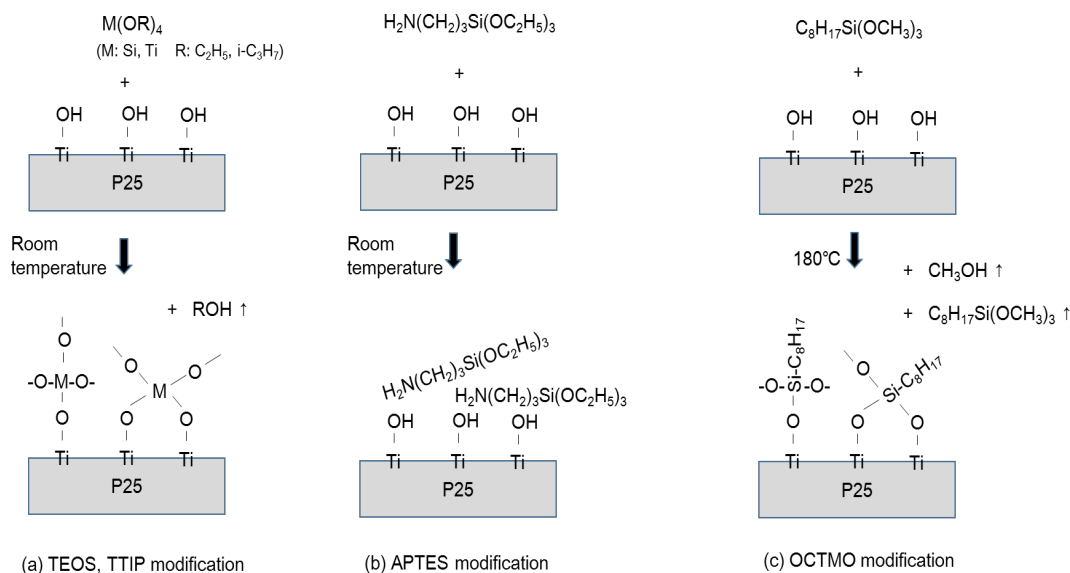
Fig. 3-3. Reaction scheme of P25 modified with metallic alkoxides (Precursors)

3.3.2 Conversion Ratio from The Anatase to The Rutile Structure

Fig. 3-4 illustrates the X-ray diffraction (XRD) patterns of the anatase (101) and the rutile (110) of the thermally-treated precursors modified with TEOS by both the dry-type and the wet-type of the surface modification. It was observed that the thermally-treated TE(2) (dry-process) showed higher rutile peak than the thermally-treated W-TE(2) (wet-process) at all temperatures. At 1400 °C, the

thermally-treated TE(2) demonstrates no anatase peak. Comparatively, the thermally-treated W-TE(2) still maintains a considerable amount of the anatase peak.

(a) TE(2) Dry-type modification

(b) W-TE(2) Wet-type modification
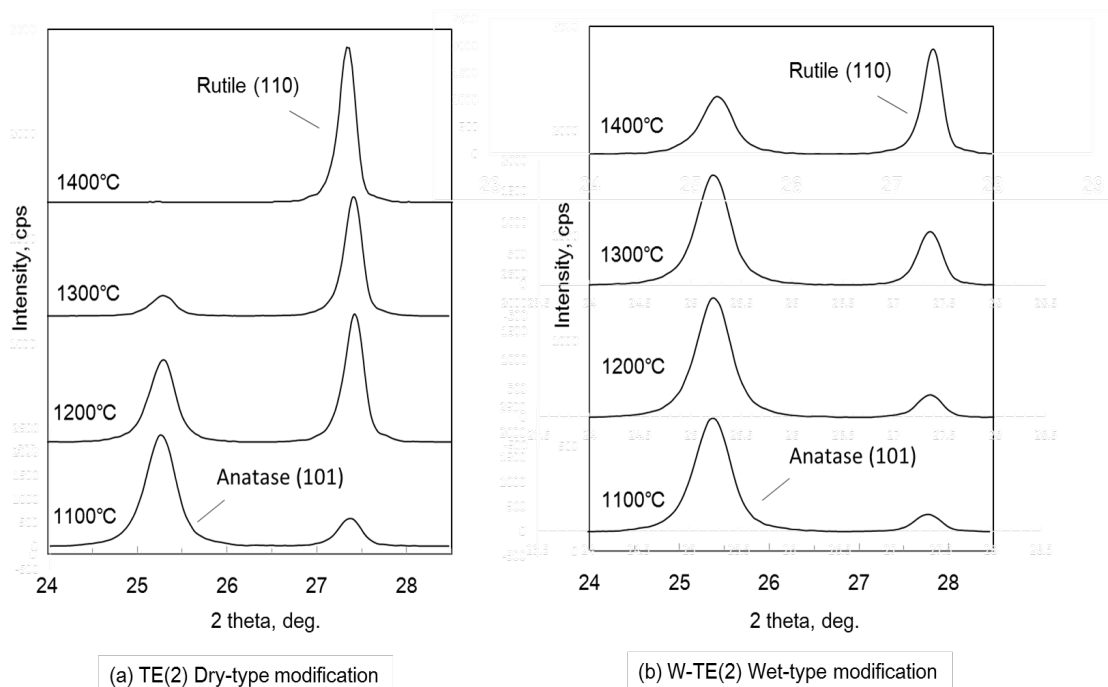
Fig. 3-4. XRD patterns of the thermally-treated P25 modified with metallic alkoxides

Fig. 3-5 confirms the content of the rutile structure of the thermally-treated precursors at several temperatures. TT(2) and TT(5) showed very similar conversion curves for the rutile structure. Both materials demonstrated 100 % of the rutile structure at 1400 ℃. AP(5) and OC(2) demonstrated low content of the rutile structure. The thermally-treated AP(5) and OC(2) at 1400 ℃ showed 84 % and 98 % of the rutile structure respectively. They did not achieve 100 % rutile structure at 1400 ℃. It has been reported that the carbon content in TiO_2 acts as the stabilizer for the anatase structure [27-28]. AP(5) and OC(2) contains a large amount of carbon as shown in Table 3-2. The carbon content probably acts as an inhibitor for the thermal transformation from anatase to rutile structure. Regarding TEOS modification, the thermally-treated TE(2) and TE(5) showed very different conversion curves of the rutile structure. TE(2) showed rapid rise of the content of the rutile structure between 1100 ℃ and 1200 ℃ and it transformed to 100 % rutile structure at 1400 ℃. Comparatively, TE(5) maintained low content of the rutile

structure from 1100 °C to 1300 °C. It remained 82 % of the rutile structure at 1400 °C. The carbon content is not attributed to the main reason for the different transformation results between TE(2) and TE(5) because these materials have similar carbon contents.
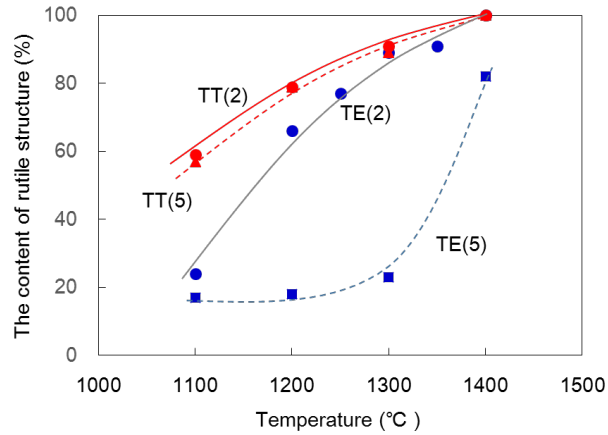
(a TEOS, TTIP modification

Fig. 3-5 (1). Rutile conversion rate for the thermally-treated P25 modified with TEOS and TTIP
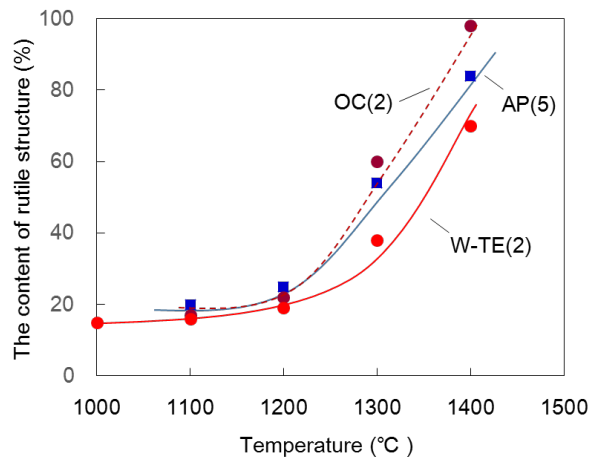
(b) OCTMO, APTES, Wet-TEOS modification

Fig. 3-5 (2). Rutile conversion rate for the thermally-treated P25 modified with OCTMO, APTES and Wet-TEOS

It was confirmed that the agglomerate before the thermal treatment is influenced on the rutile conversion ratio in Chapter 2. The particle size distributions of the precursor for TE(2) and TE(5) were measured to confirm the agglomerate size. The results are shown in Fig. 3-6.

(a) 40W 0min
(b) 40W 3min
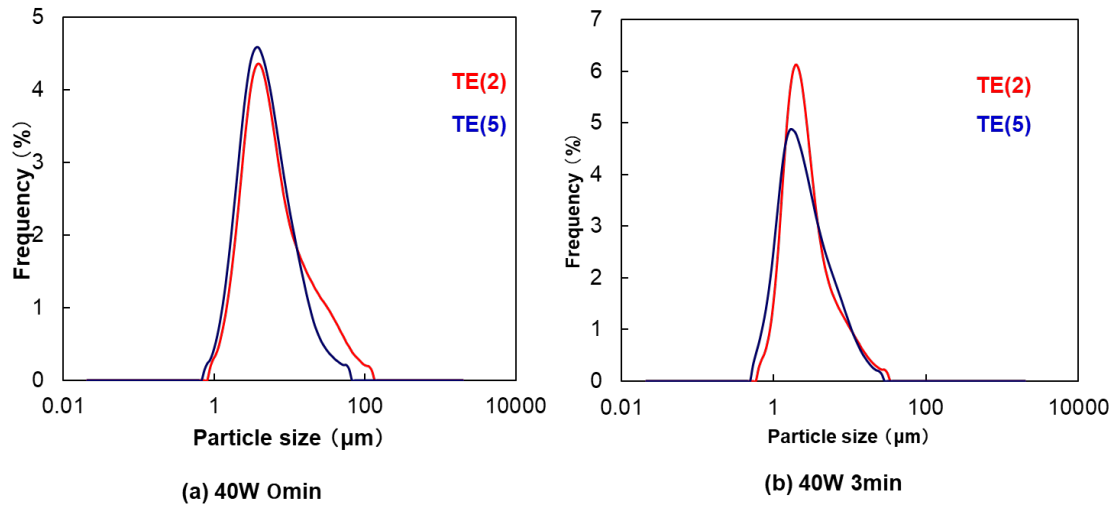
Fig. 3-6. Particle size distribution of precursor TE(2) and TE(5)

Without ultrasonic irradiation in Fig. 3-6 (a), the precursor TE(2) and TE(5) appeared very similar particle size distribution curves. Due to the ultrasonic irradiation at 40 W for 3 minutes as shown in Fig. 3-6 (b), both materials showed very similar particle size distribution curves although the main peaks of TE(2) and TE(5) shifted to smaller distribution region. The particle size distribution did not recognize the difference of agglomerate size between TE(2) and TE(5). This particle size distribution is measured in a water dispersion. Therefore, the result is influenced on the dispersibility on the media (water).   This method is not effective to confirm the agglomerate situation for this investigation.

Regarding the wet-type of surface modification, W-TE(2) showed lower content of the rutile structure for all temperatures than the dry-type TE(2). The content of the rutile structure of W-TE(2) showed still 70 % at 1400 ℃.

TE(2), TE(5) and W-TE(2) passed through the same size of mesh; 0.71 mm, for the thermal treatment. If they have the same agglomerate size; 0.71 mm and bulk densities;

0.1 Kg/L, the residence time in the electrical furnace should be the same; 0.68 seconds at 1400 °C under the Stokes's equation. To confirm the agglomerate morphology, these precursors were observed by using a scanning electron microscope (SEM). The SEM photos of the precursors TE(2), TE(5) and W-TE(2) are illustrated in Fig. 3-7. Obviously, TE(2) showed the small agglomerate around less than 5 μm. TE(5) illustrated larger and densified agglomerate than TE(2). The large quantity of the TEOS probably acts like a binder of the P25 particles in TE(5).

W-TE(2) demonstrated the large agglomerate around 5 – 20 μm. Additionally, it seems that W-TE(2) makes rigid and densified agglomerate. The terminal velocity is faster than the others due to the high densified small agglomerate. These agglomerate sizes are relatively well fit to the results of the conversion ratio from anatase to rutile structure.

(a) TE(2) Dry-type modification   (b) TE(5) Dry-type modification   (c) W-TE(2) Wet-type modification
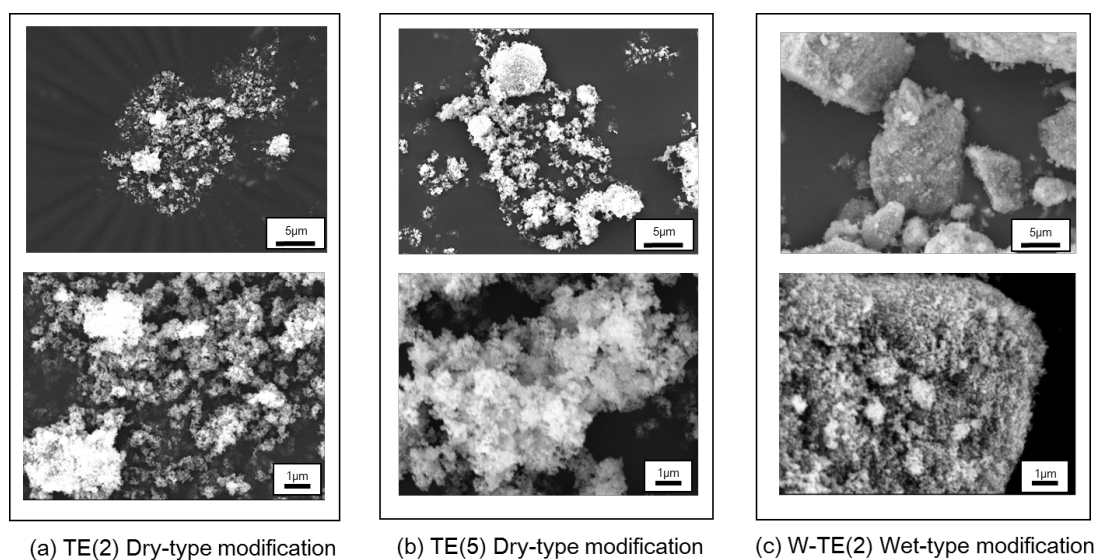
Fig. 3-7. SEM images of the surface modified P25 with TEOS (Precursors)

Carr Cohesion value was applied as the index of the agglomerate as another method. Generally, the agglomerate with low Carr Cohesion value indicates smaller / weaker agglomerate than larger one. The precursors TE(2) and TE(5) showed Carr Cohesion values; 45 and 60 respectively. These results relatively good fit to the rutile conversion results. It is suggested that the transformation from anatase to rutile structure is highly depended on the morphology of the precursors in this novel thermal treatment method.

3.3.3 Dispersibility

Fig. 3-8 demonstrates the particle size distributions of the thermally-treated TE(2), TT(2) and TT(5) at 1400 ℃ having 100 % of the rutile structure. The results of other types of TiO$_2$ with 100 % of the rutile structure produced by Chloride process (CR-EL (7m^2/g) Ishihara Sangyo Co. Ltd.) in Chapter 2. 3. 3 is quoted as a reference. Without ultrasonic irradiation in Fig. 3-8 (a), the thermally-treated TE(2), TT(2) and TT(5) appeared very similar, wide range and two major distribution peaks. Due to the ultrasonic irradiation at 40 W for 3 minutes as shown in Fig. 3-8 (b), the main peaks of TE(2), TT(2) and TT(5) shifted to smaller distribution region and made one major peak individually.　In contrast, CR-EL showed smaller particle size distribution than that of TE(2), TT(2) and TT(5) without the ultrasonic irradiation. The main peak of CR-EL shifted to smaller region although main peak was remaining in the original region under 40W of ultrasonic irradiation. These results indicate that the thermally-treated TE(2), TT(2) and TT(5) at 1400 ℃ made weak agglomerate which are easily reduced to small agglomerate by the weak ultrasonic irradiation although their particle size distributions are larger than CR-EL.

(a) Without ultrasonic irradiation

(b) With ultrasonic irradiation 40W 3 minutes
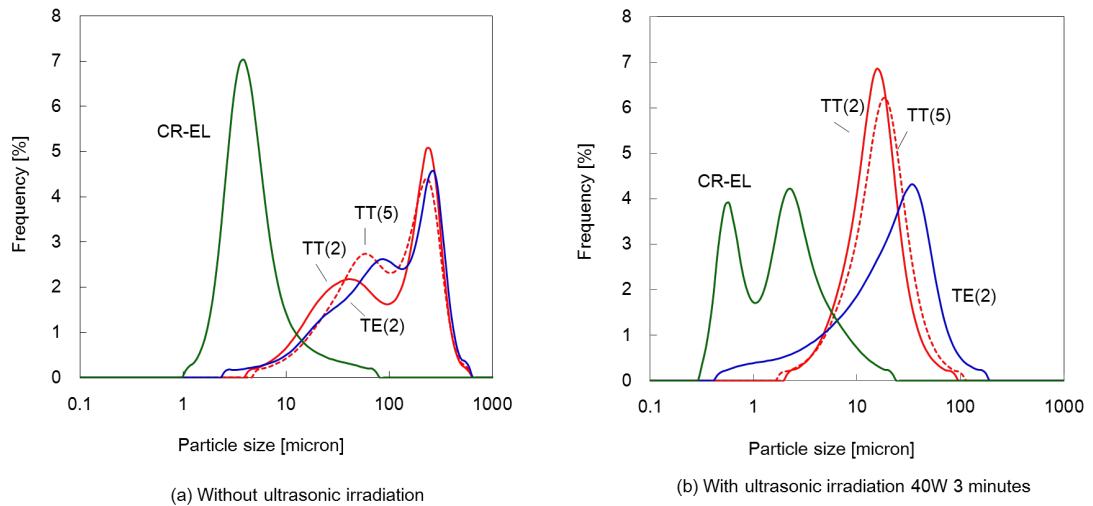
Fig. 3-8. Particle size distribution of the thermally-treated P25 at 1400 ℃

As the sedimentation test, the absorbance of the water dispersion of the thermally-treated TE(2), TT(2) and TT(5) at 1400 ℃ versus storage time were examined. CR-EL and original P25 without the thermal treatment are also illustrated as the references. The results are shown in Fig. 3-9. Very different results were obtained in the sedimentation test. The thermally-treated TE(2) maintained constant high and similar absorbance curve to the original P25. At 50 hours storage, the thermally-treated TE(2) and the original P25 demonstrated the absorbance 3.378 % and 3.584 % respectively. The thermally-treated TT(2) and TT(5) gradually reduced depended on the storage time and showed 0.460 % and 0.696 % for 50 hours storage. Comparatively, CR-EL rapidly dropped in absorbance and demonstrated 0.072 % at 50 hours. The sedimentation results of CR-EL was slightly different from the result in Fig. 2-8. This different is probably cased from the deviation of sampling point of the CR-EL.
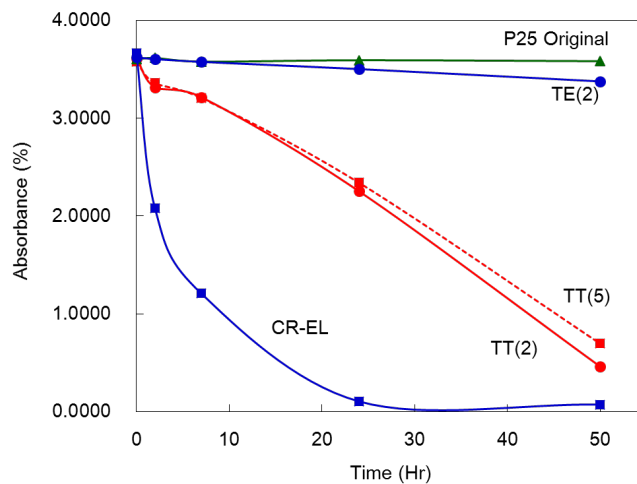
Fig. 3-9. Absorbance of the thermally-treated P25 at 1400 ℃

The absorbance value is directly related to the transparency of the water dispersion. These results suggest that the thermally-treated TE(2) has very slower sedimentation velocity and higher dispersibility in water.

For the estimation of sedimentation velocity by using the Stokes's equation, 0.56 cm/hour sedimentation velocity was obtained by applying 1 μm of average diameter for CR-EL particles and this result shows a relatively good consistency with the sedimentation test result for CR-EL as described in Chapter 2. However, this

assumption does not fit to the thermally-treated TE(2), TT(2) and TT(5) at 1400 ℃ because they showed larger particle size than CR-EL in the particle size distribution. Especially, the thermally-treated TE(2) at 1400 ℃ performed very slow sedimentation velocity.

3.3.4 Morphologies and Nanostructures

Fig. 3-10 displays the surface area ($S._{BET}$) of the thermally-treated TE(2), TT(2) and TT(5) at several temperatures. The reversed tendency observed for the conversion ratio of the content of the rutile structure. The thermally-treated TE(2) showed higher surface area than that of the thermally-treated TT(2) and TT(5) at all thermal treatment temperatures. The thermally-treated TT(2) and TT(5) demonstrated the same S. BET curves.   At 1400 ℃, the thermally-treated TE(2) demonstrated 11 m^2/g of $S._{BET}$ and both the thermally-treated TT(2) and TT(5) showed 5 m^2/g of $S._{BET.}$
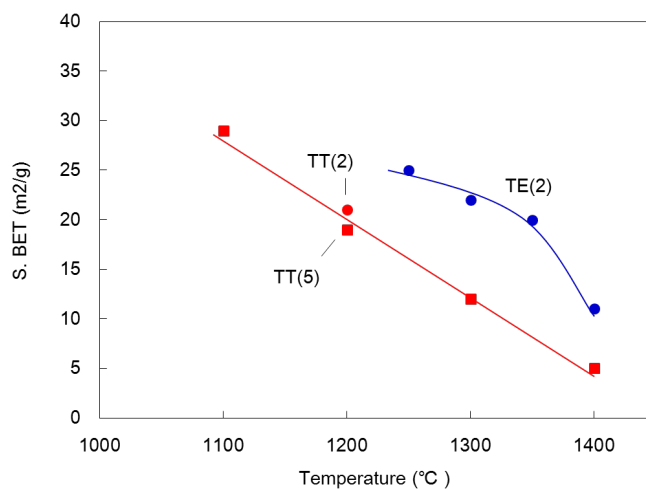
Fig. 3-10. Surface area of the thermally-treated P25 modified with metallic alkoxides

Fig. 3-11 illustrates SEM and TEM images of the thermally-treated TE(2), TT(2) and TT(5) at 1400 ℃ having 100 % of the rutile structure. It was observed that the thermally-treated TE(2), TT(2) and TT(5) make bulky agglomerates with many porous among the particles, sponge-like agglomerates. Further, the thermally-treated TE(2) demonstrated smaller particle and agglomerate size than that of the thermally-treated TT(2) and TT(5). It was reported that the growth of TiO_2 particle was suppressed by the

codeposition of SiO$_2$ for TiO$_2$-SiO$_2$ particles [29]. The coexistence of SiO$_2$ on the P25 surface inhibited the grain growth of the thermally-treated TE(2) at 1400 ℃. This result shows a relatively good consistency with the results of S.BET as shown in Fig. 3-9.

(a) TE(2) 1400℃   (b) TT(2) 1400℃   (c) TT(5) 1400℃
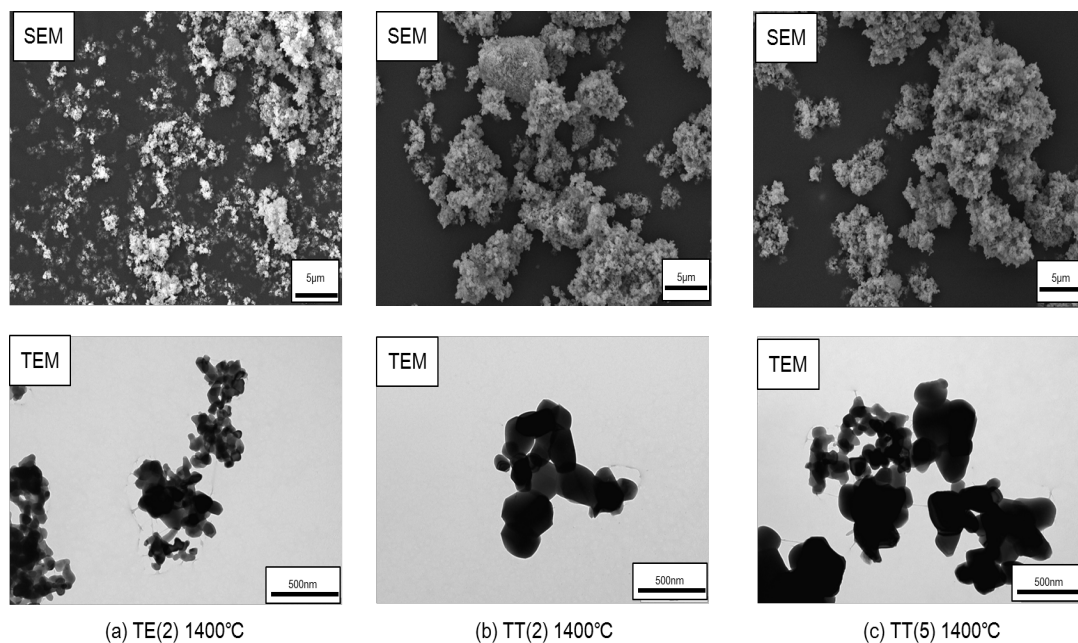
Fig. 3-11. SEM and TEM images of the thermally-treated P25 at 1400 ℃

In the thermally-treated TE(2), TT(2) and TT(5), there were no any tiny particles attached on the P25 surface by TEM observation under high magnification. The surface of the P25 was coated with a layer of SiO$_2$ or TiO$_2$. The results are shown in Fig. 3-12.

(a) TE(2) 1400℃   (b) TT(2) 1400℃   (c) TT(5) 1400℃
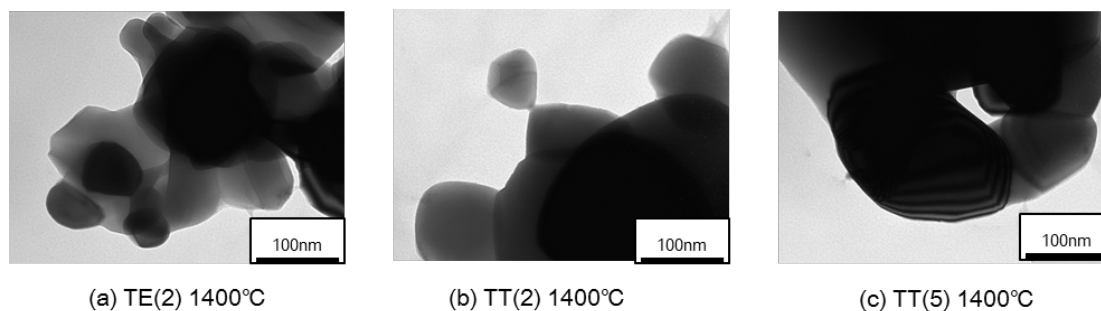
Fig. 3-12. TEM images of the thermally-treated P25 at 1400 ℃ under high magnification (×300,000)

Fig. 3-13 demonstrates the relationships between the content of the rutile structure and crystal size of the rutile structure calculated by the X-ray diffraction peak, rutile (110). The X-ray diffraction patterns are illustrated in Fig. 3-14. The thermally-treated TE(2) showed wider half-value width of rutile (110) peak than TT(2) and TT(5) at 1400 ℃. The thermally-treated TE(2) showed 38 nm crystal size for 100 % of rutile structure. Comparatively, the thermally-treated TT(2) and TT(5) showed 48 nm and 51 nm of crystal size for 100 % of rutile structure respectively. The small crystal size of TE(2) is correlated with the results of the particle size as shown in Fig. 3-11.
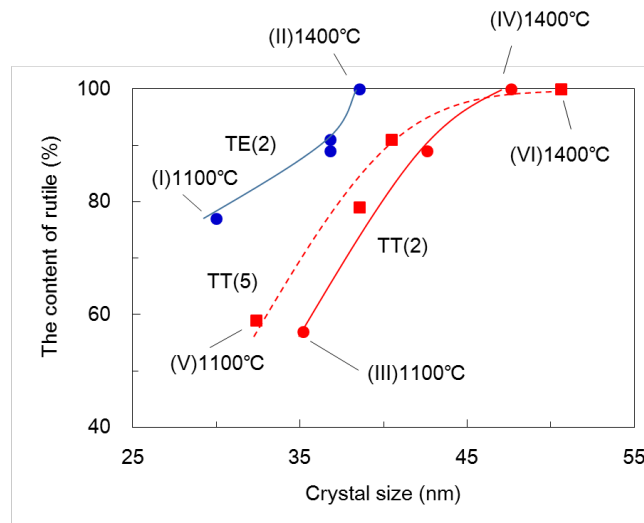
Fig. 3-13. Relationship between the content of rutile structure and crystal size of the rutile structure of the thermally-treated P25 modified with metallic alkoxides
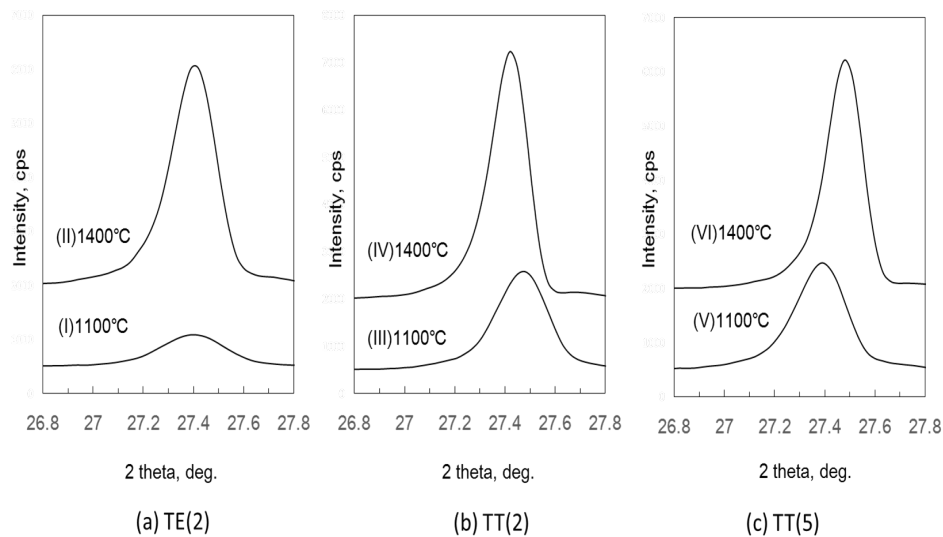
Fig. 3-14. XRD patterns (Rutile 110) of the thermally-treated P25 modified with metallic alkoxides

Fig. 3-15 presents the zeta potential of the thermally-treated TE(2) and the original P25 at several temperatures. The precursor TE(2) and the original P25 showed positive zeta potentials; 34.8 mV and 42.4 mV before thermal treatment respectively. The zeta potentials shifted from positive to negative charge with the thermal treatment. The original P25 showed -18.0 mV of the charge after thermal treatment at 1400 ℃. The shift of the zeta potential was probably caused from the decrease of a hydroxyl-group on the surface. The thermally-treated TE(2) demonstrated higher negative charges than the original P25 at all temperatures.
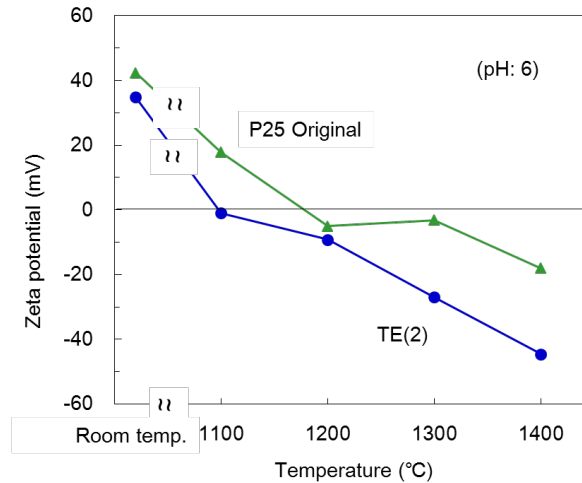
Fig. 3-15. Zeta potential of the thermally-treated P25 modified with TEOS

Table 3-3 summarizes the zeta potential of the thermally-treated TE(2), TT(2) and W-TE(2) with the results of the original P25. Before the thermal treatment, TE(2) and TT(2) demonstrated positive zeta potentials 34.8 mV and 37.8 mV relatively near to the original P25. With the thermal treatment at 1400 ℃、 the thermally-treated TE(2) and TT(2) presented high negative zeta potential, -42.0 mV and -27.5 mV respectively.

The sedimentation results of the thermally-treated TT(2) shown in Fig. 3-9 are caused from relatively similar but higher negative charge from the thermally-treated P25 shown in Fig. 2-5.

W-TE(2) performed high negative zeta potential before and after the thermal treatment at 1400 ℃, -56.8 mV and -47.9 mV. It is reported that binary metal oxides show stronger acidity than the single oxides [30]. The higher negative charge of the thermally-treated TE(2) than the original P25 was probably due to both the SiO_2 coating layer and formation of Ti-O-Si bond on the P25 surface as we expected in the beginning of this investigation.

From these results, it is confirmed that the high dispersibility of the thermally-treated TE (2) at 1400 ℃ is attributed to both the sponge-like agglomerate with low particle density and the static electricity repellence of the SiO_2 coated layer.

Table 3-3 Zeta potential of P25 modified with metallic alkoxides

	Zeta potential (mV)	(pH 6)
Sample	Before thermal treatment	After thermal treatment at 1400℃
P25 Original	42.4	-18.0
TE(2)	34.8	-42.0
TT(2)	37.8	-27.5
W-TE(2)	-56.8	-47.9

3.3.5 Brightness and Color Tone

Table 3-4 summarizes the brightness and color tone of the thermally-treated TE(2) and TT(2) at 1400 ℃. The results of the original P25, precursor W-TE(2) and CR-EL are also illustrated. The thermally-treated TE(2) and TT(2) showed shifting the b* values to positive; 2.98 and 3.25, and the a* values to negative; -0.54 and -0.81 respectively. These value shifts became near to the b* and a* values of CR-EL. Comparatively, the precursor W-TE(2) showed very near b* and a* values of the original P25. As a crystal morphology, the anatase structure usually shows slightly bluish white color while the rutile structure shows slightly yellowish white color. The color tone shifts of thermally-treated TE(2) and TT(2) were attributed to the rutile structure for these materials.

Table 3-4 Brightness and color tone of P25 modified with metallic alkoxides

Sample	Thermal treatment temperature (℃)	L*	a*	b*
P25 Original	Room temperature	99.62	-0.45	0.73
TE(2)	1400	97.95	-0.54	2.98
TT(2)	1400	97.15	-0.81	3.25
W-TE(2)	Room temperature	98.58	-0.51	0.88
CR-EL	Room temperature	96.82	-1.42	4.26

3.4 Conclusions

In this study, the effect of the dry-type of the surface modification of P25 was studied to prepare a new P25 having 100 % of the rutile structure maintaining the high dispersibility. P25 was modified with the metallic alkoxides for the preparation of the

precursors. Next, the precursors were thermally-treated with the novel natural dropping method. The carbon content and agglomerate of the precursor had influenced on the transformation ratio from anatase to rutile structure. Low carbon content and small agglomerate were preferred for the precursor for the transformation. It is confirmed that the dry-type surface modification with TEOS and TTIP without heating is very effective method to prepare the preferable precursors for the next thermal treatment. The morphology of the agglomerate for precursor is influenced on the rutile structure conversion rate. The thermally-treated TE(2), TT(2) and TT(5) at 1400 °C achieved 100 % of the rutile conversion. It is suggested that the precursors of TE(2), TT(2) and TT(5) are making small agglomerate and preserving the increase of the bulk density for the small agglomerate.

Especially, the thermally-treated TE(2) achieved both 100 % rutile structure and high dispersibility as demonstrated in the sedimentation test. The high dispersibility of the thermally-treated TE(2) is attributed to both the sponge-like structural characteristic of the agglomerate and the static electricity repellence by coated SiO_2 layer. These results revealed that the combination of dry-type surface modification and natural dropping thermal treatment is an attractive method to prepare the new fumed TiO_2 with 100 % rutile structure maintaining the high dispersibility.

References

[1] H. R. Jafry, M. V. Liga, Q. Li and A. R. Barron, Simple Route to Enhanced Photocatalytic Activity of P25 Titanium Dioxide Nanoparticles by Silica Addition, Environ. Sci. Tecnol. 45 (2011) 1563-1568.
[2] D. M. Tobaldi, A. Tucci, A. S. Škapin and L. Esposito, Effects of SiO_2 addition on TiO_2 crystal structure and photocatalytic activity, J. European Ceramic Society 30 (2010) 2481-2490.
[3] J. Zhao, M. Milanova, M. M. C. G. Warmoeskerken and V. Dutschk, Surface modification of TiO_2 nanoparticles with silane coupling agents, Colloids and Surfaces A: Physicochem. Eng. Aspects 413 (2012) 273-279.
[4] S. Pazokifard, S. M. Mirabedini, M. Esfandeh and S. Farrokhpay, Fluoroalkylsilane treatment of TiO_2 nanoparticles in difference pH values: Characterization and mechanism, Advanced Powder Technology 23 (2012) 428-436.
[5] I. Harya, F. Izinilah, I. R. Hakiki and S. Slamet, Study of Self Cleaning Fabric Modified by Cu Doped TiO_2 with the addition of Tetraethyl OrthoSilicate (TEOS), Proceeding of the 4th International Symposium on Applied Chemistry 2018, 020071-1 – 020071-7.

[6] P. Zhang, J. Tian, R. Xu and G. Ma, Hydrophilicity, photocatalytic activity and stability of tetraethyl orthosilicate modified TiO_2 film on glazed ceramic surface, Applied Surface Science 266 (2013) 141-147.

[7] X. Feng, S. Zhang and Z. Lou, Controlling silica coating thickness on TiO_2 nanoparticles for effective photodynamic therapy, Colloids and Surfaces B: Biointerfaces 107 (2013) 220-226.

[8] A. Mirabedini, S. M. Mirabedini, A. A. Babalou and S. Pazokifard, Synthesis, characterization and enhanced photocatalytic activity of TiO_2/SiO_2 nanocomposite in an aqueous solution and acrylic-based coatings. Progress in Organic Coatings 72 (2011) 453-460.

[9] J. Zhao, M. Milanova, M. M. C. G. Warmeskerken and V. Dutschk, Surface modification of TiO_2 nanoparticles with silane coupling agents, Colloids and Surfaces A: Physicochem. Eng. Aspects 413 (2012) 273-279.

[10] S. Pazokifard, S. Farrokhpay, M. Mirabedini and M. Esfandeh, Surface treatment of TiO_2 nanoparticles via sol-gel method: Effect of silane type on hydrophobicity of the nanoparticles, Progress in Organic Coatings 87 (2015) 36-45.

[11] X. Feng, S. Zhang and X. Lou, Controlling silica coating thickness on TiO_2 nanoparticles for effective photodynamic therapy, Colloids and Surfaces B: Biointerfaces 107 (2013) 220-226.

[12] A. K.-Hossini, S. M. Mirabedini and S. Pazoifard, Photocatalytic activity and colloidal stability of various combinations of TiO_2/SiO_2 nanocomposites, J. Mater Sci 51 (2016) 3219-3230.

[13] M. Tassi, A. Roevens, G. Reekmans, M. Vanhamel, V. Meynen, J. D'Haen, P. Adriaensens and R. Carleer, A detailed investigation of the microwave assisted phenylphosphonic acid modification of P25 TiO_2, Advanced Powder Technology 28 (2017) 236-243.

[14] S. Hayashi, F. Oguri and F. Kagaya, Preparation of Composite Film by Simultaneous Electrophoretic Deposition Using Titanium Oxide Nanoparticles and Submicron-sized Aluminum Oxide Particles, J. Soc. Powder Technol, Japan, 51 (2014) 686-693.

[15] M. Kim, E. Park, H. Jung, S.-T., Yun and J. Jurng, Temperature-dependent thermal stability and dispersiblity of SiO_2-TiO_2 nanocomposites via a chemical vapor condensation method, Powder Technology 267 (2014) 153-160.

[16] A. Khadem-Hosseini, S. M. Mirabedini and S. Pazokifard, Photocatalytic activity and colloidal stability of various combinations of TiO_2 / SiO_2 nanocomposites, J. Mater. Sci. 51 (2016) 3219-3230.

[17] Y. Yamashita, A. Nishihara and H. Sakurai, New Modification of Silica Powder with Sulfonic Acid Group and Their Properties, Shikizai 70 (1997) 300-307.

[18] Mitsubishi Materials, JP H9-316359.

[19] R. A. Spurr, H. Myers, Quantitative Analysis of Anatase-Rutile Mixtures with an X-ray Diffractometer, Analytical Chemistry 29 (1957) 760-762.

[20] F. Sato, H. Inoue, M. Miyata and Y. Sasaki, Experimental Investigation of Carr's Flowability Measuring Method, Journal of the Society of Powder Technology, Japan 9 (1972) 90-97.

[21] Standard Test Method for Bulk Solid Characterization by Carr Indices, ASTM D6393-08 (2008) 1-8.

[22] Y. Mitani, T. Teshima, Y. Yoshida and N. Yamazoe, Dispersibility of Fumed Silica in Simple Media, J. Ceramic Society of Japan 101 (1993) 707-712.

[23] Determination of the specific surface area of powders (solids by gas adsorption-BET method, JIS Z8830 (2013) 1-24.

[24] F. Rubio, J. Rubio and J. L. Oteo, A FT-IR study of the Hydrolysis of Tetraethylorthosilicate (TEOS), Spectroscopy Letters, 31 (1998) 199-219.

[25] S. Vives and C. Meunier, Influence of the synthesis route on sol-gel SiO_2-TiO_2 (1:1) xerogels and powders, Ceramics International 34 (2008) 37-44.

[26] C. He, B Tian and J. Zhang, Synthesis of thermally stable and highly ordered bicontinuous cubic mesoporous titania-silica binary oxides with crystalline framework, Microporous and Mesoporous Materials 126 (2009) 50-57.

[27] M. Inagaki, Suppression of Phase Transformation in Titanium Dioxide by Carbon Coating, Aichi Institute of Technology Bulletin of Research Institute for Industrial Technology 9 (2007) 67-71.

[28] M. Inagaki, T. Matsunaga, T. Tsumura and M. Toyoda, Carbon-coated TiO_2 : Photoactivity under fluorescent light, TANSO 219 (2005) 217-220.

[29] Y. Suyama, E. Ura and A. Kato, TiO_2-SiO_2 Powders Produced by the Vapor Phase Reaction of the $TiCl_4$-$SiCl_4$-O_2 System, The Chemical Society of Japan 3 (1978) 356-360.

[30] K. Shibata, T. Kiyoura, J. Kitagawa, T. Sumiyoshi and K. Tanbe, Acidic properties of Binary Metal Oxides, Bull. Chem. Soc. Japan, 46 (1973) 2985-2988.

CHAPTER 4

STUDY OF EFFECT OF EXTERNAL ADDITIVES ON A SYNTHESIS OF FUMED TITANIUM DIOXIDE WITH A HIGH CONTENT OF RUTILE STRUTURE BY A NOVEL NATURAL DROPPING THERMAL TREATMETN

4.1 Introduction

It is confirmed that the morphology of the fumed TiO_2 before thermal treatment (precursors) influenced on the transformation temperature from the anatase to the rutile structure with the novel natural dropping thermal treatment as described in Chapter 2 and Chapter 3. These results suggest that the small sized and low densified agglomerate of fumed TiO_2 tends to increase in the content of the rutile structure. Additionally, SiO_2 layer on the fumed TiO_2 surface improves the dispersibility of it with the static electricity repellence.

It is known that the addition of a small portion of fumed oxides improves the flowability of a large particle and a sticky powder. This property is utilized to an external additive of a toner material [1-3]. An organic salt is also applied as an additive to give similar functions to various powders [4-6]. The addition of these external additives with solid state have a possibility to change the morphology of the precursors prepared from the fumed TiO_2.

In this study, the sold state external additives are applied to modify the agglomerate of precursor of the fumed TiO_2 as a different type of modification process compared with metallic alkoxides. For the modification of the precursor, very simple modification; only mixing process was tried.

A surface modified fumed silica was applied as an external additive to give high dispersibility with static electricity repellence by existing SiO_2 on fumed TiO_2 surface.

A fumed Al_2O_3 was also applied as the external additive to accelerate the transformation with high thermal conductivity on the fumed TiO_2 and to confirm the effectivity of SiO_2 for the dispersibility.

Calcium stearate was used as other external additive to compare the effectiveness with the fumed SiO_2 and the fumed Al_2O_3.

The morphology of the precursors and the thermally-treated TiO_2 are investigated in relation to the agglomerate of the precursors.

Herein, in this chapter, we would like to report an available new thermal treatment technology to synthesis the new fumed TiO_2 with 100 % of the rutile structure content maintaining the high dispersibility by addition of the solid stated external additives. We focused on the evaluation of the new fumed TiO_2 with 100 % of the rutile structure content by the same reason as Chapter 3.

4.2 Experimental

4.2.1 Materials and Preparation

As fumed TiO_2, commercially produced TiO_2 and experimental sample with different surface areas and primary particle sizes, (AEROXIDE® TiO_2 P 25: 50 m^2/g; 21 nm; (P25), AEROXIDE® TiO_2 P 90: 90 m^2/g; 14nm; (P90) and VP P 75: 75 m^2/g; 19 nm; produced by Nippon AEROSIL Co., Ltd.) were used. The external additives, fumed alumina, AEROXIDE® AluC (AluC), produced by EVONIK GmbH surface modified fumed SiO_2 with dimethyldicholosilane; AEROSIL® R 972; 14 nm; (R972) ; produced by Nippon AEROSIL Co. Ltd.) and calcium stearate (Sigma-Aldrich: CP grade: Merck Co. Ltd) were used.

4.2.2. Preparation of The Fumed TiO_2 with External Additives (Precursors)

In the case of the external additives, R972 and AluC, they were mixed three times with the fumed TiO_2 using a mixer (VA-W27 Hitachi, Ltd.) at 2 times for 30 seconds intervals to prepare the precursors. Regarding the calcium stearate, it was added from the top of the mixer in several portions with stirring over 60 seconds. After finishing the addition, it was mixed two times at 30 seconds intervals.

4.2.3 Thermal Treatment of The Fumed TiO_2 with External Additives (Precursors)

The same thermal treatment was carried out with the same conditions of the electric tubular furnace described in Chapter 2.2.1. The precursors were directly dropped from the top of the furnace to the bottom by a natural dropping method through a 0.71 mm sieve fixed to the top of the electric furnace under vibration. The electric furnace was

heated at several temperatures from 1000 ℃ to 1400 ℃. Both the maximum temperature of the electric tubular furnace and the 0.71 mm sieve were selected with the same reason described in Chapter 3.2.3.

4.2.4 Characterization

The crystalline phases were analyzed by an X-ray diffractometer (XRD-6100 Shimazu Corp.) using Cu-Kα radiation peak intensity of the rutile (110) and the anatase (101) structure [7]. The average crystal size of the thermally-treated fumed TiO_2 (D in nanometers) was estimated by Scherrer's equation.

The particle size distribution was measured by a MT3300EX2 from the MicrotracBEL Corp. The surface area was measured by the BET technique (Macsorb HM-1200S Mountech Co., Ltd.) using the one-point measurement method with nitrogen as an absorbent [8].

The sedimentation test was carried out with the same method described in Chapter 2.2.2 using a spectrophotometer (V-670 JASCO Corp.) at 700 nm [9].

The appearance of the sedimentation in an aqueous medium was also visually observed. The nanostructure and morphology were determined by a transmission electron microscope (TEM, JEM-1010 JEOL Ltd.). The repose angle and the agglomerate of the powder before the thermal treatment (Precursors) were measured using a Horiba Powder tester. The Carr Cohesion value was applied as the index of the agglomerate by a weight measurement passing through the 355 μm, 250 μm and 155 μm sieves with 60 seconds of vibration [10]. The carbon content was measured by the Carbon Meter (SUMIGRAPH NC-22F, Sumika Chemical Analysis Service, Ltd.). The zeta potential of the dispersion in water was measured by nano Partica SZ-100 (HORIBA Corp.).

4.3 Results and Discussion

4.3.1 Conversion Ratio from The Anatase to The Rutile Structure

Fig. 4-1 shows the X-ray diffraction (XRD) patterns of the anatase (101) and the rutile (110) for the thermally-treated P25 without the external additive and the thermally-treated P25 with 5 wt.% R972. The XRD data indicated that the transformation from the anatase to the rutile was significantly affected by the addition of R972. It was observed that the thermally-treated P25 with R972 showed a lower

anatase content than the thermally-treated P25 without the external additive at all temperatures. At 1400 ℃, the thermally-treated P25 with R972 demonstrates no anatase content. It shows 100 % rutile structure content although the anatase still remained in the thermally-treated P25 without the external additive.
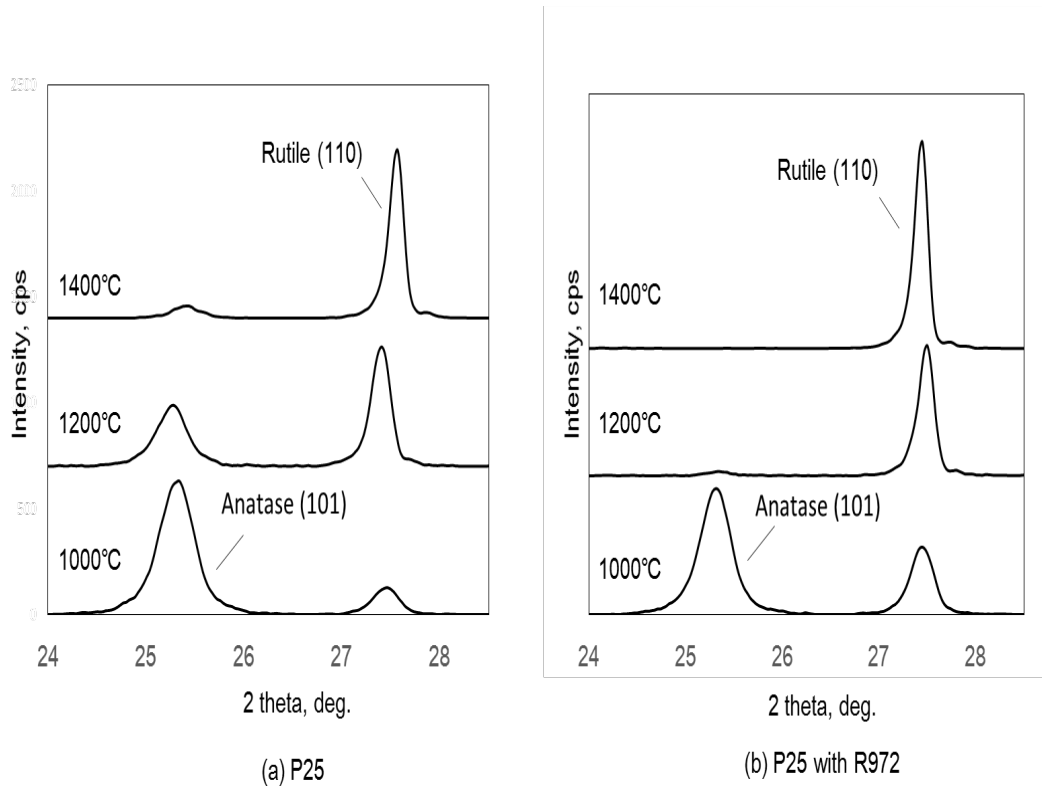
Fig. 4-1. XRD patterns of the thermally-treated P25

Fig. 4-2 confirms the rutile structure content for the thermally-treated P25 with the external additives compared to the thermally-treated P25 without the external additives at several different temperatures. It is observed that the addition of the external additives has a significant effect on increasing the rutile structure content. The order of the increase in the rutile structure content is as follows: P25 with calcium stearate > P25 with AluC > P25 with R972 >> P25 without external additive.

The thermally-treated P25 with R972 and AluC showed 100 % of rutile structure at 1350 ℃ and 1300 ℃, respectively, although the thermally-treated P25 without the external additive remained at 94 % rutile content even though the thermal treatment temperature was higher than 1400 ℃. The thermally-treated P25 with calcium stearate

showed 100 % rutile content at a relatively low temperature; 1200 ℃. This temperature is more than 100 ℃ lower than that of the addition of R972 and AluC, and more than 250 ℃ lower than the thermally-treated P25 without the external additive.

(a) P25 with R972 (b) P25 with AluC (c) P25 with Calcium Stearate
(d) P25 without external additive
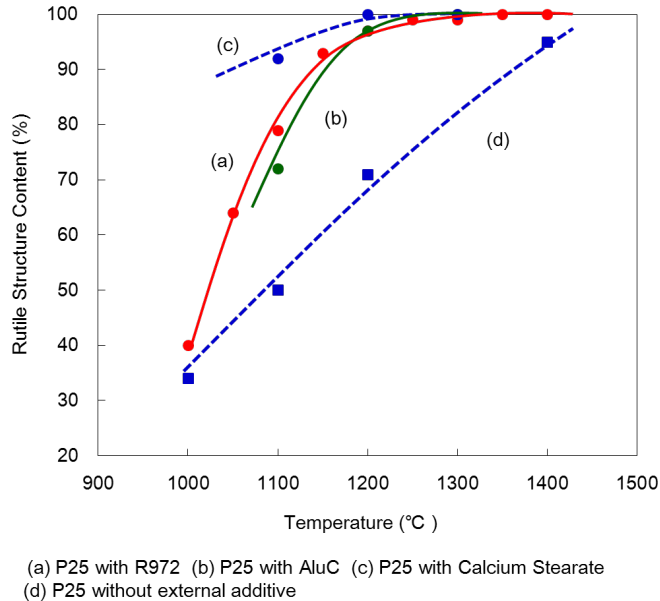
Fig. 4-2. Rutile conversion rate of the thermally-treated P25 with external additive

4.3.2 Surface Area

Fig. 4-3 displays the surface areas ($S._{BET}$) of the thermally-treated P25 with the external additives compared to the thermally-treated P25 without the external additives from 1000 ℃ to 1400 ℃. It is evident that a decrease in the surface area was observed in all cases depending on the rise in the thermal treatment temperature. The order of the decrease in the surface area is, thermally-treated P25 with calcium stearate > P25 with AluC > P25 with R972 > P25 without the external additive. This result demonstrated the reversed tendency of the conversion ratio of the rutile structure as shown in Fig.4-2. Specifically, the thermally-treated P25 with calcium stearate shows a very low surface area even though at a relatively low thermal treatment temperature.

When 5 wt.% of R972 and AluC are mixed with P25, the surface area of the mixed powder was calculated to be 52.5 m^2/g by the surface area of R972 and AluC. This estimation indicates that the addition of 5 wt.% for both R972 and AluC has less

influence on the surface area for the resulting fumed TiO_2 powders.

(a) P25 with R972 (b) P25 with AluC (c) P25 with Calcium Stearate
(d) P25 without external additive
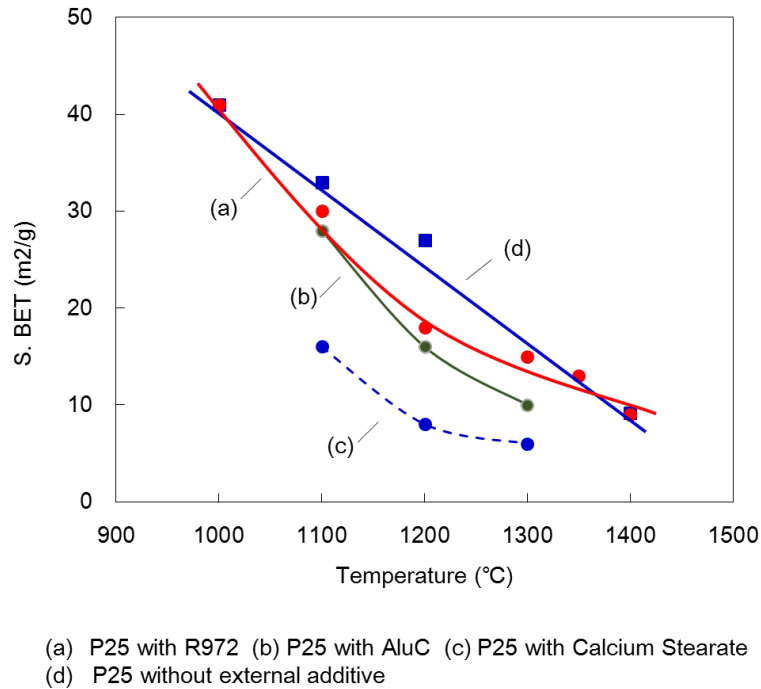
Fig. 4-3. Surface area of the thermally-treated P25 with external additives

4.3.3 Dispersibility

Fig. 4-4 confirms the particle size distributions of the thermally-treated P25 with the external additive having 100% rutile structure content; P25 with R972 at 1350 °C, P25 with AluC at 1300 °C and P25 with calcium stearate at 1200 °C. Without ultrasonic sonication, the thermally-treated P25 with R972 and AluC showed a very wide particle size distribution and they demonstrated three or two major constituents, respectively. Regarding the thermally-treated P25 with calcium stearate, it shows a narrower particle size distribution than that of the thermally-treated P25 with R972 and AluC. It shows one major constituent. Due to the ultrasonic sonication at 40 W for 3 minutes, the main constituents of the thermally-treated P25 with R972 and AluC shift to a smaller distribution region for which the thermally-treated P25 with calcium stearate shows less shift to the smaller region. This result indicates that the thermally-treated P25 with R972 and AluC have weak agglomerate behaviors which are easily disrupted by the ultrasonic sonication. On the other hand, the thermally-treated P25 with calcium stearate has a

strong agglomerate tendency which is not affected by the sonication at the ultrasonic frequency of 40 W for 3 minutes.

(a) Without Ultrasonic sonication   (b) With Ultrasonic sonication 40W 3 minutes

(a) P25 with R972 (1350℃)   (b) P25 with AluC (1300℃) (c) P25 with Calcium Stearate (1200℃)
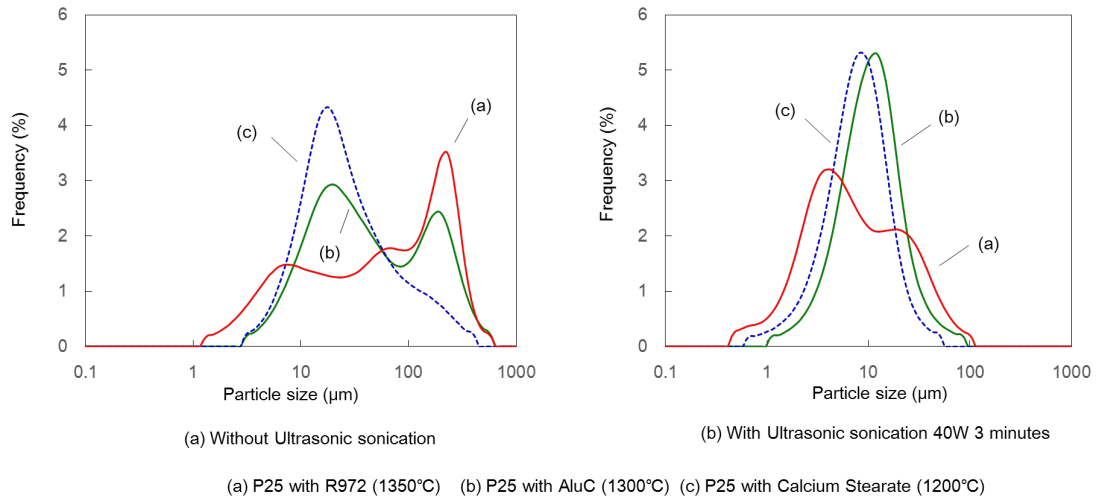
Fig. 4-4. Particle sized distribution of the thermally-treated P25 with the external additives

Fig. 4-5 indicates the absorbance of the dispersion in water versus storage time for the thermally-treated P25 with external additives having 100 % of the rutile structure as a sedimentation test. These were the same samples used for the particle size distribution. In this investigation, the other types (Chloride process) of TiO_2 (CR-EL (7 m^2/g) Ishihara Sangyo Co. Ltd.) with the rutile structure and similar surface area, and the original P25 without any external additives and thermal treatment were also applied as references. The results of CE-EL was slightly different from the results shown in Fig. 2-5 and Fig. 3-9. This difference is also probably cased from the deviation of sampling point of the CR-EL. Very different results were obtained from the sedimentation test. The thermally-treated P25 with R972 maintained a constant high and stable absorbance curve. This curve is very similar to the original P25. It showed an excellent dispersibility with 100 % rutile structure content. The thermally-treated P25 with AluC showed slightly lower dispersibility than the thermally-treated P25 with R972.
Regarding the thermally-treated P25 with calcium stearate, the absorbance rapidly dropped and showed a very similar curve to CR-EL.
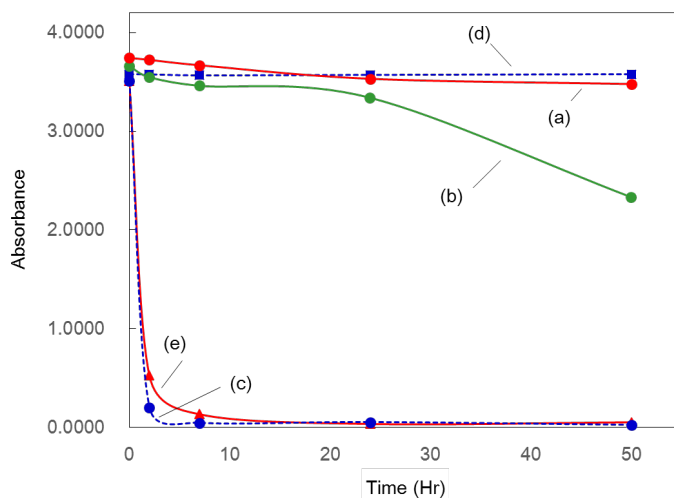
(a) P25 with R972 (1350℃)　(b) P25 with AluC (1300℃)　(c) P25 with Calcium Stearate (1200℃)
(d) Original P25 (without external additive and thermal treatment)　(e) CR-EL

Fig. 4-5. Absorbance of TiO_2 dispersion in water

The thermally-treated P25 with calcium stearate has higher sedimentation velocity in water than the thermally-treated P25 with R972 and AluC although it displays similar particle size distribution to the thermally-treated P25 with AluC under ultrasonic sonication at 40 W for 3 minutes as shown in Fig. 4-4 (b).

The photos of the fumed TiO_2 dispersion in water for the sedimentation test are displayed in Fig. 4-6. It is noted that the dispersion of the thermally-treated P25 with R972 (a) shows a turbid appearance with a low transparency similarly to the original P25 without any external additives and the thermal treatment during 50 hours of storage. The dispersion of the thermally-treated P25 with calcium stearate becomes transparent in just 2 hours of storage similarly to CR-EL produced by the chloride process. Both these powders show very poor dispersibility due to the fast sedimentation velocity.

The mixture of the thermally-treated P25 without any external additives at 1400 ℃ and 5 % AEROSIL® 130 (which is a core particle of R972) was dispersed in the water and another sedimentation test was carried out to confirm whether the excellent dispersibility of the thermally-treated P25 with R972 was due to the thickening effect of AEROSIL® 130. The dispersion did not show a high absorbance value, 2.4 % for 7 hours, 1.2 % for 24 hours and 0.28 % after 50 hours of storage. The color of the

dispersed material gradually became clear by a visual inspection. These results suggest that the high dispersibility of the thermally-treated P25 with R972 is not caused by the thickening property from the core particles of R972, AEROSIL® 130.

(a) 0 Hour

(b) 2 Hours

(c) 7 Hours

(d) 50 Hours

(a) P25 with R972 (1350℃)   (b) P25 with AluC (1300℃) (c) P25 with Calcium Stearate (1200℃)
(d) P25 without external additive and thermal treatment
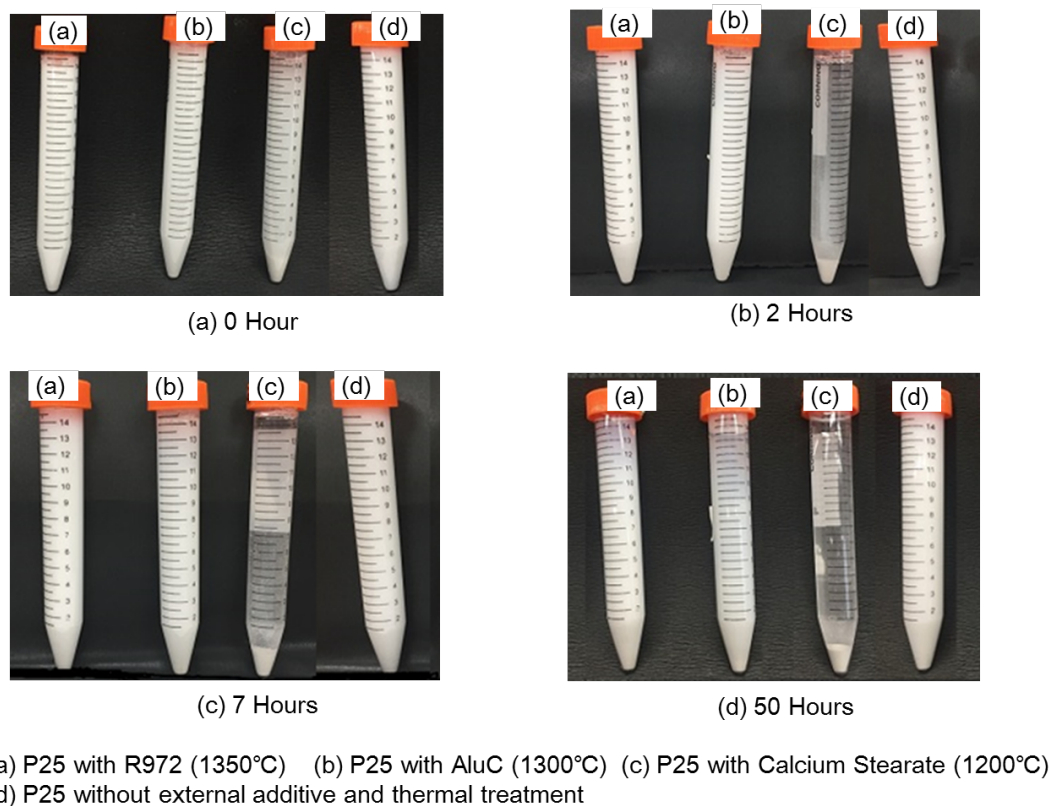
Fig. 4-6. Photos of TiO$_2$ dispersion in water for the sedimentation test

4.3.4 Nanostructure of The Thermally-Treated Fumed TiO$_2$ with An External Additive

Fig. 4-7 shows the transmission electron microscope (TEM) images including under high magnification for the thermally-treated P25 with the external additives which are the same materials from the previous sedimentation test.

It is observed that both the thermally-treated P25 with R972 and with AluC contain both large particles (possibly made by partial sintering / grain growth) and many small particles. These results are very different from the results of the thermally-treated TE (2), TT (2) and TT (5) as shown in Fig. 3-11. Chapter 3, although all materials show 100 %

of rutile structure. In Fig. 3-11, there were no any tiny particles attached on the P25 surface due to coating of a layer of SiO_2 or TiO_2. Comparatively, the thermally-treated P25 with R972 and with AluC contain the small particles on the P25 surface after the thermal treatment.

On the other hand, the thermally-treated P25 with calcium stearate shows no small particles. This TEM result supports the sintering / grain growth of P25 by the addition of calcium stearate

(a) P25 with R972 (1350℃)   (b) P25 with AluC (1300℃)   (c) P25 with Calcium Stearate (1200℃)
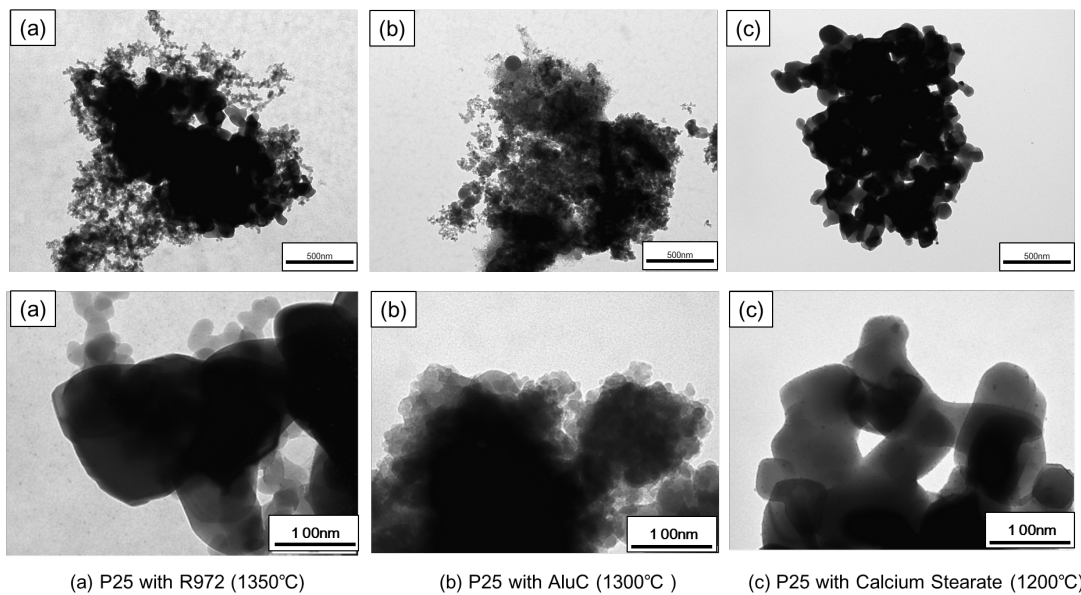
Fig. 4-7. TEM images of the thermally-treated P25 with the external additives

When 3 μm diameter of the agglomerate of the thermally-treated P25 with calcium stearate is roughly applied to the Stokes's equation from not particle size distribution but the TEM observation in this case as shown in Fig. 4-7 (c), a 5 cm/h sedimentation velocity was estimated. This result shows a relatively good consistency with the result of the sedimentation test shown in Fig. 4-6.

The thermally-treated P25 with R972 and AluC show very slow sedimentation velocities although they have a similar particle size of the agglomerates compared to the thermally-treated P25 with calcium stearate. This result indicates that the particle density can influence on the sedimentation velocity as well as the particle size. The thermally-treated P25 with R972 and AluC would have a much lower powder density

even with many pores in the agglomerate and exhibit pseudo-large particles in the particle size distribution.

The thermally-treated P25 with R972 demonstrated higher dispersibility than the thermally-treated P25 with AluC as shown in Fig. 4-5. The thermally-treated P25 with R972 at 1400 °C showed -47.8 mV of the zeta potential. These results suggest that the high dispersibility is probably caused from not only the sponge-like agglomerate but also the static electricity repellence of the attached SiO_2 on the P25 surface as we intended in this investigation.

Fig. 4-8 shows the relationship between the rutile structure content and crystal size of the rutile structure calculated from the X-ray diffraction peak, rutile (110). It was observed that 100 % rutile structure content is obtained from over 36 nm of crystal size.
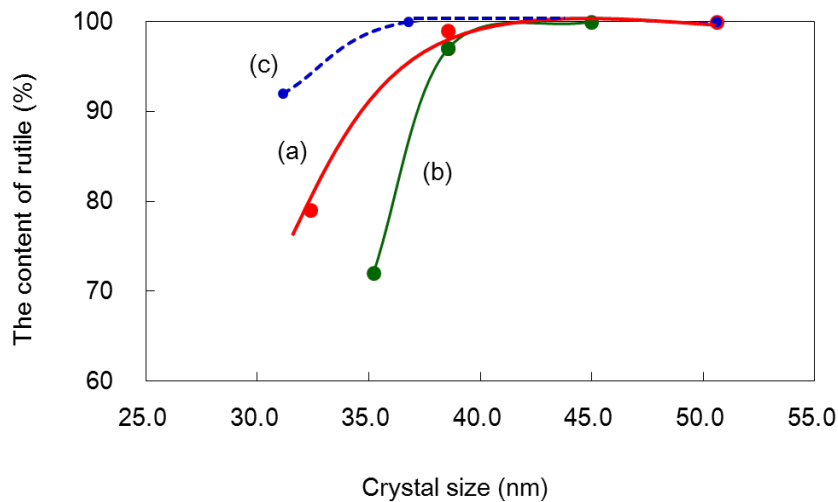
(a) P25 with R972   (b) P25 with AluC   (c) P25 with Calcium Stearate

Fig. 4-8. Crystal size of the thermally-treated P25 with the external additives

4.3.5 The Effect of Fumed TiO_2 Agglomerate before Thermal Treatment

The agglomerated situation of P25 with the external additives (Precursors) was measured to confirm the effect of the external additives on the transformation from the anatase to rutile structure.

Table 4-1 summarizes the relationships between the repose angle, Carr Cohesion value of P25 with the external additive before the thermal treatment (Precursor) and the

temperature of 100 % of rutile structure observed. The order of the repose angle from small to high is as follows: original P25 > P25 with R972 ≒ P25 with AluC > P25 with calcium stearate.

Table 4-1 Repose angle and Carr Cohesion of P25 with the external additive

Fumed TiO$_2$	External additive	Before thermal treatment (Precursor)			After thermal treatment	
		Repose angle (°)	Carr Cohesion (%)		Temperature for 100% rutile structure (℃)	Estimated agglomerate size (mm)
P25	-	39.5	69		Over 1400	
	R972	41.1	55		1350	0.71
	Alu C	42.9	49		1300	0.67
	Ca-Stearate	44.8	28		1200	(0.58)

Sieve: 0.71mm

On the other hand, the order of the Carr Cohesion value is as follows: P25 with calcium stearate < P25 with AluC < P25 with R972 < original P25. It is known that the Carr Cohesion value is a good index to demonstrate the affinity for agglomeration [11-12]. This Carr Cohesion tendency shows relatively good relationships between the temperature for 100 % rutile structure. P25 powder with the low Carr Cohesion value would pass through the sieve as smaller agglomerates than that of the agglomerate with the high Carr Cohesion value.

In the Table 4-1, the estimated agglomerate size is also summarized. The size was calculated by the back calculation based on the assumption that 80 Kcal/mol of heat energy point under the temperature for 100 % rutile structure by using the unsteady heat transfer equation described in Chapter 2.3.4. In this assumption, the thermal capacity of the agglomerate with the external additive was set depended on the weight percentage. The estimated agglomerate size also shows good relationship to the temperature for 100 % of rutile structure. The agglomerate with small estimated agglomerate size shows low crystal transformation temperature for 100 % of rutile structure.

The following residence times under the same temperature for 100 % of rutile structure are calculated based on the terminal velocity of the Stokes's equation for each agglomerate.

-P25 with R972: 0.45 seconds

-P25 with Alu C: 0.66 seconds

-P25 with calcium stearate: 0.70 seconds.

For the addition of AluC, other effect besides for low agglomerate is expected. Al_2O_3 has around 5 times higher thermal conductivity than TiO_2. Therefore, the AluC particle on the P25 surface would conduct the heat more effectively than the air and would result decrease in the crystal transformation temperature.

As for P25 with calcium stearate, it seems to have longer residence time in the electrical furnace even though lower temperature than others by this assumption.

The carbon content of P25 with calcium stearate was 3.05 wt.% before the thermal treatment and the value changed to 0.22 wt.% after the 1200 °C thermal treatment. A previous report determined that the carbon contamination prevents the transformation from the anatase to the rutile structure when the sol-gel process was implemented [13]. Our result suggests that the thermally-treated P25 with calcium stearate had the opposite effect.

It is assumed that an alkyl-group of the calcium stearate is oxidized by the thermal treatment under air and heated the P25 as an additional heat source by the burning by the result of the carbon content. The local temperature of the agglomerate would be risen compared with no burning condition by this oxidation. This additional heat accelerates the transformation and sintering / grain growth of the thermally-treated P25 with calcium stearate. P25 with calcium stearate shows very low Carr Cohesion value before the thermal treatment. It makes small agglomerate and long residence time in the electrical furnace, and additionally the heat seems to be quickly propagated within the agglomerate.

Generally, the thermal treatment of organic compounds in air can be difficult due to the oxidation reaction. However, in this case, the thermally-treated P25 with calcium stearate passes through the sieve in very small portions and the heating time is quite short. The speed and volume of P25 can be controlled through the sieve. This novel natural drop method has the advantage of providing a thermal treatment with oxidization of the organic material under safe conditions as a new thermal treatment method.   This is depicted in Fig. 4-9.
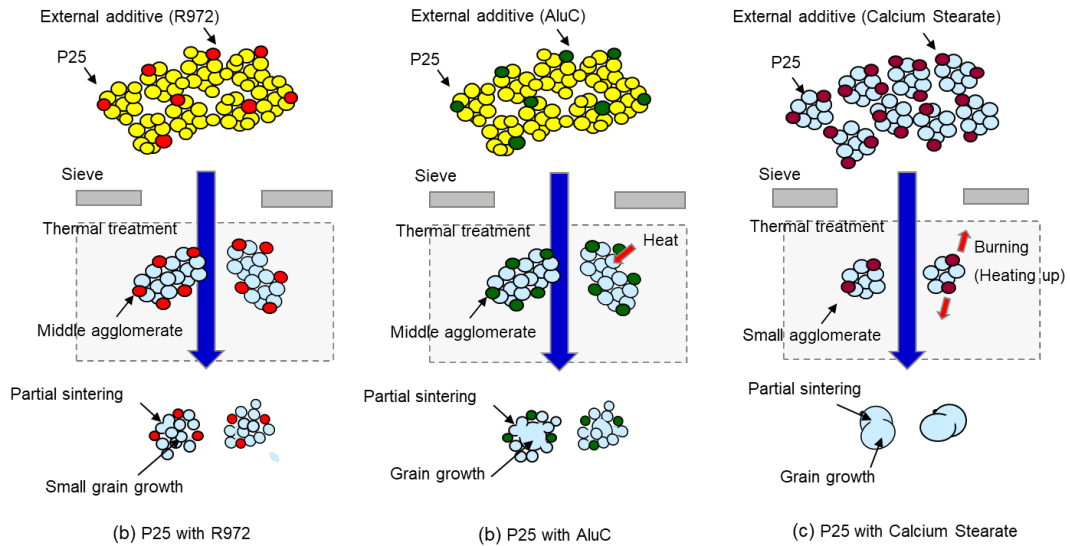
Fig. 4-9. Scheme of the thermal treatment of the fumed TiO$_2$ with the external additive

Table 4-2 shows the Carr Cohesion value of other several fumed TiO$_2$ with R972 before the thermal treatment (Precursor) and the relative rutile content after the thermal treatment at 1250 ℃. The addition of R972 to the fumed TiO$_2$ reduces the Carr Cohesion value of not only the P25 but also other fumed TiO$_2$ which have smaller primary particle sizes than P25. The contents of the rutile structure of the thermally-treated P75 and P90 with R972 were higher than the thermally-treated P25 with R972 although the Carr Cohesion value is a similar value. This result suggests that the primary particle size of the fumed TiO$_2$ is also another factor for the attainable transformation temperature of the fumed TiO$_2$. Especially, the thermally-treated P90 with R972 shows 100 % rutile structure content. The densified small agglomerate seems to be reduced by the pulverization by the mixing process with R972.

Table 4-2 Physicochemical properties of the fumed TiO_2 with external additives

TiO$_2$		External additive		Before thermal treatment	Thermal treatment temperature (℃)	After thermal treatment	
Product name	Primary Particle size (nm)	Product name	Addition quantity (wt%)	Carr Cohesion (%)		Rutile ratio (%)	S_{BET} (m^2/g)
P25	21	-	-	69.4	-	16	51
		R972	5	54.9	1250	89	20
P75	18	-	-	71.5	-	7	71
		R972	5	57.2	1250	99	13
P90	14	-	-	79.5	-	10	96
		R972	5	52.1	1250	100	11

4.4 Conclusions

The effect of the external additives on the synthesis of fumed TiO_2 with 100 % of a rutile content was investigated by a novel natural dropping thermal treatment. The addition of R972, AluC and Calcium stearate to P25 achieved to 100 % rutile structure conversion ratio.

As for the addition of surface modified fumed SiO_2; R972, it resulted in complete conversion of the anatase morphology to rutile as well as an excellent dispersibility for P25. The dispersibility is caused from both a sponge like porous-agglomerate structure and a static electrical repellence of SiO_2 on the fumed TiO_2 surface.

As for the addition of the fumed Al_2O_3, it resulted the decrease of the transformation temperature due to small sized and low densified agglomerate of the precursor, and high thermal conductive particle; Al_2O_3 on the P25 surface.

Regarding the addition of calcium stearate, remarkable decrease with the crystal transformation temperature and large grain growth / sintering of agglomerate were observed. These grain growth / sintering result a low dispersibility as the reverse effect. This result would be cased from not only a small sized and low densified agglomerate but also an additional heating from burning of the alkyl-groups of calcium stearate.

The contents of the rutile structure for the resulting fumed TiO_2 with the external additives are highly related to the agglomerate size of the precursors. The Carr Cohesion value seems to be the good index for the agglomerate. The low Carr Cohesion value resulted in a high rutile structure content due to long residence time in the electrical furnace. The mixing process seems to be effective to make small sized and low densified agglomerate.

References

[1] EVONIK. AEROSIL® Fumed Silica and AEROXIDE® Fumed Metal Oxides for Toner, Technical Information 1222 (2008) 1-20.

[2] N. Naito, Introduction of Novel External Additive of Toner, The Imaging Society of Japan 54 (2015) 133-139.

[3] M. Aoki, Y. Chikashige, T. Komatsubara and M. Ueda, Surface Structure of Fumed Silica, The Imaging Society of Japan 54 (2015) 140-147.

[4] K. Yoshimura, Characteristics of Fine Metallic Soap Particles Using Jet-Mixing Method, The Imaging Society of Japan 54 (2015) 162-166.

[5] K. Tsunematsu, K. Jinnai, H. Tateyama and K. Kimura, Dispersion of Clayer Fine Particles in Dry System by Addition of Metallic Stearate - On the mineral preparation test of weathered granite in dry system (3rd Report) -, Journal of the Mining and Metallurgical Institute of Japan 1135 (1998) 953-956.

[6] M. M. Jalili, K. Davoudi, E. Z. Sedigh and S. Farrokhpay, Surface treatment of TiO_2 nanoparticles to improve dispersion in non-polar solvents, Advanced Powder Technology 27 (2016) 2168-2174.

[7] R. A. Spurr, H. Myers, Quantitative Analysis of Anatase-Rutile Mixtures with an X-ray Diffractometer, Analytical. Chemistry 29 (1957) 760-762.

[8] Determination of the specific surface area of powders (solids by gas adsorption-BET method, JIS Z8830 (2013) 1-24.

[9] Y. Mitani, T. Teshima, Y. Yoshida and N. Yamazoe, Dispersibility of Fumed Silica in Simple Media, J. Ceramic Society of Japan 101 (1993) 707-712.

[10] Standard Test Method for Bulk Solid Characterization by Carr Indices, ASTM D6393-08 (2008) 1-8.

[11] F. Sato, H. Inoue, M. Miyata and Y. Sasaki, Experimental Investigation of Carr's Flowability Measuring Method, Journal of Research of Powder Association of Powder Technology 9 (1972) 90-97.

[12] T. Yokoyama and K. Urayama, Apparatus for Measuring Flowability of Powders by Carr's Method, Journal of the Research Association of Powder Technology, Japan. 6 (1969) 264-272.

[13] M. Inagaki, Suppression of Phase Transformation in Titanium Dioxide by Carbon Coating, Aichi Institute of Technology Bulletin of Research Institute for Industrial Technology 9 (2007) 67-71.

CHAPTER 5
THE EXTENDED APPLICATION OF THE NOVEL NATURAL
DROPPING THERMAL TREATMENT

5.1 Introduction

The novel natural dropping thermal treatment has been only applied to the fumed TiO_2 as described in Chapter 2, Chapter 3 and Chapter 4. It is obviously known that the fumed process can produce not only the fumed TiO_2 but also the fumed SiO_2 and the fumed Al_2O_3. These fumed oxides are applied to the various industrial fields [1]. The fumed SiO_2 has amorphous crystalline morphologies [2]. This is one of the big advantages of the fumed SiO_2 with no harmful effect for our health.

The SiO_2 has many crystalline morphologies depended on the temperature and pressures [3]. It is transforms from amorphous to tridymite through various crystalline morphologies depended on the rise of thermal treatment temperature from 600 ℃ to 1200 ℃ for 6 hours [4].

$$amorphous \rightarrow keatite \rightarrow quartz \rightarrow cristobalite \rightarrow tridymite \qquad (5\text{-}1)$$
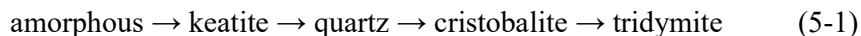
Regarding the fumed Al_2O_3, it has δ-type of alumina structure [5]. The Al_2O_3 also has many crystalline morphologies [6]. It is reported that the transformation to α-Al_2O_3 is confirmed by the thermal treatment over 1173 K for 2 hours [7].

In this study, the novel natural dropping thermal treatment is applied to the fumed SiO_2 and the fumed Al_2O_3 to confirm the possibility of the new thermal treatment process. The crystal structure and morphology of resulted the thermally-treated fumed oxides are examined. Furthermore, the effect of an external additives for the fumed Al_2O_3 is also investigated whether they can promote the phase transformation or not as a basic investigation. Herein, we would like to report the results of these new trials to confirm the possibility of the novel natural dropping thermal treatment.

5.2 Experimental
5.2.1 Materials and Preparation

Commercially-produced fumed SiO_2, (AEROSIL® 50: 50 m²/g; 30 nm; (AE50), Nippon

AEROSIL Co., Ltd.) was used. As the fumed Al_2O_3 with different surface areas and primary particle sizes, (AEROXIDE® AluC: 100 m^2/g; 13 nm; (AluC), AEROXIDE® Alu 65: 65 m^2/g; 20 nm; (Alu65); produced by EVONIK GmbH) were used.

As the external additive mixed with AluC, surface modified fumed SiO_2 with dimethyldicholosilane; AEROSIL® R 972; 14 nm; (R972); produced by Nippon AEROSIL Co., Ltd.) and calcium stearate (Sigma-Aldrich: CP grade: Merck Co. Ltd) were used. The external additives were mixed with AluC with the same method described in Chapter 4.2.

5.2.2 Thermal Treatment

The same thermal treatment was carried out at 1450 ℃ with the same conditions of the electric tubular furnace described in Chapter 2.2.1 besides for the change of the fumed oxides. The 0.71 mm sieve was applied to the thermal treatment with the same reason described in Chapter 3.2.3.

5.2.3 Characterization

Basically, the same characterization is applied as described in Chapter 2.3. The crystalline phases were analyzed by an X-ray diffractometer (XRD-6100 Shimazu Corp.) using Cu-Kα radiation. The particle size distribution was measured by a MT3300EX2 from the MicrotracBEL Corp. The surface area was measured by the BET technique (Macsorb HM-1200S Mountech Co., Ltd.) using the one-point measurement method with nitrogen as an absorbent [8].

5.3 Results and Discussion

5.3.1 Crystal Structure

AE50 showed no change of the crystal structure. It demonstrated amorphous phase in both before and after thermal treatment at 1450 ℃.

Fig. 5-1 shows the X-ray diffraction (XRD) patterns of the fumed Al_2O_3 (AluC and Alu65) before and after the thermal treatment at 1450 ℃. They demonstrated very similar XRD patterns before and after the thermal treatment.
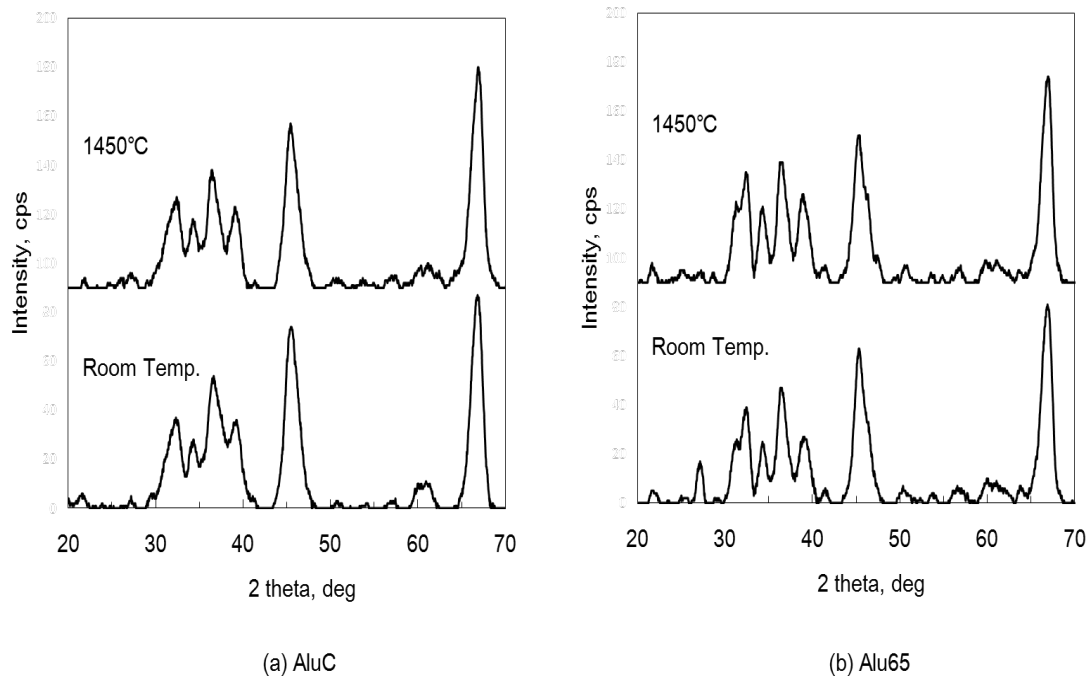
Fig. 5-1. XRD patterns of the thermal treated AluC and Alu65

A 5 wt.% of R972 and calcium stearate were mixed with AluC as the external additives for the preparation of precursors which modify the morphology of the agglomerate. These precursors were thermally-treated at 1450 °C. The XRD patterns of them are shown in Fig. 5-2 for before and after the thermal treatment. In both cases, they showed very similar XRD patterns although the thermally-treated AluC with calcium stearate at 1450 °C showed slightly increase in the crystallization with low noise for the signal. There was no observation of the crystal transformation.

The residence time of AluC is calculated at 1.25 seconds at 1450 °C by the Stokes's equation applying the bulk density of AluC. The residence time is around two times longer than P25. However, the natural dropping thermal treatment at 1450 °C is still insufficient for the crystal transformation of the fumed Al_2O_3 to α-Al_2O_3. It is reported that δ-Al_2O_3 synthesized by vapor phase reaction with $AlCl_3$ and O_2 transforms to α-Al_2O_3 by the additional thermal treatment at 1200 °C for 2 hours [9]. These conditions are more severe than that of the transformation from anatase to rutile in TiO_2. It was confirmed that the natural dropping thermal treatment is insufficient to the

crystallization he fumed SiO_2 and the crystal transformation of the fumed Al_2O_3.

(a) AluC + R972 (1450℃)　　　　　　　　(b) AluC + StCa (1450℃)
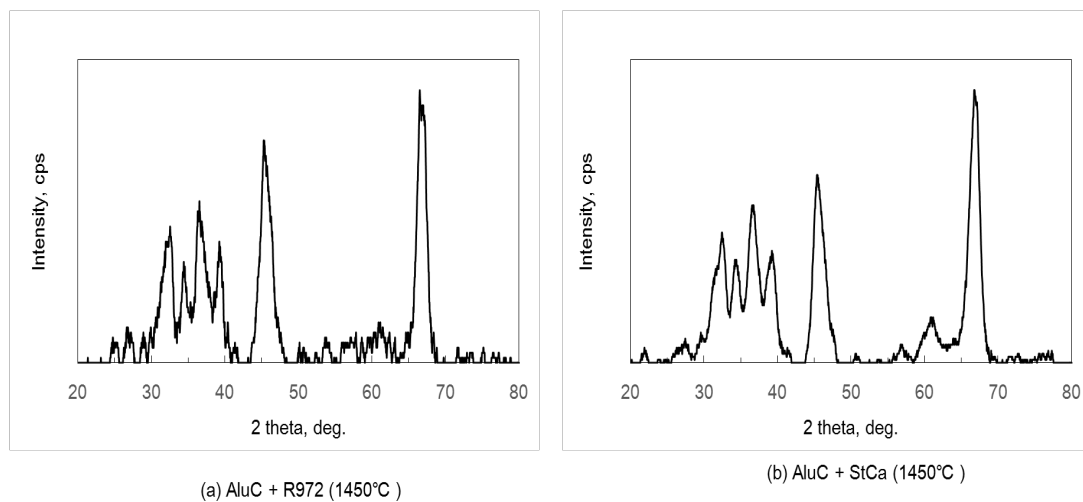
Fig. 5-2. XRD patterns of the thermally-treated AluC with external additives

5.3.2 Morphology

Table 5-1 summarizes in the surface area of AE50, AluC and Alu65 before and after the thermal treatment at 1450 ℃. In all materials, around from 10 to 20 % of the decrease with the surface area were observed.

Table 5-1 Surface area of the fumed oxides before and after thermal treatment

	S_{BET} (m^2/g)	
	Room Temp.	1450℃
AE50	50	41
AluC	100	89
Alu65	65	56

There were no differenced of the bulk densities for the thermally treated AE50, AluC and Alu65 from before the thermal treatment in all cases.

This result suggests that partially sintering occurred for the fumed SiO_2 and the fumed Al_2O_3 although these materials did not change the crystal structures.

5.3.3 Dispersibility

Fig. 5-3 confirms the particle size distributions of the thermally-treated AE50, AluC and

Alu65 at 1450 ℃. Without ultrasonic sonication Fig. 5-3 (1-3) (a), all fumed oxides showed relatively similar particle size distribution pattern in before and after the thermal treatment although the thermally-treated ones demonstrated slightly larger agglomerate. Due to the ultrasonic sonication at 40 W for 3 minutes Fig. 5-3 (1-3) (b), the main constituents of the before thermally-treated AE50, AluC and Alu65 shift to a smaller distribution region for which the thermally-treated AE50, AluC and Alu65 remained the similar region to without ultrasonic sonication. These results indicated that the thermally-treated AE50, AluC and Alu65 make slightly strong agglomerates which are not easily disrupted by the ultrasonic sonication at 40 W for 3 minutes.

(a) Without Ultrasonic sonication   (b) With Ultrasonic sonication 40W 3 minutes
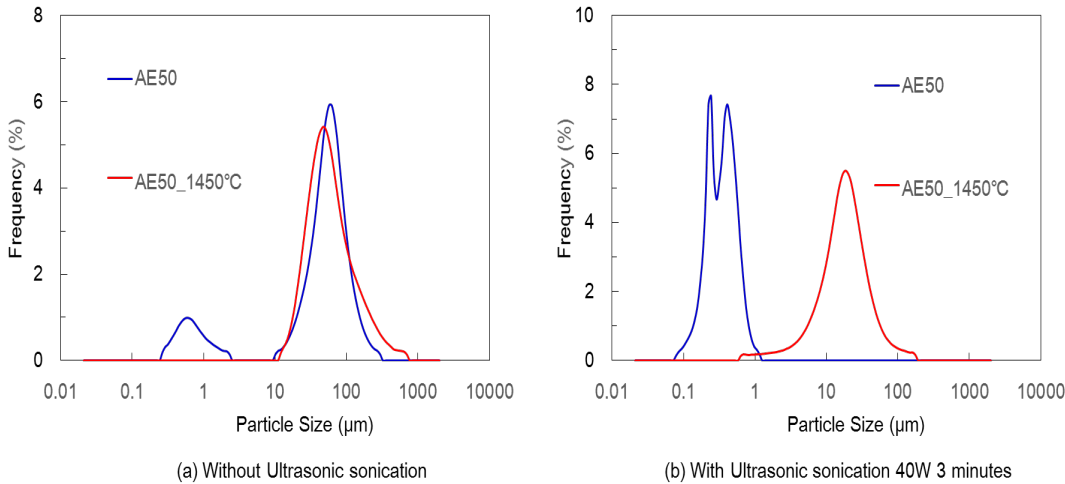
Fig. 5-3 (1). Particle size distribution of the thermally-treated AE50 at 1400 ℃

(a) Without Ultrasonic sonication   (b) With Ultrasonic sonication 40W 3 minutes
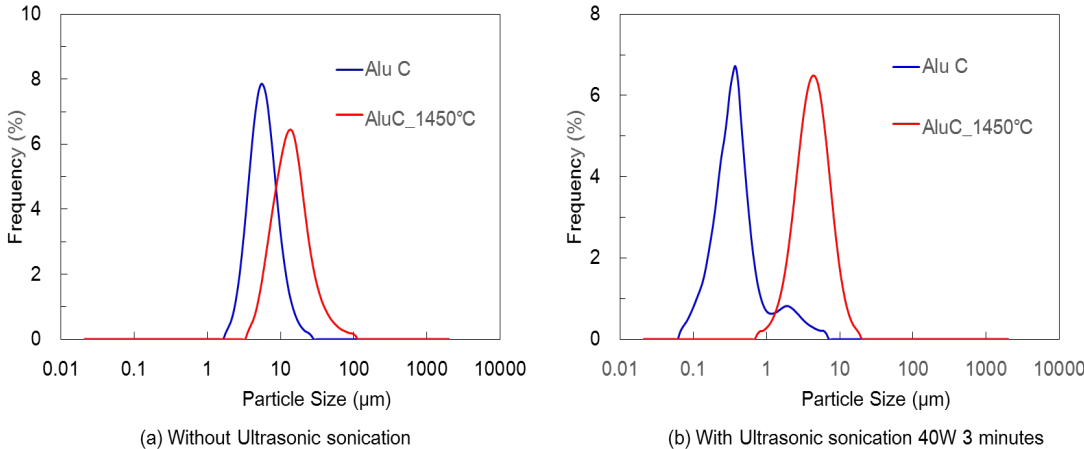
Fig. 5-3 (2). Particle size distribution of the thermally-treated AluC at 1400 ℃

<div align="center">(a) Without Ultrasonic sonication   (b) With Ultrasonic sonication 40W 3 minutes</div>
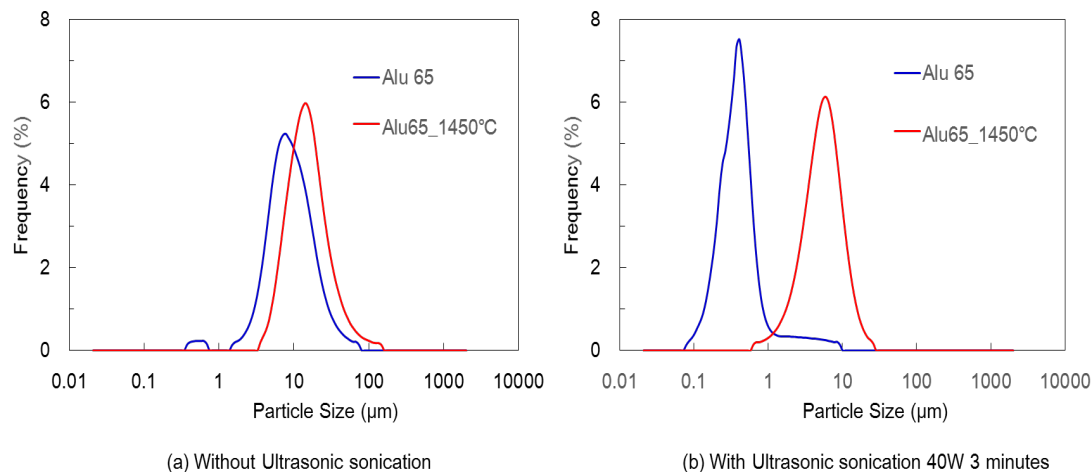
<div align="center">Fig. 5-3 (3). Particle size distribution of the thermally-treated Alu65 at 1400 °C</div>

These results suggest that the fumed SiO_2 and Al_2O_3 were modified only the agglomerate maintaining the original crystal structure. The slightly strong agglomerates were probably caused from the partial sintering of small particles which are assumed by varying the surface area. In other words, the natural dropping thermal treatment has a possibility to change the only morphology of the fumed SiO_2 and Al_2O_3 maintaining their original crystalline polymorphs.

5.4 Conclusions

The possibility of the novel natural dropping thermal treatment is investigated to apply to fumed SiO_2 and fumed Al_2O_3 besides for fumed TiO_2. The fumed SiO_2 showed no crystallization. The fumed Al_2O_3 resulted no crystal transformation even though addition of external additives, R972 and calcium stearate which showed very effective performance for the crystal transformation of the fume TiO_2.

Both thermally-treated fumed SiO_2 and fumed Al_2O_3 made slightly strong agglomerate due to probably partial sintering.

It is confirmed that the natural dropping thermal treatment is only applied to the crystal transformation of the fumed TiO_2 in this investigation. Otherwise, the morphology change maintaining the original crystalline polymorphs is possible to the fumed SiO_2

and fumed Al_2O_3. The morphology change with the amorphous phase is an advantage for the fumed SiO_2 as the point of safety material.

References

[1] Degussa, Technical Bulletin Fine Particles -Basic Characteristics of AEROSIL® Fumed Silica 11 (2003) 1-70.
[2] Nippon AEROSIL, AEROSIL effects on human body, AEROSIL Technical report 1 (1972) 1-7.
[3] K. Kihara, Crystal Structures of Silica Polymorphs and the Phase Transitions, Journal of the Crystallographic Society of Japan 43 (2001) 218-226.
[4] M. Higuchi and Y. Azuma, Effect of Alkali Metal Oxide Addition on Crystallization and Phase Transformation of Sintered Spherical Silica, Journal of the Ceramic Society of Japan 105 (1997) 385-390.
[5] Nippon AEROSIL, Aluminum Oxide C, Titanium Dioxide P25, Two Highly Dispersed Metallic Oxides from Degussa Produced by the AEROSIL-Process, AEROSIL technical report 5 (1973) 1-10.
[6] K. Sakamoto, Aluminum hydroxide and Alumina, J. JILM 22 (1972) 295-308.
[7] H. Noda and H. J. Kim, Dependence of Optical Properties on Annealing Process of Transparent Nano-Structured γ-Al_2O_3 Ceramics, Journal of the Ceramic Society of Japan 110 (2002) 1062-1066.
[8] Determination of the specific surface area of powders (solids by gas adsorption-BET method, JIS Z8830 (2013) 1-24.
[9] A. Kato, S. Kawazoe and I. Mochida, Preparation of Finely-Divided Alumina by Vapor Phase Reaction between Aluminum Chloride and Oxidizing Gases, and its Properties, Zairyo 21 (1972) 540-543.

CHAPTER 6
CONCLUDING REMARKS AND
POTENTIAL DIRECTION FOR FUTURE RESEARCH

6.1 Concluding Remarks.

This thesis successfully developed a new fumed TiO_2 with high rutile structure content maintaining the excellent dispersibility. The new fumed TiO_2 was synthesized by a novel natural dropping thermal treatment for very short calcination time. The suitable thermal treatment conditions were investigated by controlling the morphology of the fumed TiO_2 agglomerate based on the residence time in the electrical furnace during the thermal treatment. The preferable fumed TiO_2 precursors were produced with the dry-type of surface modification without heating or mixing with the external additive. The crystalline structure and a morphology of the resulted thermally-treated fumed TiO_2 were investigated. The precursor modified with tetraethoxysiane (TEOS) or an addition of surface modified fumed SiO_2 (R972) achieved 100 % of rutile structure content maintaining the high dispersibility with the sponge-like structure with many pores in the agglomerate and the static electricity repellence by SiO_2 on the fumed TiO_2 surface after the thermal treatment. Further, the addition of the external additive remarkably decreased with the crystal transformation temperature. The summary and conclusion of this thesis work are itemized as follows:

In chapter 1, general introduction of TiO_2 and the fumed TiO_2 were described. The fumed TiO_2 is a targeted material in this investigation. The necessary to increase the rutile structure for the fumed TiO_2 with high dispersibility is reported. The purpose of this study is described.

In chapter 2, a pure fumed TiO_2 (P25) was calcined by the novel additional thermal treatment, the natural dropping method. A drastic increase of the rutile structure content for the thermally-treated fumed TiO_2 (P25, 94 %) was confirmed by passing the sieves fixed on the top of the electrical furnace although the thermally-treated fumed TiO_2 without passing the sieve showed very less change of the rutile structure content (18 %) at the same thermal treatment temperature.   The thermally-treated P25 demonstrated

the high dispersibility in the water dispersion. These results suggest that many open pore spaces of the agglomerated P25 would be partially closed by partial sintering of the particles of the agglomerate and it makes a sponge-like type of agglomerate. The thermal treatment conditions are investigated depended on the agglomerate size related to the residence time under setting temperature in the electrical furnace. It was assumed that the applied heat energy is utilized not only the crystal transformation but also the sintering of the fumed TiO_2. The remained rutile structure contents at 94 % for the thermally-treated P25 is probably cased from the deviation of the bulk density of the small agglomerates in P25.

In chapter 3, the effect of the dry-type of the surface modification on the fumed TiO_2 was studied for the same purpose to develop the new fumed TiO_2 having high content of the rutile structure maintaining the high dispersibility. Especially, 100 % of the rutile structure content was aimed. The fumed TiO_2 (P25) was modified with silicone alkoxides designing to give high dispersibility with the static electrical repellence of SiO_2 layer on the fumed TiO_2 surface. Titanium alkoxide is also applied as the surface modifier comparing to the effectiveness versus silicone alkoxides for the preparation of the precursors. It was confirmed that the dry-type surface modification with tetraethoxysilane (TEOS) and titanium tetraisopropoxide (TTIP) without heating is very effective method to prepare the preferable precursors to give 100 % of rutile structure contents after the thermal treatment. The thermally-treated P25 modified with TEOS or TTIP at 1400 ℃ achieved 100 % of the rutile conversion ratio. Especially, the thermally-treated P25 modified with TEOS showed both 100 % rutile structure and excellent dispersibility attributed to both the sponge-like structural characteristic of the agglomerate and the static electricity repellence by SiO_2 coating layer.

In chapter 4, the effect of the external additives on the synthesis of the fumed TiO_2 with a high rutile content was investigated by using more simple mixing method to prepare the preferred precursors. The addition of surface modified fumed silica; R972 resulted in complete conversion of the anatase morphology to rutile structure (100 %) as well as an excellent dispersibility of the original P25 with both a sponge-like porous structure and the static electrical repellence of SiO_2 layer as we intended.

As for the addition of the fumed Al_2O_3; AluC, it resulted the decrease of the transformation temperature due to a high thermal conductive particle on the fumed TiO_2 surface.

Regarding the addition of calcium stearate, 100 % of the rutile structure and large grain growth / sintering were observed due to additional heating with burning of the alkyl-groups on calcium stearate. It resulted a low dispersibility as the reverse effect.

The contents of the rutile structure for the resulting fumed TiO_2 with the external additives are highly related to the Carr Cohesion value of the precursors before the thermal treatment. The agglomerate with low Carr Cohesion values resulted in a high rutile structure conversion ratio due to making a small agglomerate, preserving the dentification of the small agglomerate and prolonging the residence time in the electrical furnace.

In chapter 5, the possibility of the novel natural dropping thermal treatment was investigated to extend this method to the other fumed oxides, fumed SiO_2 and the fumed Al_2O_3. The fumed SiO_2 showed no crystallization by the natural dropping thermal treatment.

The fumed Al_2O_3 resulted no crystal transformation for the pure ones and mixing with external additives; surface modified fumed SiO_2; R972, and calcium stearate which showed positive performance for the crystal transformation of the fumed TiO_2. Both thermally-treated fumed SiO_2 and fumed Al_2O_3 showed partial sintering of the agglomerate and change of the morphologies.

It is confirmed that crystal transformation of the fumed oxides was observed only the fumed TiO_2 in this natural dropping thermal treatment at present.

6.2 Advantages and Disadvantages of These Approaches.

Evidently, the new fumed TiO_2 with 100 % of rutile structure maintaining the high dispersibility has an advantage with no anatase structure. This material has a possibility to apply a UV cutting sunscreen for cosmetics as an improved skin sensitivity material. For the production process, the novel natural dropping thermal treatment has a big advantage as the new thermal treatment process with very short calcination time. It can

modify the crystalline polymorphs and morphology of the fumed TiO_2 with very short heating time and produce unique sponge-like type agglomerate.

As another process, the dry-type of the surface modification without heating also has an advantage to prepare the precursor by a simple process, no heating reactor and less energy consumption. Furthermore, it is confirmed that the dry-type of the surface modification with tetraethoxysilane (TEOS) can achieve high dispersibility of the fumed TiO_2 with the static electrical repellence of the SiO_2 layer on the fumed TiO_2 surface.

More simple modification method, only mixing process achieved the decrease in the crystal transformation temperature of the fumed TiO_2.

A unique result was obtained by the addition of calcium stearate to the fumed TiO_2. A 100% rutile structure of the fumed TiO_2 with large particle size was generated by burning of the calcium stearate. This process has an advantage that the production of large particle sized fumed TiO_2 with very short calcination time and relatively low temperature.

As a disadvantage, this natural dropping thermal treatment is applied to only the fumed TiO_2 for the crystalline transformation at present. Other fumed oxides, fumed SiO_2 and fumed Al_2O_3 were not crystalized and transformed by this thermal treatment process. However, this is also considered as another big advantage of this calcination process because only morphology of the fumed oxides can be modified with maintaining the original crystalline polymorphs.

6.3 Potential Directions for Future Research.

In this study, the materials are focusing on the fumed TiO_2. However, the natural dropping thermal treatment can be applied not only fumed oxides but also other materials. If some materials need to modify the crystalline polymorphs and agglomerate situations, the natural dropping thermal treatment has a big potential to achieve them.

In this investigation, it is confirmed that the crystal transformation is applied to not the fumed SiO_2 and the fumed Al_2O_3 but only the fumed TiO_2. However, it seems to be possible to simulate whether this method can be applied to other materials compared with the fumed TiO_2 based on the basic properties such as heat capacity, thermal conductivity, primary particle size, bulk density and transformation temperature.

Additionally, it also has a possibility to apply not thermal transformation but thermal decomposition and reaction by changing the atmosphere.

For the dry-type of the surface modification, it also has a possibility to apply other materials as a simple and easy surface modification process.

Further detail investigation should be done on the external additive with different properties with core particle. The species of the external additives have a possibility to change the morphology of the particle and crystalline polymorphs drastically.

These aspects of the new fumed TiO_2 with high rutile structure content and the production processes offers exciting opportunities for newcomers to the fields.

RESEARCH ACTIVITIES

1. (Oral presentation) <u>**Y. Yamashita**</u>, K. Ishiguro, D. Nakai and M. Fuji, The Synthesis of a porous-type of TiO_2 with rutile structure, The JSPM International Conference on Powder and Powder Metallurgy, Nov. 7-9 2017.

LIST OF PUBLICATIONS

1. <u>**Y. Yamashita**</u>, K. Ishiguro, D. Nakai and M. Fuji, The synthesis of a porous-type of TiO_2 with rutile structure, Advanced Powder Technology, 29(2018) 2521-2526.

2. <u>**Y. Yamashita**</u> and M. Fuji, Development of the fumed TiO_2 having high content of rutile structure and dispersibility using the dry-type of surface modification and the thermal treatment, Advanced Powder Technology, 30(2019) 3040-3049.

3. <u>**Y. Yamashita**</u>, K. Ishiguro, D. Nakai and M. Fuji, The study of the effect of external additives on the synthesis of fumed TiO_2 with a high content of rutile structure by the novel natural dropping thermal treatment、Advanced Powder Technology, 30(2019) 1051-1057.

4. 山下行也、内藤直弘、中井大介、石黒慶、藤正督、二酸化チタン凝集粉末及びその製造法、特開2019-77597.

ACKNOWLEDGEMENTS